

# **DESIGN AND DEVELOPMENT OF GRID INTEGRATED PV SYSTEM WITH ENHANCED POWER QUALITY**

**A DISSERTATION SUBMITTED IN PARTIAL FULFILLMENT OF  
THE REQUIREMENTS FOR THE AWARD OF THE DEGREE  
OF**

**MASTER OF TECHNOLOGY  
IN  
POWER SYSTEMS**

**SUBMITTED BY:**

**HARSH CHATURVEDI**

**(2k17/PSY/05)**

**UNDER THE SUPERVISION OF**

**Prof. RACHANA GARG**



**DEPARTMENT OF ELECTRICAL ENGINEERING  
DELHI TECHNOLOGICAL UNIVERSITY**

**(Formerly Delhi College of Engineering)**

**Bawana Road, Delhi-110042**

**2019**

**DEPARTMENT OF ELECTRICAL ENGINEERING**  
**DELHI TECHNOLOGICAL UNIVERSITY**  
(Formerly Delhi College of Engineering)  
Bawana Road, Delhi-110042

**CERTIFICATE**

I, Harsh Chaturvedi, Roll No. 2k17/PSY/05 student of M. Tech. (Power System), hereby declare that the dissertation titled “**Design and Development of Grid Integrated PV System with Enhanced Power Quality**” is a bonafied record of the work carried out by me under the supervision of **Prof. Rachana Garg** of Electrical Engineering Department, Delhi Technological University in partial fulfillment of the requirement for the award of the degree of Master of Technology and has not been submitted elsewhere for the award of any other degree or diploma.

Place: Delhi

**(Harsh Chaturvedi)**

Date:

**(Prof. RACHANA GARG)**  
**SUPERVISOR**

## **ACKNOWLEDGEMENT**

I would like to express my sincere gratitude to Prof. Rachana Garg for her guidance in the dissertation. I am thankful to her for allowing me to work under her and providing all the necessary equipment required for my project work. It would have not been possible for me to complete my project work without her invaluable support and advise. I sincerely appreciate her readiness to address all my doubts and queries regarding the project work and her consistent encouragement to carry my work forward. Working under her has been a great experience and it helped me to gain a lot of personal and professional learnings.

I would like to thank Prof. Madhusudan Singh, Prof. Priya Mahajan, Prof M.Rizwan, Prof. Suman Bhowmick and all the faculties in Electrical department, DTU for their kind support and knowledge that helped me in completing my project work.

I am also thankful to my colleagues Mr. Animesh Patra, Mr. Ajay Kumar Sahu, Mr. Allu Bharghav, Mr. Tushar Srivastava, my seniors Mrs. Pallavi Verma, Mr. Hemant Saxena, Mr. Avdhesh Kumar and all the other colleagues and senior research scholars in Electrical department, DTU who have selflessly helped me and kept me motivated for my research work. I would also like to thank complete Electrical department of DTU for helping me in all possible ways to complete my project work.

Finally, I am grateful to my family for their love, support and encouragement. They have always provided me with all the needful resources and guidance to excel in life. I am fortunate to have them. All my capabilities are because of them and all of achievements truly belongs to them.

Date:

**(Harsh Chaturvedi)**

## **ABSTRACT**

Electricity is a utility, all kind of industries, commercial buildings, households, agriculture etc. require electricity to function efficiently, thus electrical energy important to every country for its development and growth. Thermal power plants based on coal and other fossil fuels have been the major source of electrical energy for the whole world till date. However due to limited availability of fossil fuels and emission of greenhouse gases it is necessary to regulate the use of fossil fuels and develop renewable energy resources which are sustainable and environment friendly. Renewable energy sources like wind and solar have become standard electrical energy sources these days and there is a lot of research work going in field of renewable energy to further improve their efficiency and feasibility. In recent years, the power generation through photovoltaic (PV) systems have grown rapidly all over the world. The grid connected PV system have become popular across the globe and are a great aspect to cater major portion of electrical energy demand in future. Grid connected PV systems have capability to transfer solar energy into the grid and also improve power quality at point of common coupling.

In the present work “DESIGN AND DEVELOPMENT OF GRID INTEGRATED PV SYSTEM WITH ENHANCED POWER QUALITY”, the electrical modelling of PV cell, conventional MPPT techniques and two-stage grid connected PV system are studied. The equivalent electrical model of a photovoltaic cell is studied to understand the PV characteristics and its dependence on solar irradiance and temperature. Design and application of boost converter for MPPT in PV system is discussed. MATLAB SIMULINK model for MPPT in PV system using boost converter is developed and simulation results are presented for dynamic solar irradiance, temperature and load conditions. A hardware model for MPPT in PV system using boost converter is also developed and results are obtained for different solar irradiance, temperature and load conditions.

Design and development of two-stage grid connected PV system is presented and its capability to integrate PV power into the grid and power quality enhancement is discussed. MATLAB SIMULINK models of two-stage grid connected PV system for several control techniques are developed and their results are presented. Hardware model of DSTATCOM is developed to demonstrate its capability to compensate load reactive power, load harmonics and unbalance in three-phase load. The performance of hardware models is tested for several control techniques and obtained results are presented in the work.

# TABLE OF CONTENT

COVER PAGE	i
CERTIFICATE	ii
ACKNOWLEDGEMENT	iii
ABSTRACT	iv
TABLE OF CONTENT	vi
LIST OF FIGURES	x
LIST OF TABLES	xiv
LIST OF ABBREVIATIONS	xv
<b>CHAPTER 1 INTRODUCTION</b>	<b>1</b>
1.1 General	1
1.2 Solar Energy	1
1.3 Power Quality	1
1.4 Grid Connected Two-stage PV System	2
1.5 Outline of Chapters	3
<b>CHAPTER 2 LITERATURE REVIEW</b>	<b>5</b>
2.1 General	5
2.2 Solar Energy in India	5
2.3 Photovoltaics and MPPT Techniques	5
2.4 Power Quality	6
2.5 Grid Connected Two-stage PV System	7
2.6 Conclusion	8

<b>CHAPTER 3 PHOTOVOLTAIC MODELLING AND MAXIMUM POWER POINT TRACKING</b>	<b>9</b>
3.1 General	9
3.2 Photovoltaics	9
3.3 Electrical Model of a Photovoltaic Cell	10
3.4 Concept of Maximum Power Point Tracking in Photovoltaic System	13
3.5 MPPT in Photovoltaic System Using Boost Converter	14
3.5.1 System Configuration	14
3.5.2 Boost Converter Design	15
3.5.3 Conventional Algorithms for MPPT	16
3.6 MATLAB Simulation Results for MPPT in Photovoltaic System Using Boost Converter	18
3.6.1 Simulation Results for MPPT Under Dynamic Solar Irradiance Condition	19
3.6.2 Simulation Results for MPPT Under Dynamic Temperature Condition	21
3.6.3 Simulation Results for MPPT Under Dynamic Load Condition	23
3.7 Hardware Implementation of MPPT in Photovoltaic System Using Boost Converter	25
3.7.1 Gate Driver Circuit	26
3.7.2 Sensor Circuit	26
3.7.3 Controller	27
3.7.4 Hardware Results for MPPT	27
3.8 Conclusion	29
<b>CHAPTER 4 GRID CONNECTED TWO-STAGE PV SYSTEM</b>	<b>30</b>
4.1 General	30
4.2 Grid Connected Two-stage PV System	30
4.3 Design of Grid Connected Two-stage PV System	31
4.3.1 Specification of PV Array	31
4.3.2 Inductor for Boost Converter	32
4.3.3 Selection of Diode and IGBT for Boost Converter	33
4.3.4 Choice of DC-Link Voltage	33
4.3.5 Sizing of DC-Link Capacitor	33

4.3.6 Interfacing Inductor	33
4.3.7 Voltage Source Inverter	34
4.4 Control of Grid Connected Two-stage System	34
4.5 Reference Current Generation for Voltage Source Inverter	35
4.5.1 Unit Template Based Current Control Algorithm	35
4.5.2 IRPT Based Current Control Algorithm	36
4.5.3 SRFT Based Current Control Algorithm	37
4.5.4 Indirect Current Control Algorithm Based on SRFT	39
4.6 Hysteresis Current Controller for Voltage Source Inverter	40
4.7 MATLAB Simulation of Grid Connected Two-Stage PV System	40
4.8 Simulation Results for Grid Connected Two-Stage PV System	44
4.8.1 Results for Unit Template Control	44
4.8.2 Results for IRPT Control	51
4.8.3 Results for SRFT Control	58
4.8.4 Results for Indirect SRFT Control	65
4.9 Observations	72
4.10 Conclusion	73
<b>CHAPTER 5 HARDWARE IMPLEMENTATION OF DSTATCOM</b>	<b>74</b>
5.1 General	74
5.2 DSTATCOM	74
5.3 Hardware Setup of DSTATCOM	75
5.3.1 Choice of DC-Link Voltage	76
5.3.2 Sizing of DC-Link Capacitor	76
5.3.3 Interfacing Inductor	76
5.3.4 Voltage Source Inverter	77
5.3.5 Gate Driver Circuit	77
5.3.6 Sensor Circuit	77
5.4 Control of DSTATCOM Using MicroLabBox	77
5.5 Specifications of Hardware Model for DSTATCOM	79



5.6 Hardware Results for DSTATCOM	79
5.6.1 Grid Voltage and Current Profile for Different Types of Load without Compensation	80
5.6.2 Results for Unit Template Control	82
5.6.3 Results for IRPT Control	86
5.6.4 Results for SRFT Control	90
5.6.5 Results for Indirect SRFT Control:	94
5.6.6 Results for Compensation of Composite Load through SRFT Control:	98
5.7 Observations	102
5.8 Conclusion	106
<b>CHAPTER 6 CONCLUSION AND FUTURE WORK</b>	<b>107</b>
6.1 Main Conclusion	107
6.2 Future Work	107
<b>REFERENCES</b>	<b>108</b>

## LIST OF FIGURES

Figure 1-1. Grid connected two-stage PV System.....	3
Figure 3-1. Structure of PV array .....	9
Figure 3-2. Double-diode model of a PV cell.....	10
Figure 3-3. Single-diode model of a PV cell .....	10
Figure 3-4. I-V and P-V characteristic of PV cell .....	11
Figure 3-5. I-V characteristic of PV cell at different solar irradiance .....	12
Figure 3-6. I-V characteristic of PV cell at different temperature .....	12
Figure 3-7. Concept of MPPT in PV system .....	13
Figure 3-8. System configuration for MPPT in photovoltaic system using boost converter .....	14
Figure 3-9. Flowchart of P&O algorithm for MPPT in photovoltaic system using boost converter .....	16
Figure 3-10 Flowchart for Incremental conductance algorithm for MPPT in photovoltaic system using boost converter .....	17
Figure 3-11 MATLAB model for MPPT in photovoltaic system using boost converter... ..	18
Figure 3-12 Simulation results for MPPT under dynamic solar irradiance condition....	20
Figure 3-13. Simulation results for MPPT under dynamic temperature condition .....	22
Figure 3-14. Simulation results for MPPT under dynamic load condition.....	24
Figure 3-15. Hardware setup for MPPT in photovoltaic system using boost converter.	25
Figure 3-16. Gate Driver Circuit.....	26
Figure 3-17. Sensor Circuit.....	27
Figure 3-18. Arduino Uno .....	27
Figure 4-1. Grid connected two-stage PV system .....	30
Figure 4-2. PV array characteristics used for grid connected two-stage system .....	32
Figure 4-3. Unit template current control algorithm.....	35
Figure 4-4. IRPT based current control algorithm.....	37
Figure 4-5. SRFT based current control algorithm.....	38
Figure 4-6. Indirect current control algorithm using SRFT .....	39
Figure 4-7. Hysteresis current controller .....	40
Figure 4-8. MATLAB SIMULINK model for grid connected two-stage PV system ....	41
Figure 4-9. Solar irradiance input to PV array.....	42
Figure 4-10. Results of Unit template control for dynamic switching of linear load .....	44

Figure 4-11. Results of Unit template control for dynamic switching of linear load showing real and reactive power of grid, VSI and load respectively .....	45
Figure 4-12. Results of Unit template control with linear load and change in solar irradiance .....	46
Figure 4-13. Results of Unit template control with unbalanced load .....	47
Figure 4-14. Results of Unit template control with non-linear load .....	48
Figure 4-15. Current profiles in unit template control for non-linear load.....	49
Figure 4-16. Harmonic profile in Unit template for non-linear load .....	50
Figure 4-17. Results of IRPT control for dynamic switching of linear load .....	51
Figure 4-18. Results of IRPT control for dynamic switching of linear load showing real and reactive power of grid, VSI and load respectively .....	52
Figure 4-19. Results of IRPT control with linear load and change in solar irradiance ..	53
Figure 4-20. Results of IRPT control with unbalanced load .....	54
Figure 4-21. Results of IRPT control with non-linear load .....	55
Figure 4-22. Current profile in IRPT control for non-linear load.....	56
Figure 4-23. Harmonic profile in IRPT control for nonlinear load .....	57
Figure 4-24. Results of SRFT control for dynamic switching of linear load .....	58
Figure 4-25. Results of SRFT control for dynamic switching of linear load showing real and reactive power of grid, VSI and load respectively .....	59
Figure 4-26. Results of SRFT control with linear load and change in solar irradiance..	60
Figure 4-27. Results of SRFT control with unbalanced load .....	61
Figure 4-28. Results of SRFT control with nonlinear load.....	62
Figure 4-29. Current profile in SRFT control for non-linear load.....	63
Figure 4-30. Harmonic profile in SRFT control for non-linear load .....	64
Figure 4-31. Results of Indirect SRFT control for dynamic switching of linear load ....	65
Figure 4-32. Results of Indirect SRFT control for dynamic switching of linear load showing real and reactive power of grid, VSI and load respectively .....	66
Figure 4-33. Results of Indirect SRFT control with linear load and change in solar irradiance .....	67
Figure 4-34. Results of Indirect SRFT control with unbalanced load .....	68
Figure 4-35. Results of Indirect SRFT control with nonlinear load .....	69
Figure 4-36. Current profile for Indirect SRFT control for non-linear load.....	70
Figure 4-37. Harmonic spectrum in Indirect SRFT control for non-linear load.....	71
Figure 5-1. Block diagram for hardware setup of DSTATCOM.....	74

Figure 5-2. Hardware setup of DSTATCOM .....	75
Figure 5-3. Block diagram for control of DSTATCOM using MicroLabBox .....	78
Figure 5-4. Grid voltage and current respectively in case of linear load without compensation .....	80
Figure 5-5. Grid Power analysis in case of linear load without compensation .....	81
Figure 5-6. Grid voltage and current respectively in case of non-linear load without compensation .....	81
Figure 5-7. Compensated grid voltage and current in case of linear load with Unit template control .....	82
Figure 5-8. Reference grid currents, actual grid currents and dc-link voltage in case of linear load with unit template control .....	83
Figure 5-9. Grid power analysis in case of linear load with unit template control.....	84
Figure 5-10. Compensated grid voltage and current in case of non- linear load with Unit template control .....	84
Figure 5-11. Reference grid currents, actual grid currents and dc-link voltage in case of non-linear load with unit template control.....	85
Figure 5-12. Compensated grid voltage and current in case of linear load with IRPT control .....	86
Figure 5-13. Reference VSI currents, actual VSI currents and dc-link voltage in case of linear load with IRPT control .....	87
Figure 5-14. Grid power analysis in case of linear load with IRPT control .....	88
Figure 5-15. Compensated grid voltage and current in case of non- linear load with IRPT control .....	88
Figure 5-16. Reference VSI currents, actual VSI currents and dc-link voltage in case of non-linear load with IRPT control .....	89
Figure 5-17. Compensated grid voltage and current in case of linear load with SRFT control .....	90
Figure 5-18. Reference VSI currents, actual VSI currents and dc-link voltage in case of linear load with SRFT control .....	91
Figure 5-19. Grid power analysis in case of linear load with SRFT control .....	92
Figure 5-20. Compensated grid voltage and current in case of non- linear load with SRFT control .....	92
Figure 5-21. Reference VSI currents, actual VSI currents and dc-link voltage in case of non-linear load with SRFT control .....	93

Figure 5-22. Compensated grid voltage and current in case of linear load with Indirect SRFT control.....	94
Figure 5-23. Reference grid currents, actual grid currents and dc-link voltage in case of linear load with Indirect SRFT control .....	95
Figure 5-24. Grid power analysis in case of linear load with Indirect SRFT control.....	96
Figure 5-25. Compensated grid voltage and current in case of non- linear load with Indirect SRFT control .....	96
Figure 5-26. Reference grid currents, actual grid currents and dc-link voltage in case of non-linear load with Indirect SRFT control.....	97
Figure 5-27. Grid voltage and current in case of composite load without compensation .....	98
Figure 5-28. Phasors of grid voltage and current with power analysis in case of composite load.....	99
Figure 5-29. Compensated grid voltage and current waveforms and THD in case of composite load with SRFT control .....	99
Figure 5-30. Reference VSI currents, actual VSI currents in case of composite load with SRFT control.....	100
Figure 5-31. Actual DC-link voltage in case of composite load with SRFT control ...	101
Figure 5-32. Phasors of grid voltage and current with power analysis in case of composite load with SRFT control.....	101

## LIST OF TABLES

Table 3-1. Specification of PV panel used for MPPT in photovoltaic system using boost converter .....	15
Table 3-2. Specification of MATLAB model for MPPT in photovoltaic system using boost converter.....	19
Table 3-3. Results for photovoltaic system without MPPT.....	28
Table 3-4. Results for MPPT in photovoltaic system using boost converter .....	28
Table 4-1. PV array specification for grid connected two-stage PV system .....	31
Table 4-2. Specification of MATLAB model for grid connected two-stage PV system .....	41
Table 4-3. Grid current and voltage THD in case of non-linear load with different control techniques .....	73
Table 5-1. Specifications for hardware model for DSTATCOM.....	79
Table 5-2. Hardware Results for compensation of linear load using DSTATCOM.....	103
Table 5-3. Hardware Results for compensation of non-linear load using DSTATCOM .....	104
Table 5-4. Hardware Results for compensation of composite load using DSTATCOM .....	105

## LIST OF ABBREVIATIONS

PV	Photovoltaic
MPPT	Maximum power point tracking
VSI	Voltage Source Inverter
P&O	Perturb and Observe
INC	Incremental Conductance
AC	Alternating Current
DC	Direct Current
IGBT	Insulated Gate Bipolar Transistor
SRFT	Synchronous Reference Frame Theory
IRPT	Instantaneous Reactive Power Theory
HCC	Hysteresis Current Controller
THD	Total Harmonic Distortions
PLL	Phase Locked Loop
PCC	Point of Common Coupling
DSTATCOM	Distribution static compensator
DVR	Dynamic voltage restorer
UPQC	Unified power quality conditioner

## **CHAPTER 1 INTRODUCTION**

### **1.1 General**

Electricity is a utility, all kind of industries, commercial buildings, households, agriculture etc. require electricity to function efficiently, thus electrical energy is important to every country for its development and growth. The demand for electricity in the world is increasing daily with increase in population, urbanization and industrialization.

Several sources of electrical energy are available such as thermal power plant based on fossil fuels, hydroelectric power plants, nuclear power plants, wind power plants, solar power plants etc. Thermal power plants based on coal and other fossil fuels have been the major source of electrical energy for the whole world till date. However, combustion of fossil fuels has harmful effect on the environment and also fossil fuels are present in limited quantity which will exhaust with time. It is therefore necessary to regulate the use of fossil fuels and develop renewable energy resources which are sustainable and environment friendly.

### **1.2 Solar Energy**

There are several renewable energy sources available today like hydro energy, wind energy, solar energy, geothermal energy, tidal energy etc. However solar energy out of all seems to be the future of electricity as many countries across the world are developing capacity for solar energy generation to meet their current and future energy demands. Most of the solar projects developed today are based on Photovoltaic system. Photovoltaic (PV) are semiconductor devices that directly convert solar radiations into electricity. There has been a tremendous research and development in field of PV which has resulted in their reduced cost and increased efficiency. The PV based projects are cost-effective, space-efficient and have a low operation and maintenance cost therefore making them a more reasonable choice when compared to wind or hydro projects [1-3].

### **1.3 Power Quality**

Apart from availability of electricity other important issue is quality of power. The term power quality is very clear from its name, it describes the quality of power supply available at consumer terminal. Power quality of a three-phase supply at consumer terminal is characterised by magnitude of 3-phase voltage, frequency of voltage, balance of 3-phase voltages and waveform of the voltage. Most of the electrical appliances and



machinery installed in industries, commercial buildings, households etc. are designed to work at a balanced 3-phase sinusoidal voltage supply of rated magnitude and frequency. On the other hand every utility would also want to transmit balanced 3-phase current containing only fundamental component at unity power factor to minimize losses in their network and regulate magnitude, frequency, THD (total harmonic distortion) and balance of 3-phase terminal voltage, however due to ever changing load in a distribution network balanced 3-phase load cannot be guaranteed, there is variety of loads connected demanding reactive power and drawing harmonic current from distribution network, there is sudden changes in loads causing voltage sag and voltage swell, notches in supply voltage, all these problems are termed as power quality issues. In order to deal with power quality issue custom power devices which, include distribution static compensator (DSTATCOM), dynamic voltage restorer (DVR), and unified power quality conditioner (UPQC) can be used according to suitability [24,25].

#### **1.4 Grid Connected Two-stage PV System**

Grid connected two-stage PV system is a solution which can be used for integrating PV output power into the grid. It can also serve functions of a DSTATCOM to act against power quality issues due to non-ideal nature of grid current like load reactive power compensation, load unbalance compensation, load harmonic compensation.

Figure 1.1 shows a basic block diagram of a grid connected two-stage PV system. A two-stage system consist of a DC-DC converter as its first stage and a Voltage Source Inverter (VSI) as its second stage. The DC-DC converter stage performs function of Maximum Power Point Tracking (MPPT) in PV array. MPPT is a control technique that helps to extract maximum power from a PV in given environmental conditions. In MPPT technique the output current and voltage of PV array are sensed and given as input to a controller which based on a MPPT algorithm controls duty cycle of DC-DC converter to extract maximum power from PV array. There are conventional maximum power point tracking algorithms available such as Perturb and Observe algorithm (P&O), Incremental Conductance (INC), fractional voltage, fractional current, etc. and also there are MPPT algorithm based fuzzy logic control, neural network, and other artificial intelligent techniques. [8,9].

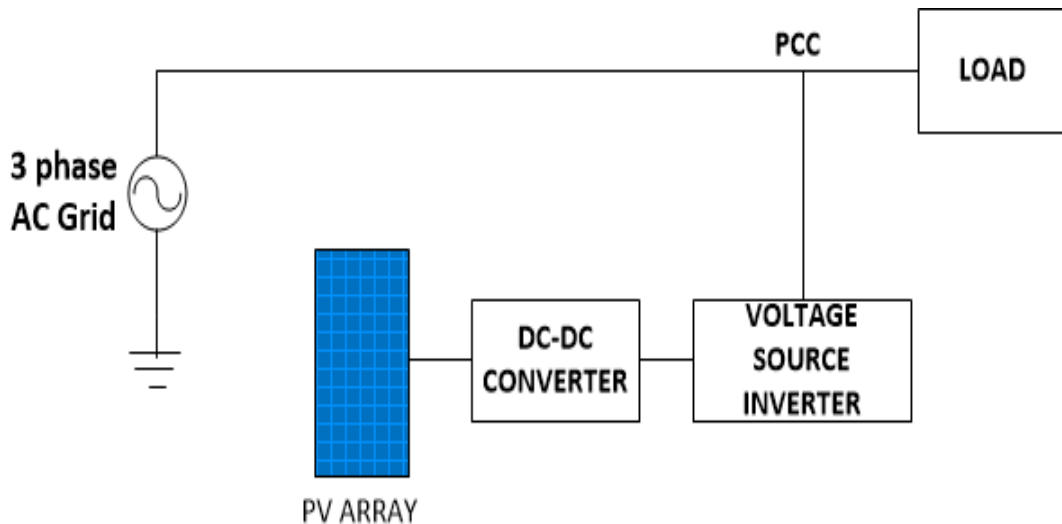


**Figure 1-1. Grid connected two-stage PV System**

The output of DC-DC converter is dc (direct current) power which is fed to the voltage source inverter. The voltage source inverter converts this power from dc to ac (alternating current) and injects it into the grid. As seen in figure 1.1 Voltage source inverter is connected at point of common coupling (PCC) such that it is in parallel to the grid. It is controlled as a current source which can injects current in the grid such that it compensate load reactive power, load unbalance, load harmonics and also inject PV power into grid. Thus, in addition to transfer of PV power to the grid VSI also serves functions of a DSTATCOM. There are several control techniques available for DSTATCOM which are also applicable for VSI control in grid connected two-stage PV like Instantaneous reactive power theory (IRPT), Synchronous reference frame theory (SRFT), Power balance theory, Conductance based current algorithm, etc [27,28].

### **1.5 Outline of Chapters**

The thesis consists of following chapters:

Chapter 1: This chapter gives a brief review on solar energy, power quality and grid connected two-stage system.

Chapter 2: This chapter gives the literature review done in related for the present work “DESIGN AND DEVELOPMENT OF GRID INTEGRATED PV SYSTEM WITH ENHANCED POWER QUALITY”. The literature review is done to understand the future scope of solar energy, modelling of photovoltaics, MPPT techniques in PV system, power quality standards and mitigation of power quality problems and grid connected two-stage systems.

Chapter 3: This chapter gives an introduction on PV and its electrical modelling to derive its output characteristics and understand their dependence on solar irradiance and temperature. This chapter explains application of MPPT in PV systems to improve their efficiency. Design and application of boost converter for MPPT in PV system using conventional techniques ‘Perturb and Observe’ and ‘Incremental Conductance’ is discussed. MATLAB-SIMULINK model and a hardware model for MPPT in PV system by application of boost converter are designed and presented.

Chapter 4: In this chapter design and controlling of a grid connected two-stage system is discussed. A MATLAB-SIMULINK for the system is developed and its performance to integrate power from PV to grid and simultaneously compensate current related power quality issues is analysed for different control techniques under varying solar input and different loading conditions.

Chapter 5: This chapter gives design and development of hardware model for DSTATCOM. The control of DSTATCOM is done using MicroLabBox (dSPACE product). The performance of DSTATCOM is analysed for different control algorithms and the results are recorded and presented using FLUKE 435 Series II three phase power quality and energy analyzer.

Chapter 6: This chapter gives the main conclusion of the work done and also includes scope for future work.

## **CHAPTER 2 LITERATURE REVIEW**

### **2.1 General**

In present work “DESIGN AND DEVELOPMENT OF GRID INTEGRATED PV SYSTEM WITH ENHANCED POWER QUALITY”, the electrical modelling of PV cell, conventional MPPT techniques and grid connected two-stage PV system are studied. Design and application of boost converter for MPPT in PV system is discussed. MATLAB-SIMULINK model for MPPT in PV system by application of boost converter is developed and simulation results are presented for dynamic solar irradiance, temperature and load conditions. A hardware model for MPPT in photovoltaic system using boost converter is also developed and results are obtained for different solar irradiance, temperature and load conditions. Design and development of grid connected two-stage PV system is presented and its capability to integrate solar power into the grid and power quality enhancement is discussed. MATLAB-SIMULINK models of grid connected two-stage PV system for several control techniques are developed and their results are presented. Hardware model of DSTATCOM is developed to demonstrate its capability to compensate load reactive power, load harmonics and unbalance in 3-phase load. The performance of hardware models is tested for several control techniques and obtained results are presented in the work. The literature review for this work is carried out in the related areas and is detailed in this chapter.

### **2.2 Solar Energy in India**

The present installed capacity of renewable energy in India is about 34.6 % of total installed capacity. The major sources of renewable energy are hydroelectric plants followed by wind energy and then solar energy. However, inception of PV has made solar power a promising option for the future energy demands. PV systems can either be used as standalone system (up to several kilowatt) or as grid connected system (several megawatt) [1-3]. Sahoo et al. [1] gives a review of solar energy development in India and government policies to support solar energy development.

### **2.3 Photovoltaics and MPPT Techniques**

The fundamental component of PV system is a photovoltaic cell which is a semiconductor device that generate dc voltage when solar radiation falls on its surface. PV cells and their characteristics can be analysed with help of equivalent electrical model of PV cell [4,5]. Bellia et al. [4] gives details on MATLAB simulation of a PV cell using single-diode

equivalent model. Kumar et al. [5] presents an two-diode equivalent model for a PV cell and investigates its accuracy compared to single-diode model. PV systems employ MPPT techniques to maximize their output power, there are several papers available explaining mathematical modelling of PV and comparing different MPPT algorithm [6-9]. Karami et al. [8] explains and classifies 40 different MPPT techniques. Ram et al. [9] gives a review on timeworn conventional MPPT techniques, latest soft computing algorithms and compares them on basis of complexity of algorithm, tracking of MPP under dynamic shading condition. Verma et al. [10] gives a comparison of intelligent and conventional techniques to track maximum power under partial shading in PV system. Mohan et al. [11] have given explanation on working and design of DC-DC converters and magnetic components used. There are several papers which discuss the hardware implementation of MPPT in PV systems [12-14]. Hohm et al. [12] compares different MPPT techniques on a programmable test bed.

#### **2.4 Power Quality**

The problems in electric supply like voltage sag and swell, notches in supply voltage, harmonics in supply voltage and current, supply power factor and unbalancing in 3-phases are termed as power quality issues. Choi et al. [15] explains voltage sag and swell is a decrease and increase respectively in supply voltage for a short duration (less than a minute) whereas variations for longer time period are termed as undervoltage and overvoltage. Heydt et al. [16] explains how the increased usage of non-linear loads like power electronic devices e.g. ac-dc converter, electronic devices like personal computers, mobile chargers etc. result in harmonic injection at distribution level due which supply current and voltage to become non-sinusoidal. Ozgonenel et al. [17] explains the reactive power demand at load side reduces power factor of the supply and causes overloading in supply cables and a voltage drop at load end. There is unbalance in supply currents due to unbalanced 3-phase loads. There may be excessive neutral current in 3-phase four wire systems due to zero sequence harmonics injected by non-linear loads. The power quality problems may result in derating of end-user equipment, malfunctioning or failure of equipment, higher power loss in system etc. A failure in critical equipment in industries, commercial offices, sub-stations, hospitals may result in severe losses. Therefore, several standard to maintain an acceptable level related to power quality at distribution level have been developed [18]. IEEE-519-1992 standard [19], is a guideline for mitigation and control of problems related to harmonics at distribution level. This standard forms

guidelines for the design of electric power system with nonlinear loads to that the non-linear equipment installed at a user end does not degrade power quality for other users connected to the same utility. IEEE-1159-1995 [20] is a standard for power quality monitoring and IEEE-1100-1999 [21] is standard which guides on how to power and ground electrical equipments. IEEE 1459-2010 [22] standard states that an electrical network will have maximum efficiency when grid current and PCC voltages consist of only fundamental harmonic components. With advancement in the field of power electronics, signal processing and improved sensor technology custom power devices have evolved. Custom Power devices includes distribution static compensator (DSTATCOM), dynamic voltage restorer (DVR), and unified power quality conditioner (UPQC). Custom power devices are composed of a power electronic converter with a sensor and a controller unit. These devices have become popular choice to deal with power quality issues [23-26]. Singh et al. [26] explains the digital implementation of a shunt active filter for compensating load harmonics, unbalance and reactive power.

## **2.5 Grid Connected Two-stage PV System**

Grid connected two-stage PV system is used for integrating PV power into the grid. It can also serve functions of a DSTATCOM to act against power quality issues like load reactive power compensation, load unbalance compensation, load harmonic compensation [27,28]. The grid connected PV systems can either be a single stage configuration or a two-stage configuration. In single stage configuration, PV array is interfaced directly to the dc-link of VSI. In single stage configuration the control of VSI is designed to perform MPPT in PV, transferring solar power into grid and mitigating current related power quality problems. Singh et al. [29] have proposed a single stage configuration with ILST control of VSI, the VSI transfer the extracted PV energy to three-phase grid and simultaneously helps in enhancing power quality. In two-stage configuration the PV array is interfaced to dc-link of VSI by a DC-DC converter. In two-stage configuration, DC-DC converter tracks maximum solar power and transfers it to inverter stage. It is job of the VSI to transfer this energy to grid and simultaneously mitigate power quality problems. Jain et al. [30] have proposed a two-stage solar energy conversion system which consist of a boost converter for maximum power point tracking (MPPT) in PV and a VSI to feed solar energy to the grid and provide reactive power compensation, harmonics elimination at PCC. Singh et al. [31] proposed design of two-stage PV system with details on seizing of PV array, boost converter, dc-link capacitor,

reference dc bus voltage and interfacing inductors. Singh et al. [32] have proposed grid interfaced 50 kW PV system which incorporates features for power quality enhancement using IRPT control technique. Verma et al. [33] proposed a two-stage system to improve the power factor to unity or to regulate a voltage at point of common coupling (PCC). Perturb and Observe MPPT technique is implemented using DC-DC boost converter, VSI is controlled through SRFT algorithm to compensates for harmonics currents, unbalances load and improve power factor or regulate voltage at PCC, DC bus voltage is regulated using a PI controller.

## **2.6 Conclusion**

In this chapter the literature review done in the relevant areas for the present work “DESIGN AND DEVELOPMENT OF GRID INTEGRATED PV SYSTEM WITH ENHANCED POWER QUALITY” is detailed. The literature review is done to understand the scope of solar energy in future, modelling of photovoltaics, MPPT techniques in PV system, power quality standards and mitigation of power quality problems and grid connected two-stage systems.

## CHAPTER 3 PHOTOVOLTAIC MODELLING AND MAXIMUM POWER POINT TRACKING

### 3.1 General

Invention of photovoltaics (PV) has given a boost to development of solar energy around the world. The cost of PV has come down and their efficiency has increased with time and continuous research in this field. There are large solar parks developed based on PV across the world having capacities up to several megawatts.

In order to develop and design an efficient electrical system based on PV, it is important to understand the equivalent electrical model of PV and its output characteristics. This chapter gives an introduction on PV and its electrical modelling to derive its output characteristics and understand their dependence on solar irradiance and temperature. This chapter explains application of MPPT in PV systems to improve their efficiency. Design and application of boost converter for MPPT in PV system using conventional techniques ‘Perturb and Observe’ and ‘Incremental Conductance’ is discussed. MATLAB-SIMULINK simulation and a hardware model for MPPT in photovoltaic system using boost converter is also developed and presented.

### 3.2 Photovoltaics

The smallest unit in a PV is a photovoltaic cell. Photovoltaic cell is a p-n semiconductor junction which generates dc current when light falls on its surface, the current generated is proportional to the solar irradiation.

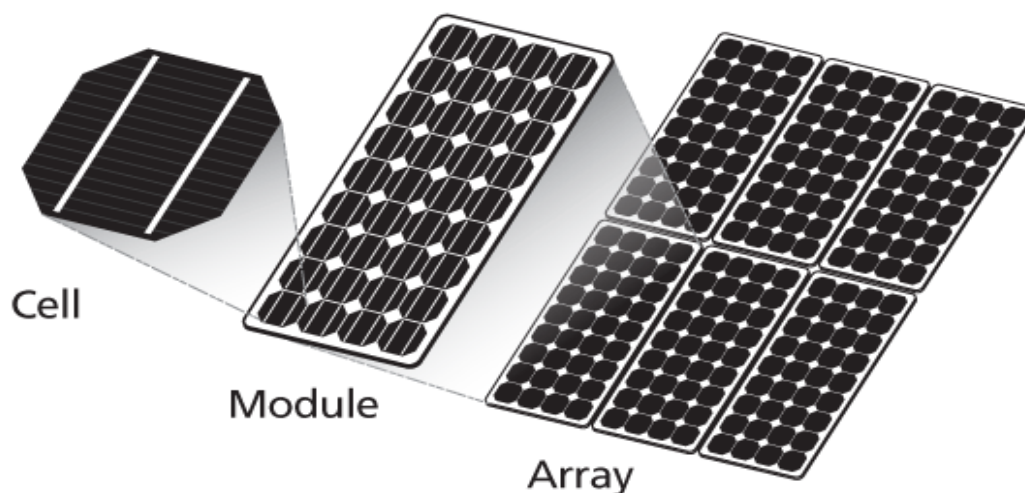


Figure 3-1. Structure of PV array



A PV cell generates a small open circuit voltage (approximately .5 to .6 volt) across its terminals when sunlight falls on it and generate a small amount of power (approximately 0.1 to 3 watt). PV cells are connected in series and laminated together to make a PV module for higher output voltage (about 15 to 20 volt) and power (about 100 to 350 watt). PV modules are further connected in series and parallel to form PV array and large arrangements of PV arrays can be designed for larger power output (in Megawatt). Figure 3.1 shows structure of PV array composed of PV modules which in turn are composed of PV cells.

### 3.3 Electrical Model of a Photovoltaic Cell

In order to analyse a PV cell and its characteristic it is important to understand its equivalent electrical model. PV cell can be modelled using double-diode model or single-diode model. Double-diode model gives a more accurate representation of a PV cell compared to single-diode model and it is shown in figure 3.2.

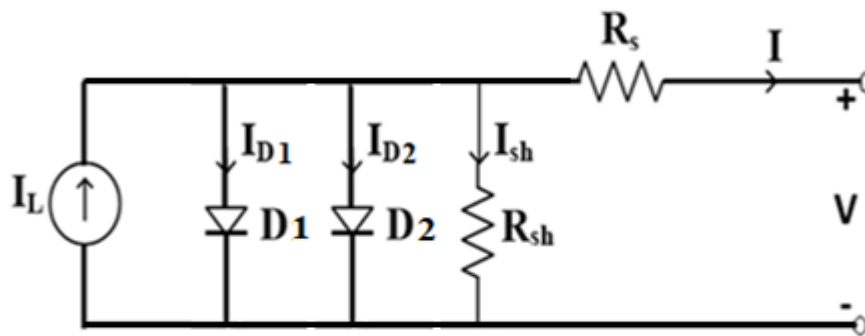


**Figure 3-2. Double-diode model of a PV cell**

Single-diode model is an approximation of double-diode model with one diode eliminated shown in figure 3.3. Single-diode model has acceptable accuracy and is widely used for analysis and design purposes [4,5].

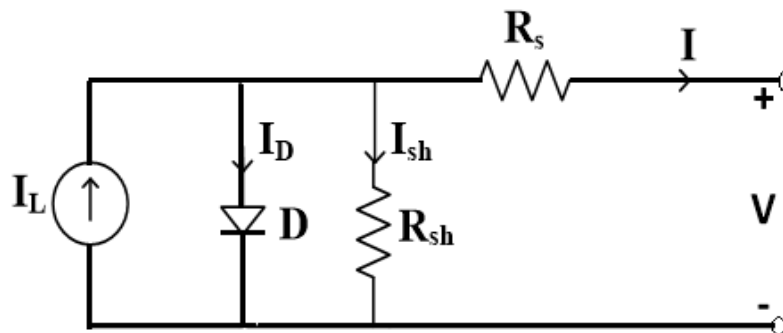


**Figure 3-3. Single-diode model of a PV cell**

In this work Single-diode model is studied and equations related to it are explained below [6]. Equation 3.1 is obtained by applying Kirchoff's current law, the output current  $I$  is expressed in terms of photo current  $I_L$ , diode current  $I_D$  and shunt current  $I_{Sh}$ .

$$I = I_L - I_D - I_{Sh} \quad (3.1)$$

$I_D$  is diode current and it can be expressed as in equation 3.2:

$$I_D = I_0 \left( e^{q \cdot \frac{V + I \cdot R_S}{K} \cdot T} - 1 \right) \quad (3.2)$$

Here  $I_0$  is reverse saturation current which depends on material/doping level,  $q$  is the charge of an electron =  $1.6 \times 10^{-19}$  coulombs,  $K$  is the Boltzmann constant (J/K),  $T$  is the cell temperature (K),  $R_S$  is effective series resistance.  $I_{Sh}$  is current through effective shunt resistance  $R_{Sh}$  and can be expressed as in equation 3.3:

$$I_{Sh} = (V + I \cdot R_S) / R_{Sh} \quad (3.3)$$

Here  $V$  is the terminal voltage of PV cell. Thus, the equation of output current of photovoltaic cell using equations 3.1 to 3.3 can be written as in equation 3.4:

$$I = I_L - I_0 \left( e^{q \cdot \frac{V + I \cdot R_S}{K} \cdot T} - 1 \right) - (V + I \cdot R_S) / R_{Sh} \quad (3.4)$$

Equation 3.4. is used to plot the characteristics of a PV cell. There are two important characteristics of a PV cell, one is I-V characteristic between output current and output voltage and other is P-V characteristics between output power and output voltage.

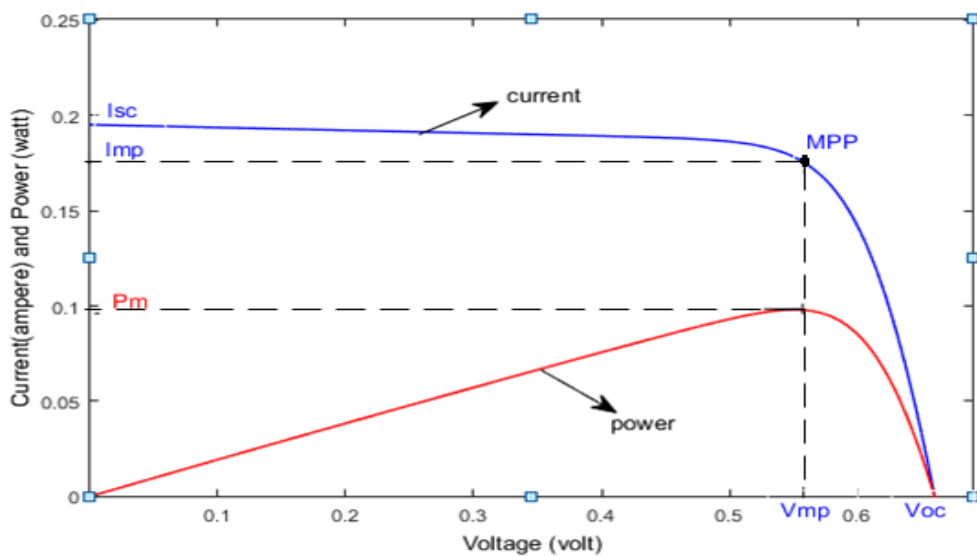
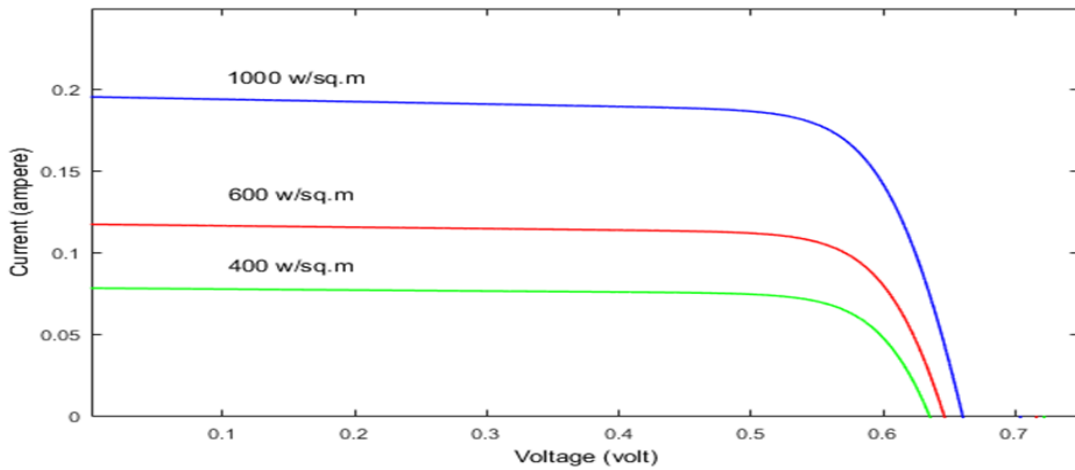


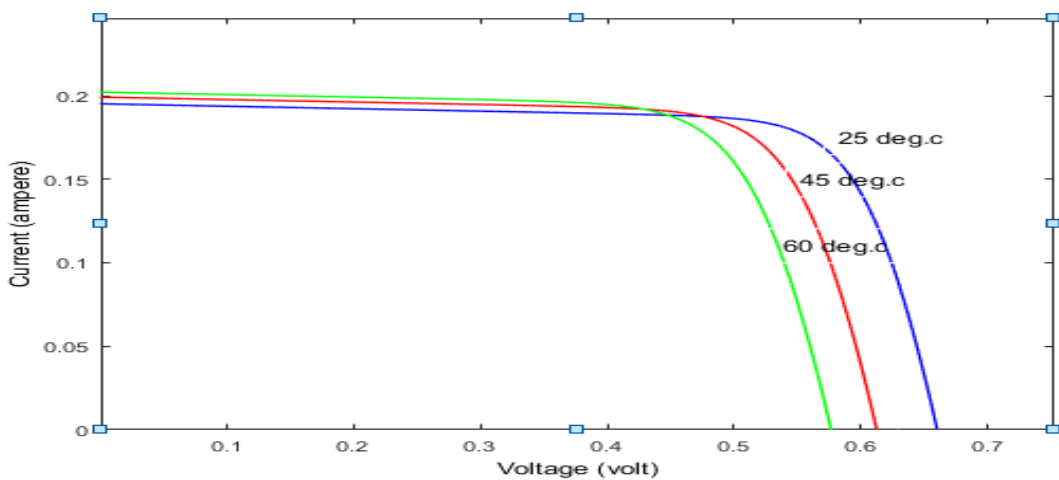
Figure 3-4. I-V and P-V characteristic of PV cell

Figure 3.4 shows the I-V and P-V characteristics of a PV cell. In the figure 3.4,  $I_{SC}$  is short circuit current,  $V_{OC}$  is open circuit voltage,  $V_{mp}$  is maximum power voltage,  $I_{mp}$  is maximum power current and  $P_m$  is maximum power.

The output of a PV cell depends upon the available solar irradiance ( $W/m^2$ ) and temperature ( $^{\circ}C$ ) of the cell itself. Figure 3.5 and 3.6 illustrates the dependence of I-V characteristics on solar irradiation and temperature respectively. With increase in solar irradiance,  $I_{SC}$  increases and there is a slight increase in  $V_{OC}$  and thus output power increase. With increase in temperature,  $V_{OC}$  decreases and there is a slight increase in  $I_{SC}$  thus the power output decreases.



**Figure 3-5. I-V characteristic of PV cell at different solar irradiance**



**Figure 3-6. I-V characteristic of PV cell at different temperature**

### 3.4 Concept of Maximum Power Point Tracking in Photovoltaic System

It can be observed in figure 3.4 that the output power of a photovoltaic cell is maximum when the output current equals  $I_{mp}$  and output voltage is  $V_{mp}$ , this operating point is called maximum power point (MPP). The maximum output power ( $P_m$ ) of a PV cell at MPP is given by equation 3.5:

$$P_m = V_{mp} \cdot I_{mp} \quad (3.5)$$

Since the I-V and P-V characteristics of PV vary with solar irradiation and temperature, the MPP of PV will also vary. If a load is connected directly across a PV, the operating point will depend on the load impedance and environmental conditions and may not always be at MPP thus underutilizing PV capacity. MPPT techniques are developed to ensure maximum utilization of PV capacity. In MPPT objective is to keep the operating point of PV at its MPP when a variable load is connected irrespective of changes in environmental conditions. In MPPT PV is interfaced to the load through a DC-DC converter. The operating point of PV is controlled by adjusting the duty cycle of DC-DC converter as shown in figure 3.7.

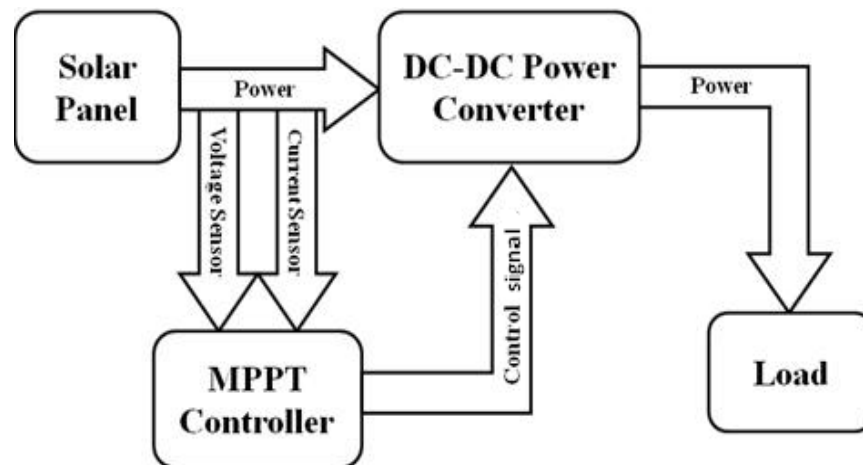


Figure 3-7. Concept of MPPT in PV system

The MPPT in a PV system can be implemented using different dc-dc converters like buck converter, boost converter, buck-boost converter etc. Several MPPT algorithms have been developed to control the duty cycle of these dc-dc converters, some examples of the MPPT algorithms are listed below:

- (i) Perturb and Observe (P&O)
- (ii) Incremental Conductance (INC)

- (iii) Fuzzy logic Control
- (iv) Neural Network

There are many more MPPT techniques developed so far which are not mentioned in the above list. However, ‘Perturb and Observe’ and ‘Incremental conductance’ algorithms are popular conventional techniques widely used whereas as neural networks and fuzzy logic control are advanced soft computing techniques developed for MPPT in PV system [8-10].

### 3.5 MPPT in Photovoltaic System Using Boost converter

As explained in the previous section that application of MPPT in PV system is necessary to improve efficiency. This section explains the design of boost converter for MPPT in PV system and application of two conventional MPPT algorithms ‘Perturb and Observe’ and ‘Incremental Conductance’.

#### 3.5.1 System Configuration

Figure 3.8 gives the description of the developed PV system. PV system consists of a PV panel interfaced to resistive load through a boost converter. The output voltage and current of photovoltaic panel are measured with help of sensors and given as input to the microcontroller. Microcontroller is programmed with P&O algorithm to control the duty cycle for boost converter for implementing MPPT in the PV system.

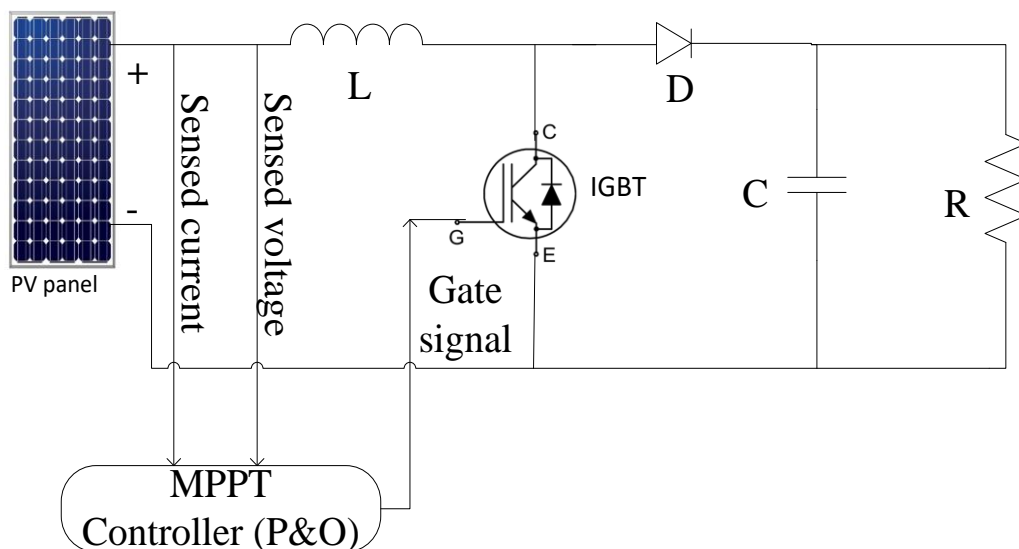


**Figure 3-8. System configuration for MPPT in photovoltaic system using boost converter**

Table 3.1 shows the rating of PV panel at standard test condition (STC). A 50  $\Omega$ , 5 amperes variable resistor (rheostat) is used as a load.

**Table 3-1. Specification of PV panel used for MPPT in photovoltaic system using boost converter**

Maximum PV Power ( $P_{mpp}$ )	100 W
Voltage at max power ( $V_{mpp}$ )	17.70 V
Current at max Power ( $I_{mpp}$ )	5.70 A
Open circuit PV voltage ( $V_{oc}$ )	21.4 V
Short circuit PV current ( $I_{sc}$ )	6.30 A
Temperature coefficient of $V_{oc}$ (% per $^{\circ}\text{C}$ )	-0.36099
Temperature coefficient of $I_{sc}$ (% per $^{\circ}\text{C}$ )	0.102

### 3.5.2 Boost Converter Design

The boost converter design depends on the ratings of the PV panel used, connected load, acceptable limits in output voltage ripple and input current ripple. The boost converter consists of an inductor, power electronic switch (MOSFET/IGBT), diode and a capacitor as shown in figure 3.8. The power electronic switch (MOSFET/IGBT) and diode are selected based on voltage level, current and switching frequency at which they have to operate in the circuit. The design of inductor and capacitor used in boost converter are explained below:

#### i) Inductor design

Inductance of the boost converter is designed to ensure operation in continuous current mode. The ripple in the input current ' $\Delta I$ ' is given by equation 3.6 [11]:

$$\Delta I = (V_{in} * D) / (2 * L * F_s) \quad (3.6)$$

$\Delta I$  is restricted to be less than 5% of input current.  $D$  is duty cycle of the boost converter,  $F_s$  is switching frequency,  $V_{in}$  is the input voltage to boost converter (at MPP). With  $\Delta I = 0.3$  A,  $D = 0.5$ ,  $V_{in} = 17.70$  V,  $F_s = 20$  KHz the calculated value of inductance is  $L = 0.74$  mH. To ensure safe operation, a higher value of  $L = 1$  mH is selected.

#### ii) Capacitor design

Output capacitor is used to minimize the output voltage ripple ' $\Delta V$ '.  $\Delta V$  is given by equation 3.7 [11]:

$$\Delta V / V_o = D / (R * F_s * C) \quad (3.7)$$

$V_o$  is the output voltage,  $\Delta V/V_o$  is restricted to be = 0.05,  $R = 20 \Omega$  (minimum load resistance), taking  $D = 0.5$ ,  $F_s = 20\text{KHz}$ , calculated values of capacitor is  $C = 25\mu\text{F}$ . To ensure safe operation, a higher value of  $C = 33\mu\text{F}$  is used.

### 3.5.3 Conventional Algorithms for MPPT

‘Perturb and Observe(P&O)’ and ‘Incremental Conductance (INC)’ are two most widely used algorithms. The application of these algorithms for MPPT using boost converter is explained below:

#### i) Perturb and Observe (P&O) Algorithm:

P&O algorithm is one of the most popular and simple MPPT algorithm. In P&O algorithm the duty cycle of boost converter is changed in small steps and changes in PV terminal voltage and current are sensed, and corresponding change in output power is calculated. It can be observed from the P-V characteristics in figure 3.4 that on the left side of MPP,  $dP/dV$  is positive and on the right side of MPP,  $dP/dV$  is negative and at MPP,  $dP/dV = 0$ . Based on these observations the flowchart for P&O algorithm is developed and is shown in Figure 3.9. [7].

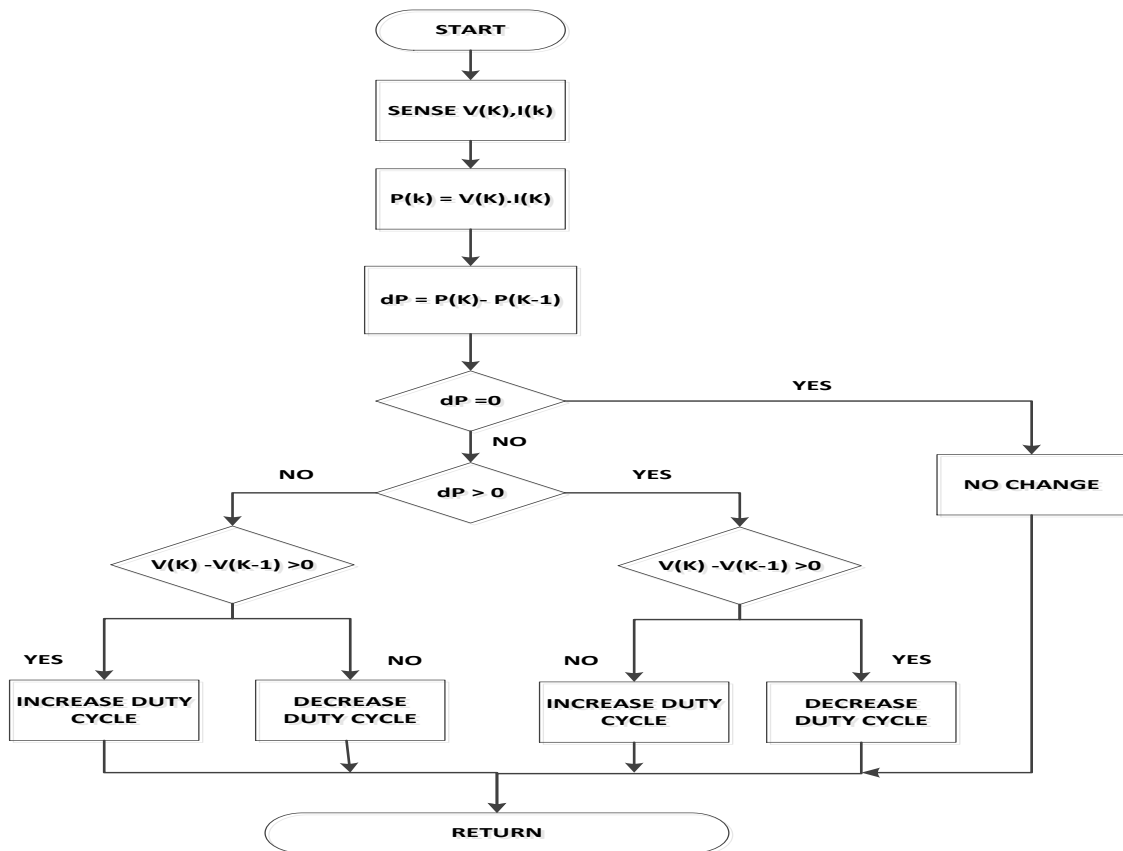


**Figure 3-9. Flowchart of P&O algorithm for MPPT in photovoltaic system using boost converter**

ii) Incremental Conductance (INC) Algorithm:

Incremental conductance (INC) is another conventional and popular MPPT technique. The mathematical background for INC algorithm is explained below [34]:

Equation 3.8 gives the output power equation of a PV, Equation 3.8 is partially differentiated with respect to voltage to obtain equation 3.9 which is simplified to obtain equation 3.10.

$$P = V \cdot I \quad (3.8)$$

$$\frac{\partial P}{\partial V} = \partial(V \cdot I) / \partial V \quad (3.9)$$

$$\frac{\partial P}{\partial V} = I + V \cdot \partial I / \partial V \quad (3.10)$$

For maximum power output from PV,  $\frac{\partial P}{\partial V} = 0$  has to be satisfied, therefore from equation 3.10 we get;

$$\frac{\partial I}{\partial V} = -I/V, \text{ at MPP} \quad (3.11)$$

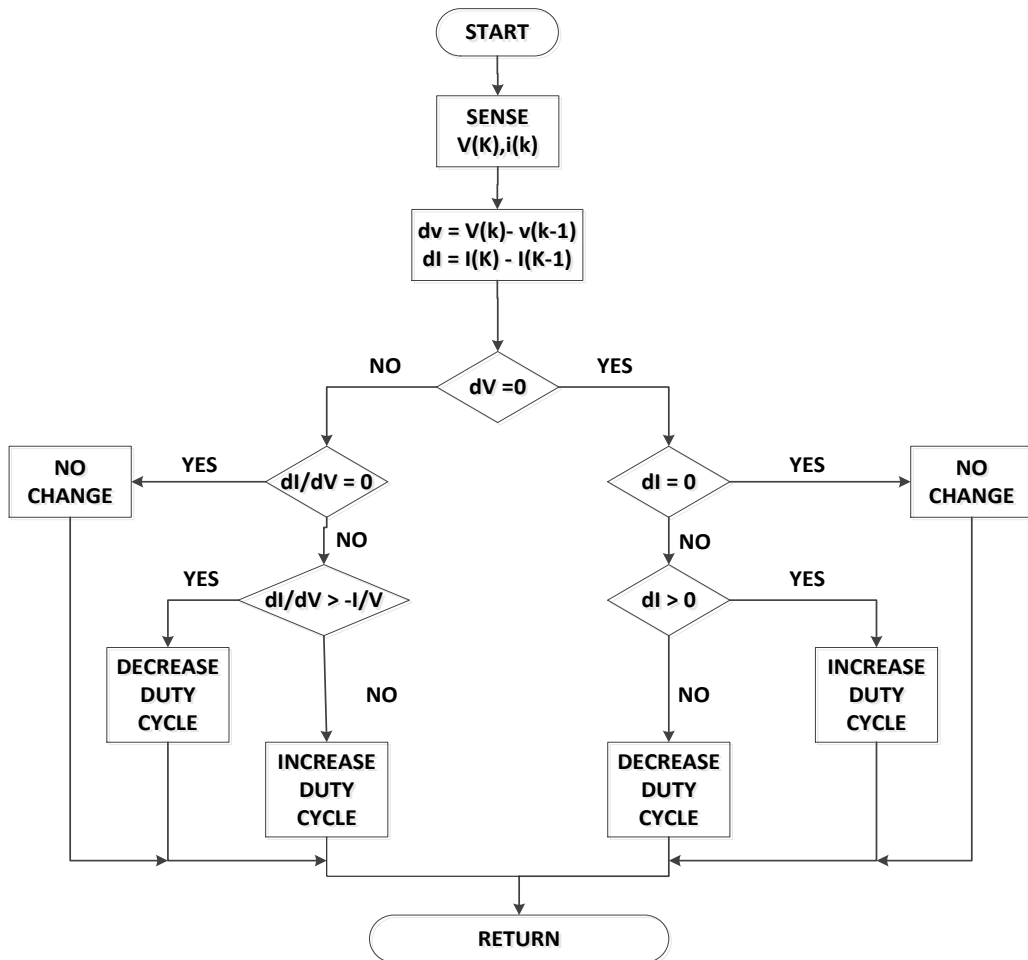


Figure 3-10 Flowchart for Incremental conductance algorithm for MPPT in photovoltaic system using boost converter



Equation 3.11 gives the condition for MPPT. It can be seen in I-V characteristics in figure 3.4, that slope of I-V characteristics is less negative in left side of the MPP point ( $V < V_{mpp}$ ) and it is more negative in right of MPP point ( $V > V_{mpp}$ ) when compared to slope at MPP ( $V = V_{mpp}$ ). This observation can be written in form of equation 3.12 and 3.13 given below:

$$\frac{\partial I}{\partial V} > -I/V, \text{ left of MPP} \quad (3.12)$$

$$\frac{\partial I}{\partial V} < -I/V, \text{ right of MPP} \quad (3.13)$$

Equations 3.11 to 3.13 forms the foundation of INC algorithm. The switching cycle of boost converter is controlled such that the condition  $\frac{\partial I}{\partial V} = -I/V$  is satisfied. The Flow chart of INC algorithm is shown in figure 3.10 [7].

### 3.6 MATLAB Simulation Results for MPPT in Photovoltaic System Using Boost Converter

A MATLAB-SIMULINK model for MPPT using boost converter in PV system designed in previous section is developed shown in figure 3.11. The specifications of the MATLAB-SIMULINK model for MPPT in photovoltaic system using boost converter is given in table 3.2. The duty cycle of boost converter is controlled using P&O algorithm. The simulation results are obtained for three different cases mentioned below:

- i) Results for MPPT under dynamic solar irradiance condition
- ii) Results for MPPT under dynamic temperature condition
- iii) Results for MPPT under dynamic load condition

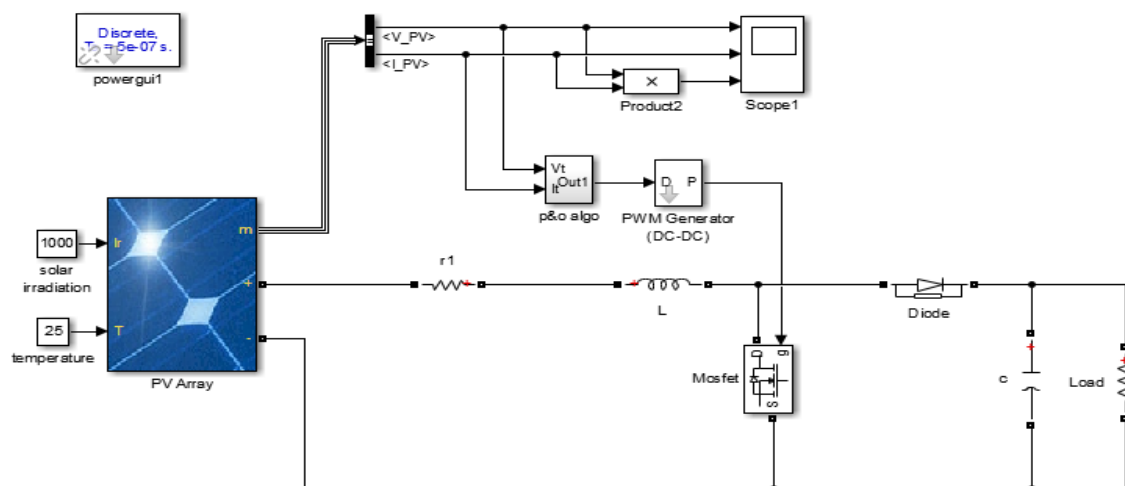


**Figure 3-11 MATLAB model for MPPT in Photovoltaic system using boost converter**

**Table 3-2. Specification of MATLAB model for MPPT in photovoltaic system using boost converter**

Maximum PV Power	100 W
<u>Boost Converter</u>	
Inductor (L)	1 mH
Capacitor (C)	33 $\mu$ F
Switching Frequency ( $F_s$ ) for Boost Converter	20 KHz
Load	Resistive (30 $\Omega$ /15 $\Omega$ )
MPPT Algorithm	P&O Algorithm

### 3.6.1 Simulation Results for MPPT Under Dynamic Solar Irradiance Condition

Figure 3.12 shows simulation results obtained for dynamic solar irradiance conditions. The results include PV voltage and current, load voltage and current, solar irradiance, temperature, duty cycle and PV power. Initially the conditions are standard with solar irradiance equal to 1000 w/m<sup>2</sup> and temperature equal to 25°C and load connected at output is 30  $\Omega$ . The output power of the PV is 100 watts which is the maximum output under standard conditions with PV voltage equal to 17.7 volts, PV current equal to 5.7 ampere, load voltage is about 53 volts and load currents is 1.75 ampere. The duty ratio of the boost converter is stable at value 0.675. Thus it can be concluded that the system is stable and operating at maximum power under standard condition and designed MPPT system is working fine under static condition of load, solar irradiance and temperature. At time 0.15 seconds there is a gradual dip in solar irradiance which reduces up to 750 w/m<sup>2</sup> at 0.2 seconds. As we know already that with reduction of solar irradiance the maximum output of the PV will reduce, and it will be equal to 75 watts at solar irradiance of 750 w/m<sup>2</sup>. It can be observed that duty cycle of boost converter reduces in steps until reaching a stable value at which PV track maximum power of 75 watts and then remain stable. It can be seen in the result (figure 3.12) that with dip in solar irradiance there is a dip in PV current and PV voltage almost remains same. At time 0.35 seconds solar irradiance gradually rises to 1000 w/m<sup>2</sup> at 0.5 seconds. The duty cycle of boost converter increases in steps up to 0.675 and becomes stable at which PV again tracks maximum power equal to 100 watts which is the maximum output under standard conditions with PV voltage equal to 17.7 volts, PV current equal to 5.7 ampere, load voltage is about 53 volts and load currents is 1.75 ampere. Thus, it can be concluded that designed MPPT system is working fine and

is stable under dynamic solar irradiance and tracks the maximum power corresponding to the available solar irradiance.

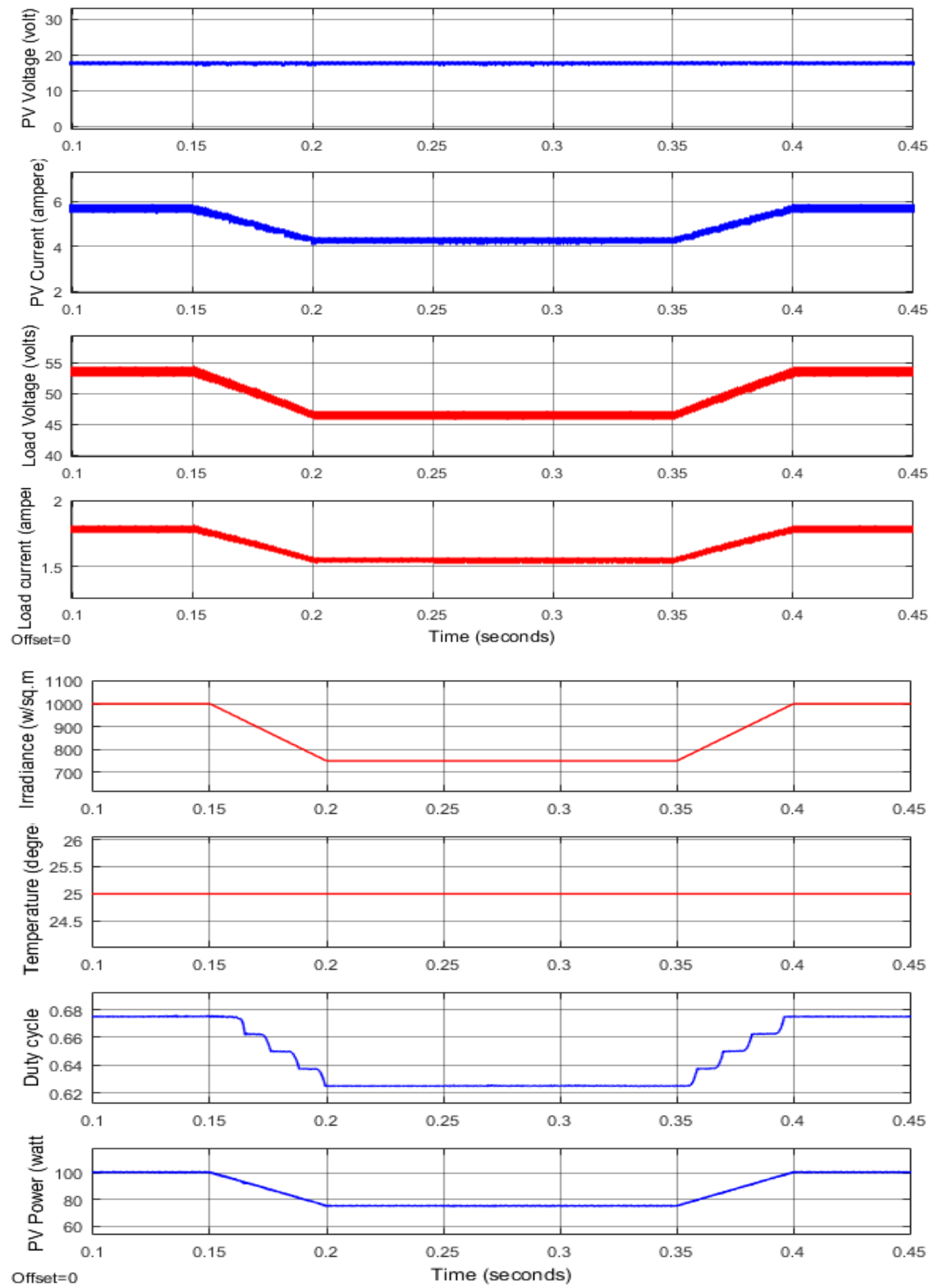


**Figure 3-12 Simulation results for MPPT under dynamic solar irradiance condition**

### 3.6.2 Simulation Results for MPPT Under Dynamic Temperature Condition

Figure 3.13 shows simulation results obtained for dynamic temperature conditions. The results include PV voltage and current, load voltage and current, solar irradiance, temperature, duty cycle and PV power. Initially the conditions are standard with solar irradiance equal to  $1000 \text{ w/m}^2$  and temperature equal to  $25^\circ\text{C}$  and load connected at output is  $30 \Omega$ . The output power of the PV is 100 watts which is the maximum output under standard conditions.

At time 0.15 seconds temperature starts gradually increasing up to  $40^\circ\text{C}$  at 0.2 seconds. As we know already that with increase in ambient temperature the maximum output of the PV will reduce, and it will be equal to 95 watts at  $40^\circ\text{C}$  temperature. It can be observed that duty cycle of boost converter increases and stabilizes at a higher value at which PV track maximum power of 95 watts at  $40^\circ\text{C}$ . It is noticed that there is one volt drop in PV voltage and minimal drop in PV current. It can be seen in the result (figure 3.13) that there is a logarithmic drop in voltage with increasing temperature and there is a small drop in maximum PV output power at higher temperature with current approximately remaining unchanged.

At 0.35 second the temperature gradually rises to  $25^\circ\text{C}$  at 0.4 second. The duty ratio of boost converter drops and becomes stable at 0.675. The PV starts tracking maximum power equal to 100 watts which is the maximum output under standard conditions with PV voltage equal to 17.7 volts, PV current equal to 5.7 ampere, load voltage is about 53 volts and load currents is 1.75 ampere. Thus, it can be concluded that designed MPPT system is working fine and is stable under dynamic temperature and tracks the maximum power corresponding to the ambient temperature.

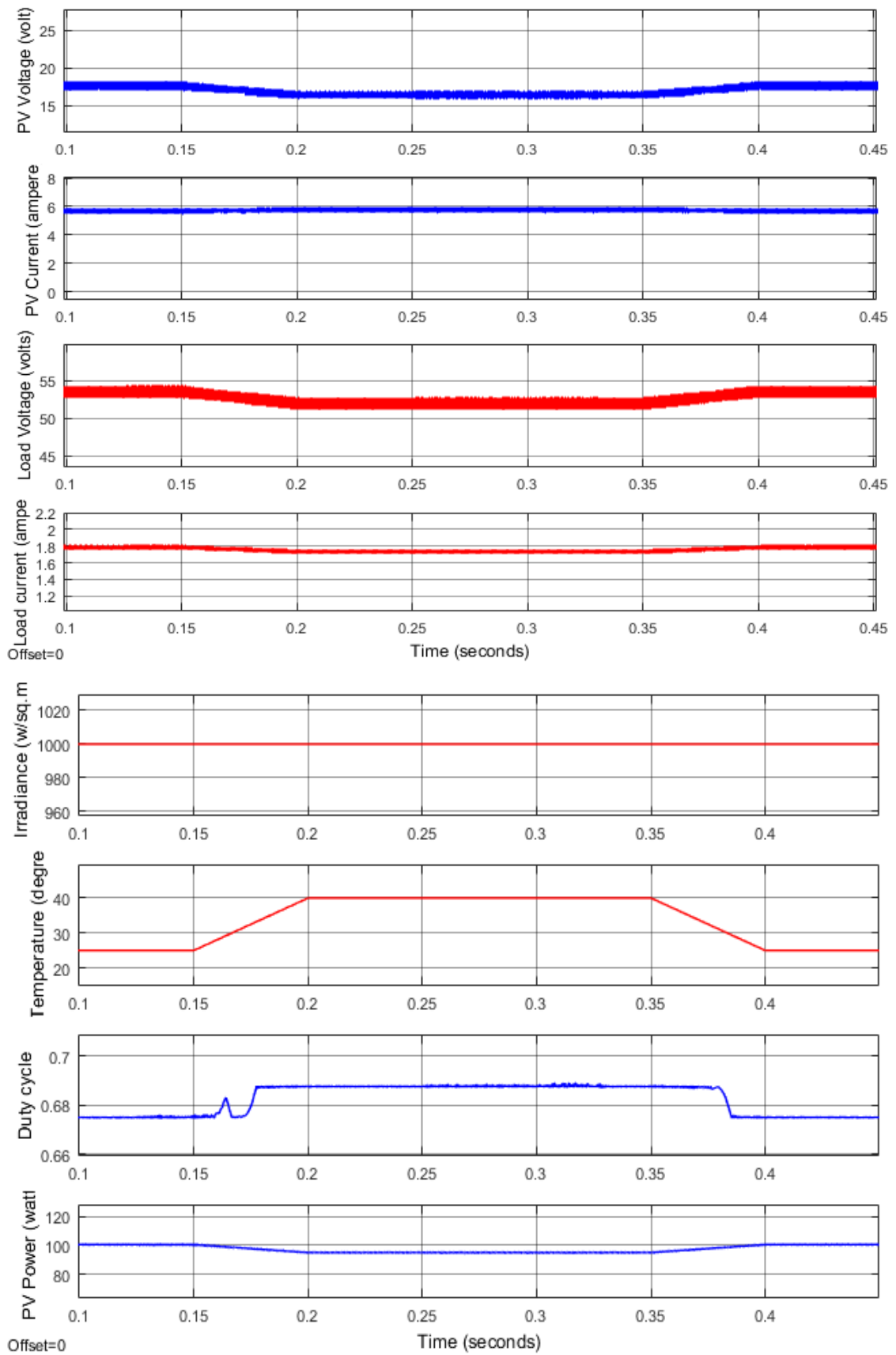


**Figure 3-13. Simulation results for MPPT under dynamic temperature condition**

### **3.6.3 Simulation Results for MPPT Under Dynamic Load Condition**

Figure 3.14 shows simulation results obtained for dynamic load conditions. The results include PV voltage and current, load voltage and current, solar irradiance, temperature, duty cycle and PV power. Initially the conditions are standard with solar irradiance equal to  $1000 \text{ w/m}^2$  and temperature equal to  $25^\circ\text{C}$  and load connected at output is  $30 \Omega$ . The output power of the PV is 100 watts which is the maximum output under standard conditions.

At time 0.15 seconds another  $30 \Omega$  load is switched in parallel to the existing  $30 \Omega$  load making equivalent load of  $15 \Omega$ . As we know, that changes in load does not affect maximum output of PV and MPPT system must continue to track 100 watts even after change in load. It can be seen in result (figure 3.14) that there are small transients in the PV voltage and current which settles quickly with no change in PV voltage, current and output power. The duty ratio of boost converter changes to help PV system in tracking maximum PV power equal to 100 watts. It is noticed that there is no change in PV voltage, current and Power with change in connected load and system continues to track maximum power. Thus, it can be concluded that the MPPT system is working fine and is stable under dynamic load conditions.

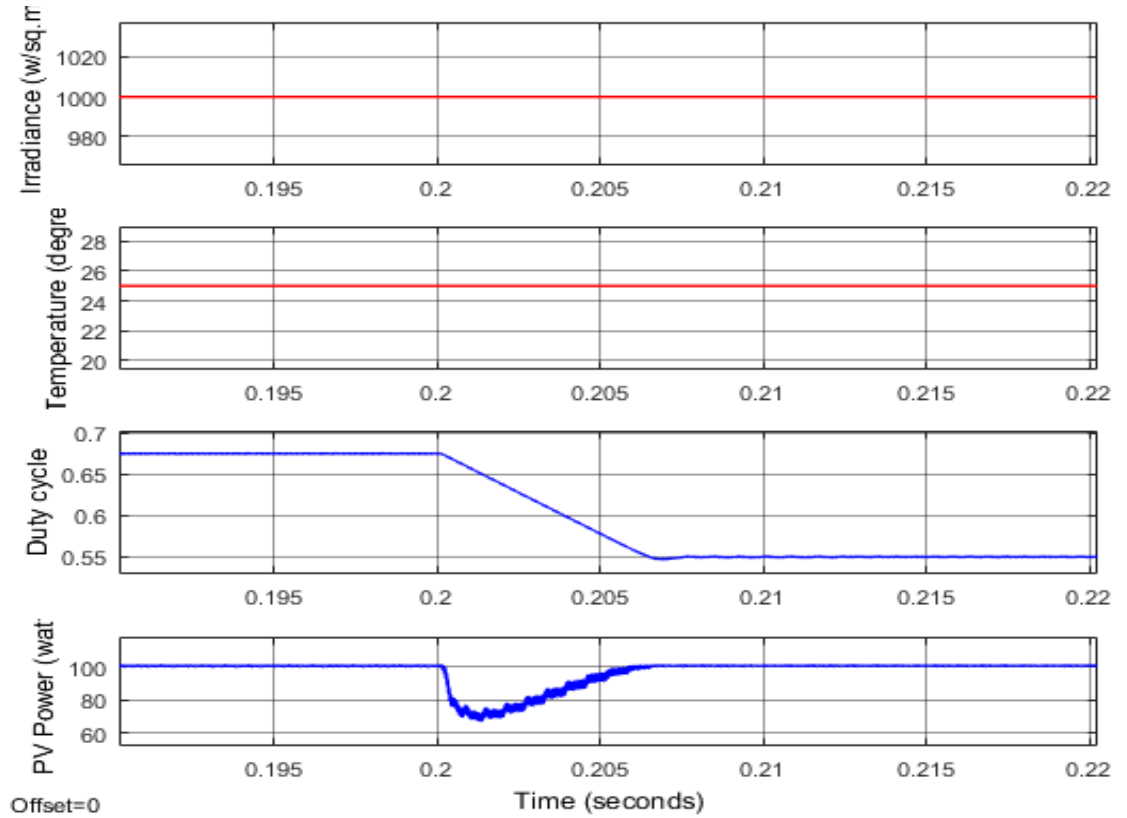
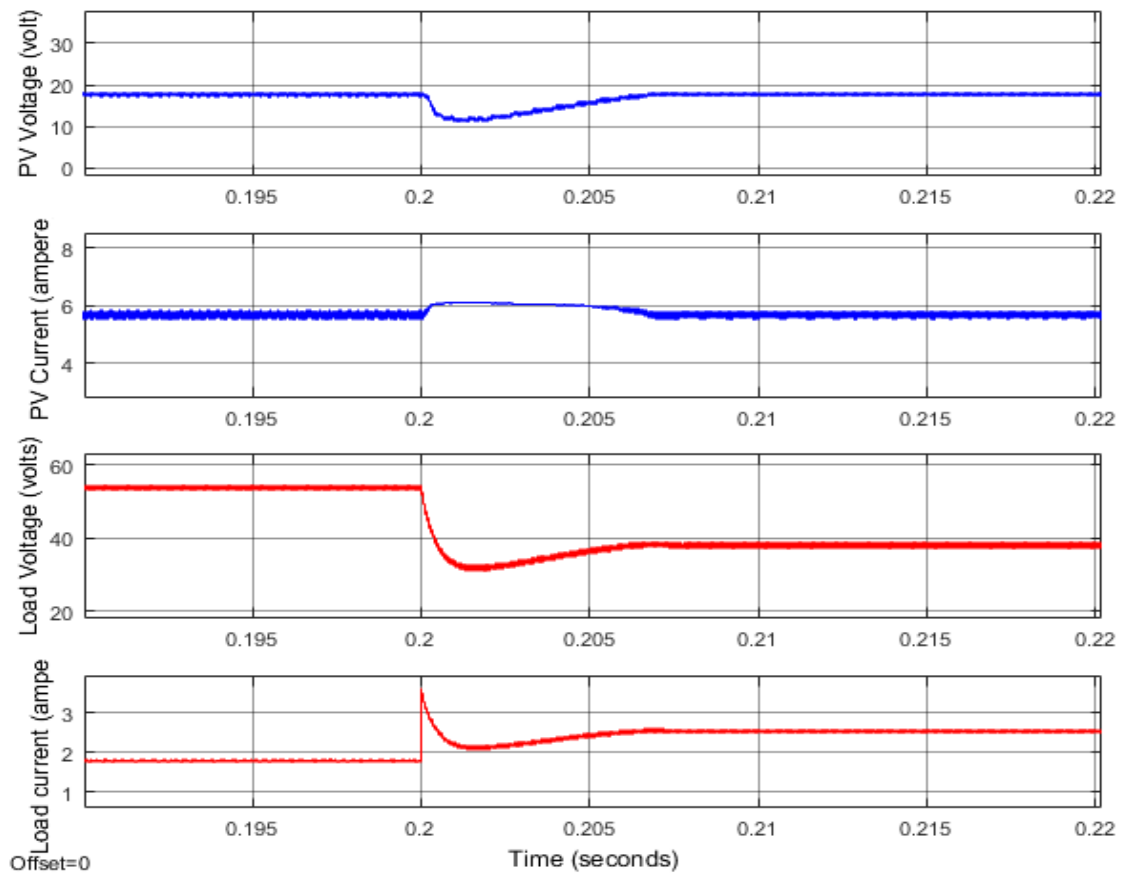


**Figure 3-14. Simulation results for MPPT under dynamic load condition**

### 3.7 Hardware Implementation of MPPT in Photovoltaic System Using Boost Converter

A hardware model for MPPT in photovoltaic system using boost converter is developed and presented in this section. Figure 3.15 shows a hardware model of the system is developed for MPPT in photovoltaic using boost converter [12-14].

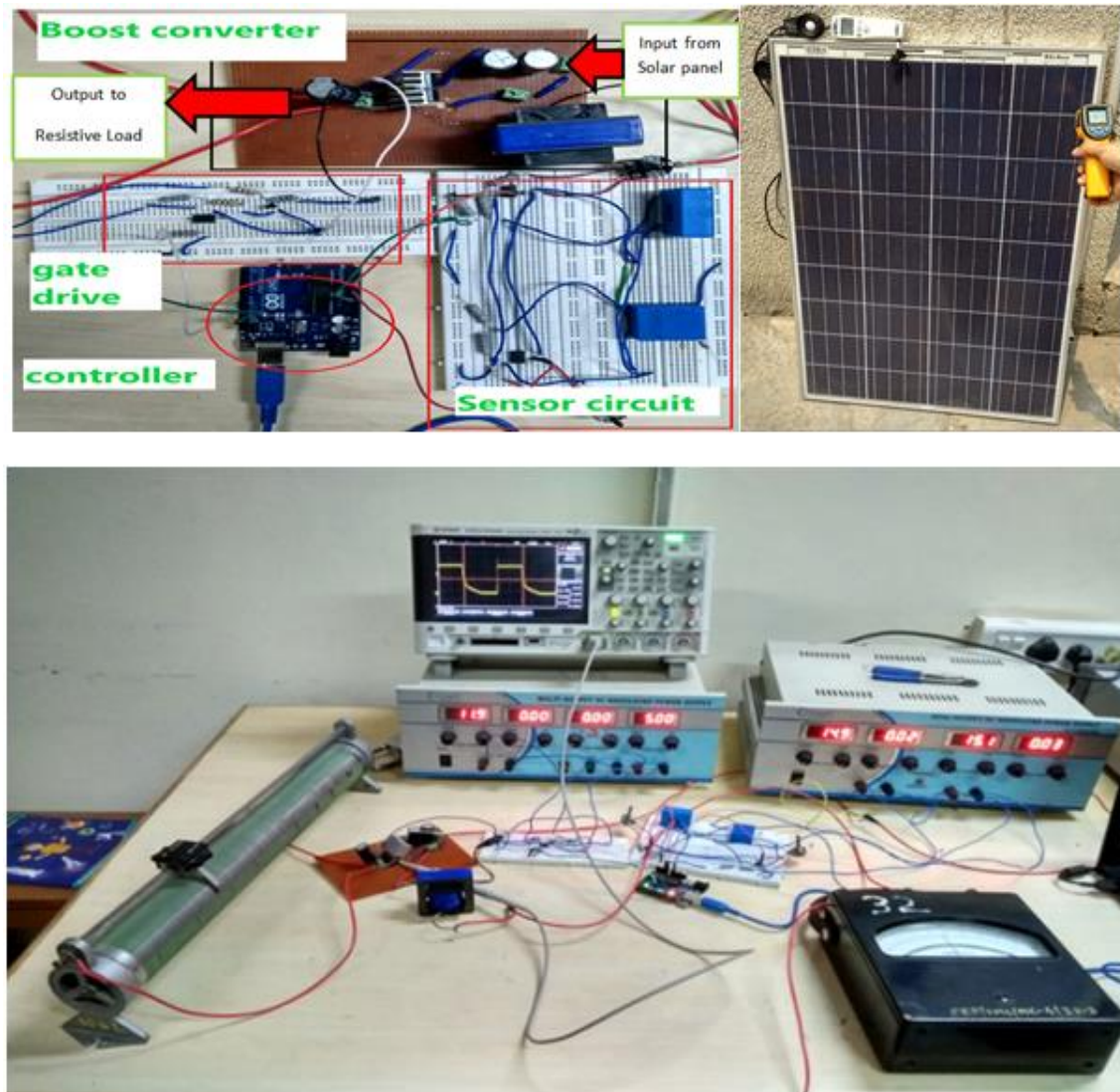


**Figure 3-15. Hardware Setup for MPPT in photovoltaic system using boost converter**

The hardware model is developed for the system designed and simulated in the previous section. The system is tested with ‘Perturb and Observe’ MPPT algorithm under varying solar irradiance, temperature and different loads for its ability to track maximum power from PV. Table 3.3 gives the system specifications for hardware model developed.



**Table 3-3. Specifications of Hardware Model for MPPT in Photovoltaic system using boost converter**

PV Panel Peak Output Power	100 W
Inductor (L)	1 mH , 6 A
Capacitor (C)	33 $\mu$ F, 100 V
Switching Frequency ( $F_s$ )	20 KHz
Power electronic Switch	FGL40N120AND (IGBT)
Voltage sensor	LV25-P
Current sensor	LA25-P
Load	50 $\Omega$ rheostat, 5 A
Controller	Arduino Uno

### 3.7.1 Gate Driver Circuit

Gate driver circuit shown in figure 3.16 is required to switch the IGBT switch in the boost converter. The selected IGBT is FGL40N120AND, its ratings are  $V_{CES} = 1200V$ ,  $V_{GES} = 25V$ ,  $I_C = 50A$ . The PWM signal generated by controller is given to the IGBT through the gate driver circuit. The gate drive circuit consist of an optocoupler (6N317) followed by BJT used as a switch. Optocoupler is used to isolate the controller from power circuit and BJT is used in switching mode to provide high and low voltage to gate of the IGBT for turn off/on operation.

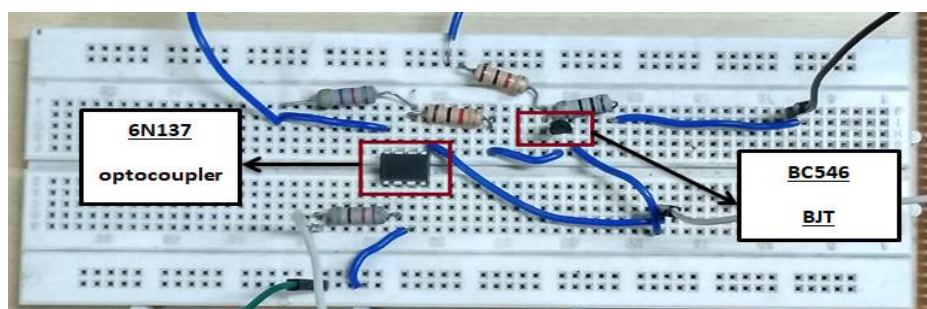


**Figure 3-16. Gate Driver Circuit**

### 3.7.2 Sensor Circuit

Sensor circuit shown in figure 3.17 is used to sense output voltage and current of PV panel. Sensor circuit consist of LV25-P (voltage sensor) and LA25-P (current sensor). A signal amplifier with adjustable gain is used for both voltage and current transducer to

limit output voltage less than 5 volts. Signal amplifier is build using OP07C (operational amplifier), the gain is adjusted using variable pot resistance.

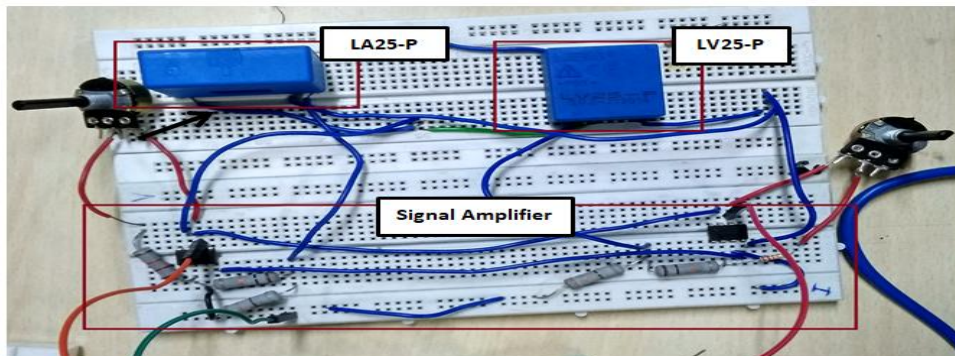


**Figure 3-17. Sensor Circuit**

### 3.7.3 Controller

Arduino Uno a microcontroller board (ATmega328) shown in figure 3.18 is used for MPPT control. Output from voltage and current sensor are given to the analog input of the microcontroller. Microcontroller is programmed with P&O algorithm. It senses the PV panel voltage and current and generates a 20 kHz PWM signal with required duty cycle at its output pin which is given to gate driver circuit.

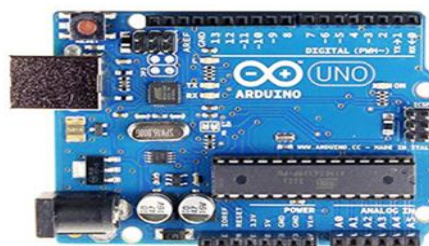


**Figure 3-18. Arduino Uno**

### 3.7.4 Hardware Results for MPPT

Table 3.3 shows results of the system without MPPT, that is when the PV panel is directly connected across the load. The value of solar irradiance is  $670 \text{ w/m}^2$  and temperature is  $45^\circ\text{C}$  The PV voltage and current are noted for three different loads  $40\Omega$ ,  $30\Omega$ ,  $20\Omega$  respectively and output power of PV is calculated. The simulation results are also presented in the table for comparison. The results show that PV power output is very less ( $<15$  watts) and varies with change in load when connected directly to load without MPPT.

Table 3.4 shows results of the system with MPPT. First set of reading gives PV voltage, current and power at solar irradiance  $600 \text{ w/m}^2$  and temperature  $36^\circ\text{C}$  for three different loads  $40\Omega$ ,  $30\Omega$ ,  $20\Omega$  respectively. The power output of PV remains close to about 50

watts irrespective of the changes in load which is much higher when compared to power output obtained without MPPT application.

The second set of reading gives PV voltage, current and power at solar irradiance 500 w/m<sup>2</sup> and temperature 40 °C for three different loads 40Ω, 30Ω, 20Ω respectively. The power output of PV remains close to about 42 watts irrespective of the changes in load. It can be inferred from the results that with application of MPPT system the output power of PV remains close to its maximum power and does not vary with changes in load unlike the case when MPPT is not used. The results show that PV output power decreases with decrease in solar irradiation and increase in temperature. The hardware results obtained are comparable to the simulation results with reasonable differences.

**Table 3-3. Results for photovoltaic system without MPPT**

			Hardware result				Simulation result		
	Solar Irradiation (W/m <sup>2</sup> )	Temperature (°C)	Load (Ω)	Voltage (V)	Current (A)	Output Power (W)	Voltage (V)	Current (A)	Output Power (W)
1.	670	45	40	19.5	0.4	7.8	19.27	0.47	9.06
2.			30	19.4	0.5	9.6	19.2	0.62	11.9
3.			20	19.2	0.8	15.36	19.07	0.91	17.3

**Table 3-4. Results for MPPT in photovoltaic system using boost converter**

			Hardware result				Simulation result		
	Solar Irradiation (w/m <sup>2</sup> )	Temperature (°C)	Load (Ω)	Voltage (V)	Current (A)	Output Power (W)	Voltage (V)	Current (A)	Output Power (W)
1.	600	36	40	17.6	2.8	49.28	17.15	3.35	57.5
2.			30	17.4	2.9	50.46	17.15	3.35	57.5
3.			20	17.3	3.1	53.63	17.15	3.35	57.5
1.	500	40	40	17.2	2.4	41.28	16.7	2.8	47
2.			30	17	2.5	42.5	16.7	2.8	47
3.			20	16.9	2.6	43.94	16.7	2.8	47

### **3.8 Conclusion**

In this chapter equivalent electrical model of a PV cell and its characteristics are discussed. The concept of maximum power point tracking is explained. MPPT in photovoltaic system using boost converter is discussed, which includes design of boost converter for MPPT in PV system, and application of conventional MPPT techniques.

A MATLAB-SIMULINK model for MPPT in photovoltaic system using boost converter is developed and its performance under dynamic solar irradiance, temperature and load conditions is studied. A Hardware model for the system is also developed and is tested under varying solar irradiance, temperature and load conditions. The hardware results and simulation results are compared for analysing the performance of hardware developed. It is found that developed hardware is performing satisfactorily and is able to track maximum power in PV and hence increasing efficiency of the system under varying load, solar irradiance and temperature condition.

## CHAPTER 4 GRID CONNECTED TWO-STAGE PV SYSTEM

### 4.1 General

In this chapter design and development of a grid connected two-stage system is discussed. A MATLAB-SIMULINK model for the system is developed and its performance to integrate power from photovoltaic into grid and simultaneously act on current related power quality issues is analysed for different control techniques under varying solar input and different load conditions.

### 4.2 Grid Connected Two-Stage PV System

Grid connected two-stage PV system are capable of transferring PV power to the grid and can also serve functions of a DSTATCOM to mitigate current related power quality issues like load reactive power compensation, load unbalance compensation, load harmonic compensation [27,28]. Figure 4.1 shows a basic block diagram of a grid connected two-stage PV system. It consists of a boost converter as its first stage and a Voltage Source Inverter (VSI) as its second stage.

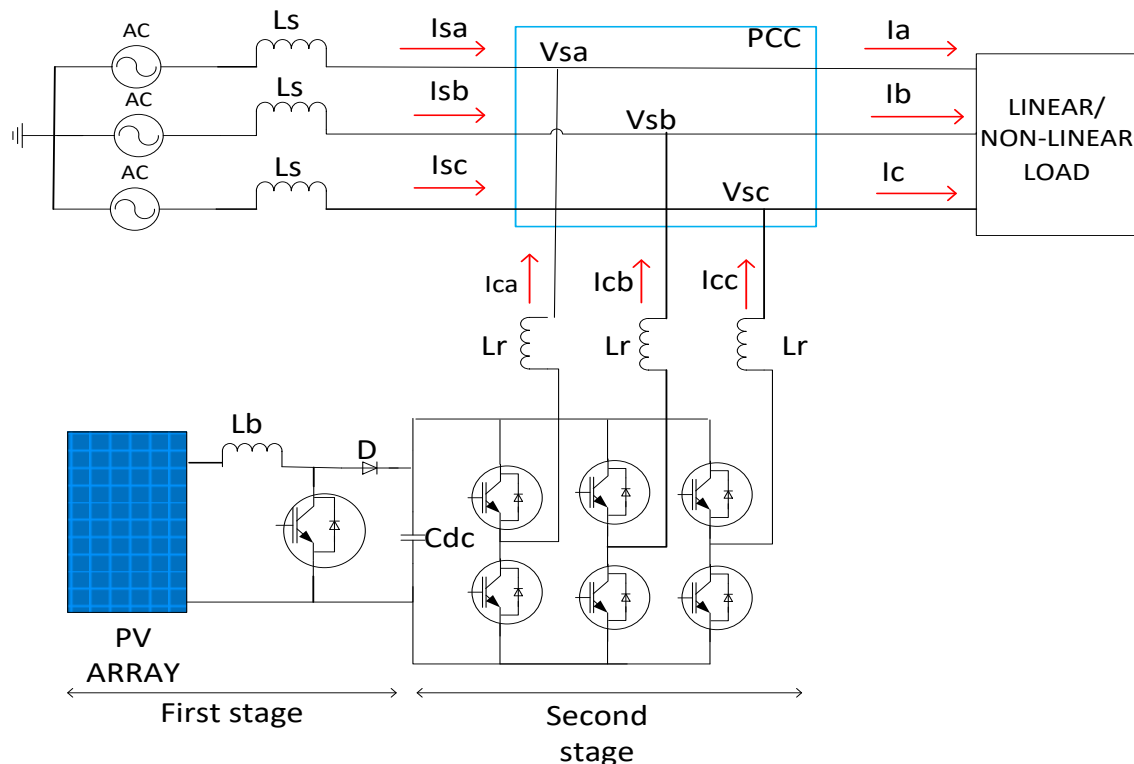


**Figure 4-1. Grid connected two-stage PV system**

The boost converter stage performs function of Maximum Power Point Tracking (MPPT) in PV array. Different MPPT algorithms like Perturb and Observe, Incremental Conductance, fractional voltage, fractional current, fuzzy logic control MPPT, neural network control MPPT can be used to control switching of boost converter. The boost converter extracts maximum possible power from PV array and feeds it into dc-link capacitor ' $C_{dc}$ ' which forms an interface between boost converter and VSI. The VSI converts dc power from boost converter into ac (alternating current) and injects it into the grid. As seen in figure 4.1, VSI is connected in parallel to the grid, VSI is controlled as a current source which can injects current in the grid such that it compensate load reactive power, load unbalance, load harmonics and also inject PV power into grid. Thus, in addition to transfer of PV power to the grid VSI also serves functions of a DSTATCOM. There are several control techniques available for DSTATCOM which are also applicable for VSI control in grid connected two-stage PV like Instantaneous reactive power theory (IRPT), Synchronous reference frame theory (SRF), Power balance theory, Conductance based current algorithm, etc.

### 4.3 Design of Grid Connected Two-Stage PV System

This section gives design of a grid connected two-stage PV system consisting of a PV array of dc capacity equal to 12.789 kW (maximum power) integrated to 3-phase grid at 415 V, 50 Hz.

#### 4.3.1 Specification of PV Array

Table 4.1 gives specifications of PV array used for grid connected two-stage PV system.

**Table 4-1. PV array specification for grid connected two-stage PV system**

Open circuit voltage ( $V_{oc}$ )	726 V
Short circuit current ( $I_{sc}$ )	23.52 A
Voltage at MPP ( $V_{mpp}$ )	580 V
Current at MPP ( $I_{mpp}$ )	22.05 A
Maximum Power ( $P_m$ )	12.789 kW
Temperature coefficient of $V_{oc}$ (% per $^{\circ}C$ )	-0.36099
Temperature coefficient of $I_{sc}$ (% per $^{\circ}C$ )	0.102

MATLAB-SIMULINK has inbuilt PV models which can be used to design PV array of desired capacity and specifications. The PV array modelled has 3 strings in parallel with 20 PV modules (connected in series) in each string.

Figure 4.2 shows I-V and P-V characteristics of the array at two temperatures 25°C and 45°C respectively.

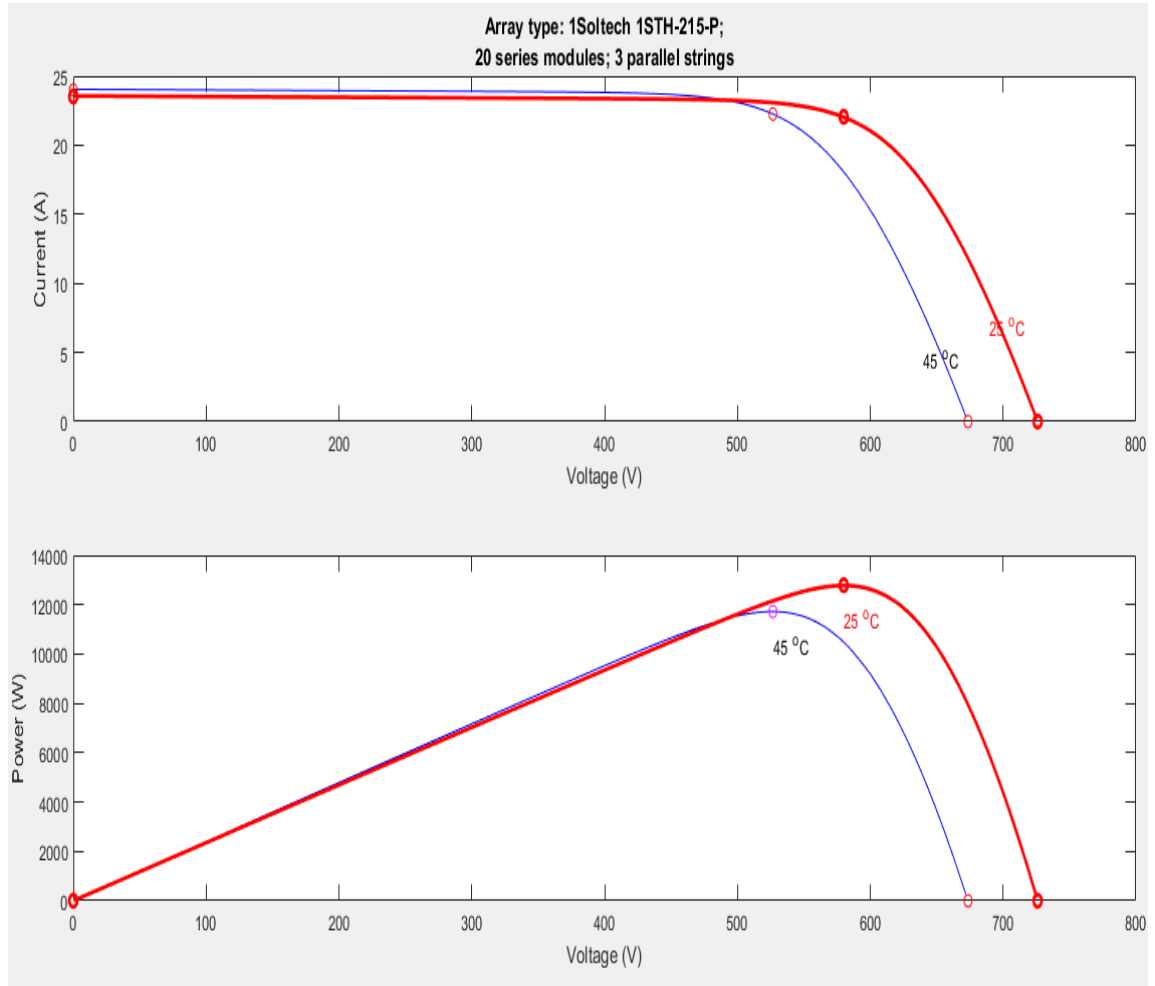


**Figure 4-2. PV array characteristics used for grid connected two-stage system**

#### 4.3.2 Inductor for Boost Converter ( $L_b$ )

The inductor  $L_b$  for boost converter shown in figure 5.1 is designed using the inductor ripple current equation 4.1 [32]:

$$\Delta i_1 = V_{dc} \cdot \frac{D(D-1)}{2 \cdot L_b \cdot F_{sw}} \quad (4.1)$$

In equation 5.1,  $\Delta i_1$  is ripple in current through boost inductor. For this design  $\Delta i_1$  is considered to be 5 percent (at maximum) of the PV array short circuit current (23.52 A) which is equal to 1.176 A.  $F_{sw}$  is switching frequency of boost converter taken to be 20 KHz.  $V_{dc}$  is the dc-link voltage taken as 800 V. D is the duty cycle of boost converter, at  $D = 0.5$  the ripple in current will be maximum therefore in order to get the minimum

value of  $L_b$  that will limit the max ripple current below 1.176 A,  $D$  should be taken equal to 0.5. The calculated value of  $L_b$  from equation 4.1 comes out to be 4.25 mH. The selected value of  $L_b$  is 5 mH.

#### 4.3.3 Selection of Diode and IGBT for Boost Converter

The voltage rating of diode and IGBT switch in boost converter should be selected such that they safely withstand/block dc-link voltage, in our design we have  $V_{dc}$  equal to 800V therefore with safety factor of 1.5 IGBT and diode voltage rating should be 1200 V. The current rating of IGBT and diode should be higher than the maximum PV output current. In our design maximum PV output current is 23.52 A, taking a safety factor of 2 the current rating of both the devices should be higher than 47 A.

#### 4.3.4 Choice of DC-Link Voltage ( $V_{dc}$ )

In order to achieve proper operation of the VSI, the minimum dc-link voltage  $V_{dc}$  should be greater than twice the peak phase voltage on the ac side of the VSI [32].

$$.V_{dc} \geq (2 * \sqrt{2} * V_{LL})/\sqrt{3} \quad (4.2)$$

Here  $V_{LL}$  is ac side line-line voltage = 415 V. The calculated value of the  $V_{dc}$  from equation 4.2 is 680 V, selected value of  $V_{dc}$  is = 800 V.

#### 4.3.5 Sizing of DC-Link Capacitor ( $C_{dc}$ )

The dc-link capacitor is designed using energy conservation principle, the boost converter feeds energy to the dc-link and VSI extracts this energy and feeds it to the grid. The capacitor sizing should ensure a stable dc-link voltage with minimum voltage ripple. The value of dc-link capacitor value can be calculated using equation 4.3 [30]:

$$C_{dc} = I_{mpp}/(2 * \omega * V_{dcripple}) \quad (4.3)$$

Here  $I_{mpp}$  is PV array current at maximum power = 22.05 A ,  $\omega$  is grid frequency = 314 rad/sec,  $V_{dcripple}$  is ripple in dc-link voltage taken to be 16 V ( 2% of  $V_{dc}$  ). The calculated value of  $C_{dc}$  from equation 4.3 comes to be 2.2 mF. The selected value of capacitor is 3 mF.

#### 4.3.6 Interfacing Inductor ( $L_r$ )

Interfacing inductor  $L_r$  shown in figure 4.1 is designed to minimise the ripple in ac side output current of VSI [26]. The basic equation governing dynamics between VSI and PCC is given by equation 4.4:

$$L_r \frac{di_c}{dt} = V_f - V_s \quad (4.4)$$



Here  $V_f$  is the instantaneous inverter pole voltage of any phase and  $V_S$  is the instantaneous PCC voltage of the corresponding phase. The ripple in current through interfacing inductor will be maximum when  $V_S$  is at its peak equal to  $V_{Sm}$ , at this instant the average value of inverter pole can be considered equal to  $1.1 * V_{Sm}$  assuming a 10% voltage drop across interfacing inductor. Thus equation 4.4 can be now modified into equation 4.5:

$$L_r \frac{di_c}{dt} = 1.1V_{Sm} - V_{Sm} \quad (4.5)$$

$$L_r \frac{di_c}{dt} = 0.1V_{Sm} \quad (4.6)$$

In equation 5.6,  $V_{Sm} = 338.84$  V,  $di_c$  is the ripple in inductor current taken to be 0.5 A (at maximum),  $dt$  is the switching time interval taken to be 0.1 ms. The calculated value of  $L_r$  comes out to be 6.8 mH. The selected value of  $L_r$  is 7mH.

#### 4.3.7 Voltage Source Inverter

A 3-phase two level VSI is used as shown in figure 4.1. VSI has three legs, each leg is made of two IGBT switches called the top switch (connected to positive of dc-link) and bottom switch (connected to negative of dc-link) of the leg. The midpoint of each leg is connected to ac output of VSI. IGBT switches have inbuilt reverse conducting diodes. The voltage rating of IGBT switches should be selected to ensure that IGBT switch will be capable of blocking dc-link voltage, in our design we have Vdc equal to 800V therefore with safety factor of 1.5 the voltage rating of IGBT should be 1200 V. The current rating of each switch depends on the current that will flow through the switch, this current is composed of the PV array power, load reactive power, load balancing and harmonic compensating currents. Thus, the current rating depends on the PV array output and load compensation required.

#### 4.4 Control of Grid Connected Two-stage System

A grid connected two-stage system has two separate control for the boost converter stage and the VSI stage. The boost converter stage has MPPT control and is implemented using INC method already explained in chapter 3. The VSI is connected in shunt at PCC and is controlled as a current source to transfer the solar energy from dc-link to the grid and also compensate for load reactive power, load harmonics and load imbalance at PCC. Control of VSI has two important aspects, first is to calculate 3-phase reference currents that the VSI should supply to the grid and second is to give switching pulses to VSI such that its output current follows the reference current in each phase.

## 4.5 Reference Current Generation for Voltage Source Inverter

There are several control algorithms available that generate reference currents for the VSI. The control algorithms used in this work are [25-28]:

1. Unit template based current control algorithm
2. IRPT based current control algorithm
3. SRFT based current control algorithm
4. SRFT based indirect current control algorithm

### 4.5.1 Unit Template based Current Control Algorithm

In Unit template based current control algorithm the 3-phase PCC voltage and dc-link voltage are sensed to generate reference currents to be supplied by the grid. Figure 4.3 shows model for Unit template current control algorithm developed in MATLAB-SIMULINK.

The peak value of per phase PCC voltage  $V_{sm}$  is calculated using equation 4.12.

$$V_{sm} = \sqrt{\left[\left(\frac{2}{3}\right) \cdot (v_{sa}^2 + v_{sb}^2 + v_{sb}^2)\right]} \quad (4.12)$$

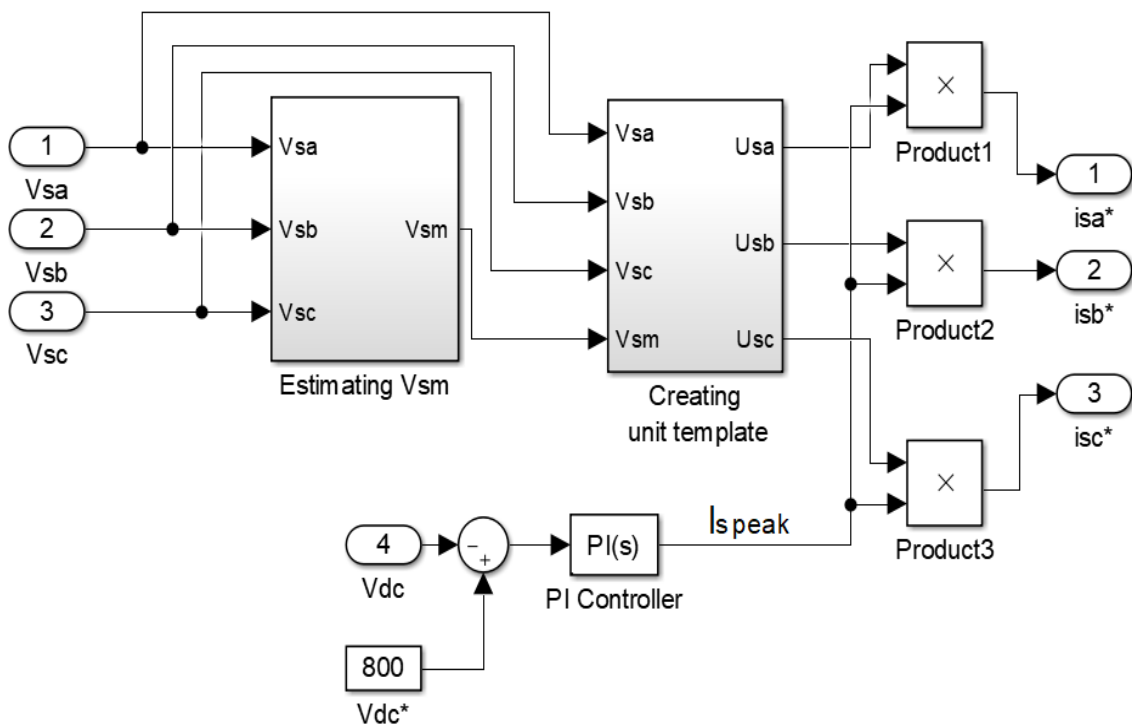


**Figure 4-3. Unit template current control algorithm**

In above equation  $v_{sa}, v_{sb}, v_{sc}$  are instantaneous PCC voltages. After  $V_{sm}$  is calculated, unit template for each grid phase current ( $u_{sa}, u_{sb}, u_{sc}$ ) is calculated using equations 4.13 to 4.15.

$$u_{sa} = \frac{v_{sa}}{V_{sm}} \quad (4.13)$$

$$u_{sb} = \frac{v_{sb}}{V_{sm}} \quad (4.14)$$

$$u_{sc} = \frac{v_{sc}}{V_{sm}} \quad (4.15)$$

The reference grid currents are obtained by multiplying these unit template with output of dc-link PI controller  $I_{speak}$  as given by equation 4.16:

$$\begin{bmatrix} i_{sa}^* \\ i_{sb}^* \\ i_{sc}^* \end{bmatrix} = I_{speak} \cdot \begin{bmatrix} u_{sa} \\ u_{sb} \\ u_{sc} \end{bmatrix} \quad (4.16)$$

$i_{sa}^*, i_{sb}^*, i_{sc}^*$  are instantaneous values of reference grid currents.

#### 4.5.2 IRPT based Current Control Algorithm

In instantaneous reactive power theory (IRPT) control algorithm the 3-phase PCC voltage and load current are sensed and transformed from a-b-c frame to  $\alpha$ - $\beta$  frame using Clarke transformation given below in equation 4.17 and 4.18.

$$\begin{bmatrix} v_{\alpha} \\ v_{\beta} \end{bmatrix} = \sqrt{\frac{2}{3}} \cdot \begin{bmatrix} 1 & -1/2 & -1/2 \\ 0 & \sqrt{3}/2 & -\sqrt{3}/2 \end{bmatrix} \cdot \begin{bmatrix} v_{sa} \\ v_{sb} \\ v_{sc} \end{bmatrix} \quad (4.17)$$

$$\begin{bmatrix} i_{\alpha} \\ i_{\beta} \end{bmatrix} = \sqrt{\frac{2}{3}} \cdot \begin{bmatrix} 1 & -1/2 & -1/2 \\ 0 & \sqrt{3}/2 & -\sqrt{3}/2 \end{bmatrix} \cdot \begin{bmatrix} i_a \\ i_b \\ i_c \end{bmatrix} \quad (4.18)$$

Figure 4.4. shows model for IRPT current control algorithm developed in MATLAB-SIMULINK. The instantaneous real and reactive power of load is calculated using  $\alpha$ - $\beta$  components of voltage and current given by equation 4.19.

$$\begin{bmatrix} p_l \\ q_l \end{bmatrix} = \begin{bmatrix} v_{\alpha} & v_{\beta} \\ v_{\beta} & -v_{\alpha} \end{bmatrix} \cdot \begin{bmatrix} i_{\alpha} \\ i_{\beta} \end{bmatrix} \quad (4.19)$$

The instantaneous powers of the load both  $p_l$  and  $q_l$  have average as well as oscillating components.

$$p_l = p_{ac} + p_{dc} \quad (4.20)$$

$$q_l = q_{ac} + q_{dc} \quad (4.21)$$

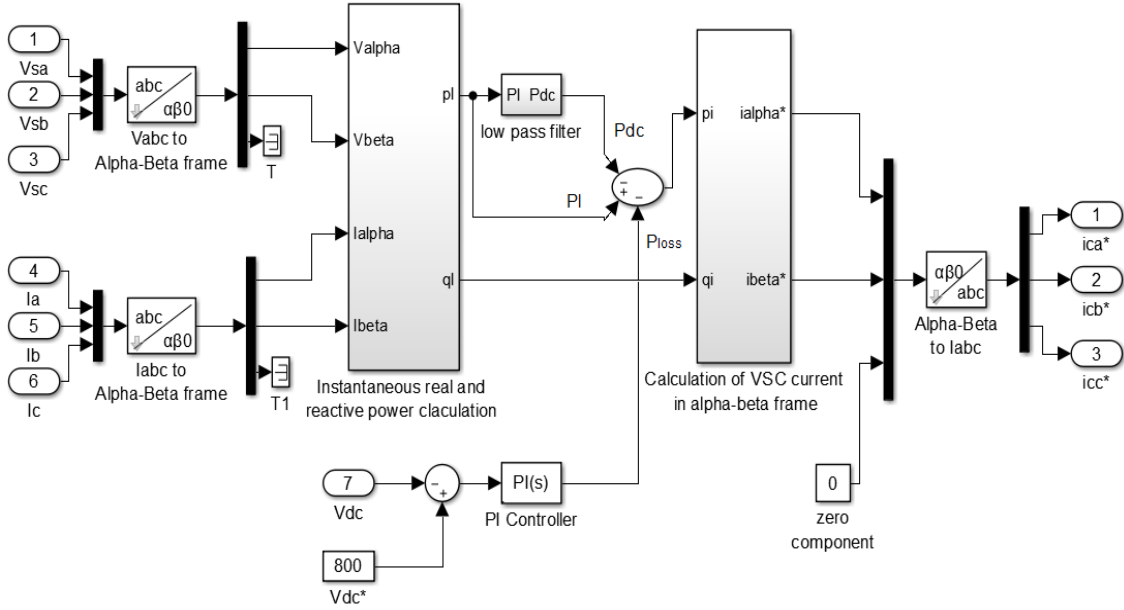


**Figure 4-4. IRPT based current control algorithm**

In order to have grid current sinusoidal and in phase with grid voltage the grid must only supply  $p_{dc}$  and VSI must supply  $p_{ac}$  and  $q_l$  component of the load.

In addition to this the voltage of the DC-link should be held constant at the designed value of 800 V to ensure proper operation of VSI and complete transfer of solar energy from dc side to the ac side of VSI. This is achieved with the help of a PI controller at dc-link. The output of PI controller  $p_{loss}$  should also be supplied by the grid to maintain dc-link voltage constant. The powers to be supplied by VSI are  $p_i$  and  $q_i$  are given by equations 4.22 and 4.23:

$$p_i = p_l - p_{dc} - p_{loss} \quad (4.22)$$

$$q_i = q_{ac} + q_{dc} \quad (4.23)$$

The VSI currents in  $\alpha$ - $\beta$  frame corresponding to these powers can be calculated using equation 4.24 and corresponding reference current in a-b-c frame are given by equation 4.25:

$$\begin{bmatrix} i_{\alpha}^* \\ i_{\beta}^* \end{bmatrix} = \frac{1}{v_{\alpha}^2 + v_{\beta}^2} \cdot \begin{bmatrix} v_{\alpha} & v_{\beta} \\ v_{\beta} & -v_{\alpha} \end{bmatrix} \cdot \begin{bmatrix} p_i \\ q_i \end{bmatrix} \quad (4.24)$$

$$\begin{bmatrix} i_{ca}^* \\ i_{cb}^* \\ i_{cc}^* \end{bmatrix} = \frac{\sqrt{2}}{3} \cdot \begin{bmatrix} 1 & 0 \\ -1/2 & \sqrt{3}/2 \\ -1/2 & -\sqrt{3}/2 \end{bmatrix} \begin{bmatrix} i_{\alpha}^* \\ i_{\beta}^* \end{bmatrix} \quad (4.25)$$

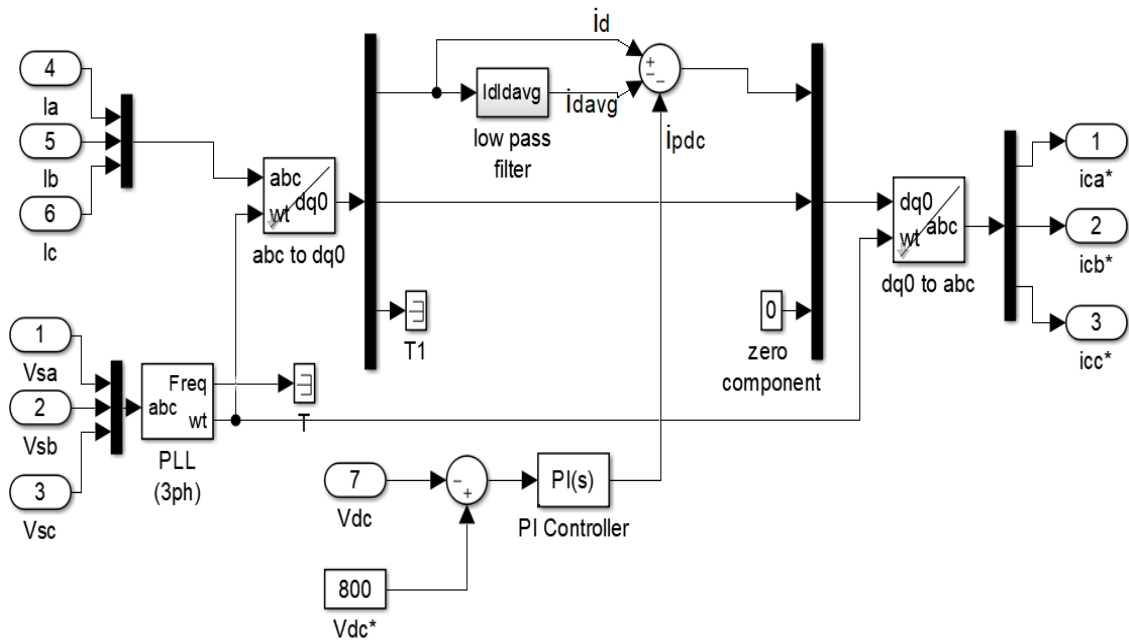
#### 4.5.3 SRFT based Current Control Algorithm

Figure 4.5 shows model for Synchronous reference frame theory (SRFT) based current control algorithm developed in MATLAB-SIMULINK. In SRFT, the 3-phase PCC

voltage and load current are sensed and transformed from a-b-c frame to  $\alpha$ - $\beta$  frame initially and then into synchronously rotating d-q frame using equation 4.26.

$$\begin{bmatrix} i_d \\ i_q \end{bmatrix} = \begin{bmatrix} \cos \omega t & \sin \omega t \\ -\sin \omega t & \cos \omega t \end{bmatrix} \cdot \begin{bmatrix} i_\alpha \\ i_\beta \end{bmatrix} \quad (4.26)$$

Here  $\omega$  is the angular frequency of the synchronous rotating frame and it is kept equal to the grid frequency so that the fundamental ac component in grid voltage and current is transformed into dc quantities in d-q frame. The grid frequency is measured with help of a phase lock loop (PLL).



**Figure 4-5. SRFT based current control algorithm**

The  $i_d$  component corresponds to the instantaneous real power of load and  $i_q$  component corresponds to instantaneous reactive power of load. The  $i_d$  has both average ( $i_{davg}$ ) and oscillatory component ( $i_{dac}$ ) given by equation 4.27, it is passed through a low pass filter (5<sup>th</sup> order Butterworth low pass filter) to extract the average instantaneous real power component  $i_{davg}$ .

$$i_d = i_{davg} + i_{dac} \quad (4.27)$$

The output of DC-link PI controller  $i_{pdc}$  together with  $i_{davg}$  component must be supplied by the grid, whereas the remaining components  $i_{dac}$  and  $i_q$  should be supplied by the VSI. The d-q components to be supplied by VSI is given by equation 4.28 and 4.29

$$i_{di} = i_{dac} \quad (4.28)$$

$$i_{qi} = i_q \quad (4.29)$$

The d-q component of VSI current is initially transformed into  $\alpha$ - $\beta$  frame using equation 4.30 and then into a-b-c frame to given by equation 4.31

$$\begin{bmatrix} i_{\alpha}^* \\ i_{\beta}^* \end{bmatrix} = \begin{bmatrix} \cos \omega t & \sin \omega t \\ -\sin \omega t & \cos \omega t \end{bmatrix} \cdot \begin{bmatrix} i_{di} \\ i_{qi} \end{bmatrix} \quad (4.30)$$

$$\begin{bmatrix} i_{ca}^* \\ i_{cb}^* \\ i_{cc}^* \end{bmatrix} = \frac{\sqrt{2}}{3} \cdot \begin{bmatrix} 1 & 0 \\ -1/2 & \sqrt{3}/2 \\ -1/2 & -\sqrt{3}/2 \end{bmatrix} \begin{bmatrix} i_{\alpha}^* \\ i_{\beta}^* \end{bmatrix} \quad (4.31)$$

#### 4.5.4 Indirect Current Control Algorithm based on SRFT

In this algorithm the dc-link voltage and 3-phase PCC voltage are sensed and reference currents to be supplied by the grid are generated. In this algorithm we do not sense the load current therefore less number of current sensors are required. Figure 4.6 shows model for Indirect current control algorithm developed in MATLAB-SIMULINK

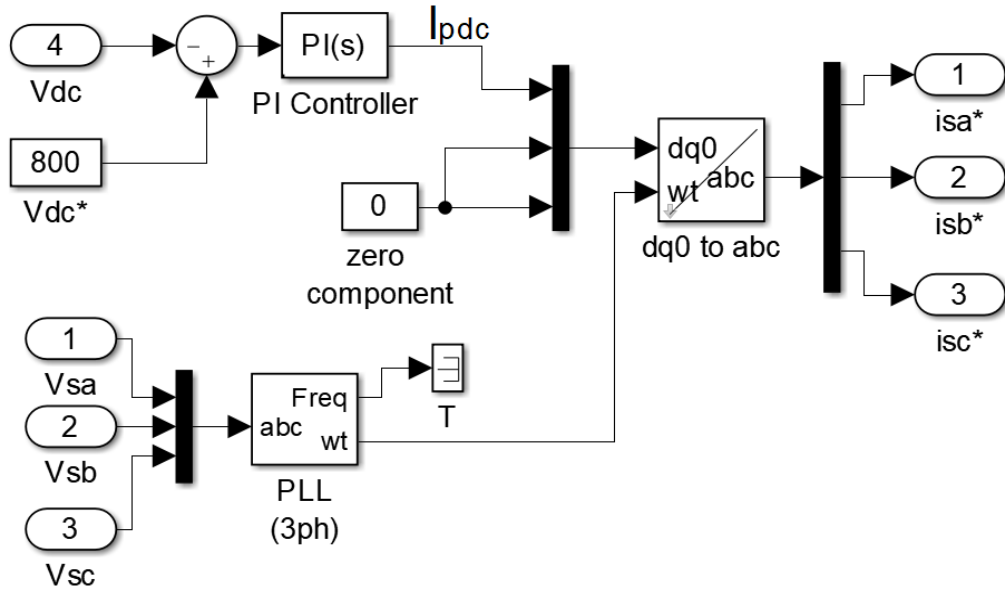


**Figure 4-6. Indirect current control algorithm using SRFT**

Therefore, the d-component of grid current  $i_{dg}$  is equal to output of PI controller  $I_{pdc}$  and q-component to be supplied by grid must be zero. the d-q components are converted into  $\alpha$ - $\beta$  components given by equation 4.32 and reference grid currents in a-b-c frame are given by equation 4.33:

$$\begin{bmatrix} i_{\alpha}^* \\ i_{\beta}^* \end{bmatrix} = \begin{bmatrix} \cos \omega t & \sin \omega t \\ -\sin \omega t & \cos \omega t \end{bmatrix} \cdot \begin{bmatrix} I_{pdc} \\ 0 \end{bmatrix} \quad (4.32)$$

$$\begin{bmatrix} i_{sa}^* \\ i_{sb}^* \\ i_{sc}^* \end{bmatrix} = \frac{\sqrt{2}}{3} \cdot \begin{bmatrix} 1 & 0 \\ -1/2 & \sqrt{3}/2 \\ -1/2 & -\sqrt{3}/2 \end{bmatrix} \begin{bmatrix} i_{\alpha}^* \\ i_{\beta}^* \end{bmatrix} \quad (4.33)$$

#### 4.6 Hysteresis Current Controller for Voltage Source Inverter

Hysteresis current control (HCC) is a popular technique for giving switching pulses to a two level VSI. In a 3-phase two level VSI, if top switch of any leg is closed(ON) with bottom switch of the same leg open(ON) then output current of the corresponding phase will increase, if the bottom switch is closed with top switch open in a leg the corresponding phase current will decrease. However, both top and bottom switch should not be ON simultaneously as this will short circuit the dc-link. This property of two level VSI makes it possible to control output current of each phase independently by giving switching pulses to the corresponding leg. The switching of the VSI should be done such that the VSI output current follows the generated reference current in each phase. In HCC the reference currents are compared with actual current within a hysteresis band and switching pulses are generated accordingly as shown in figure 4.7.

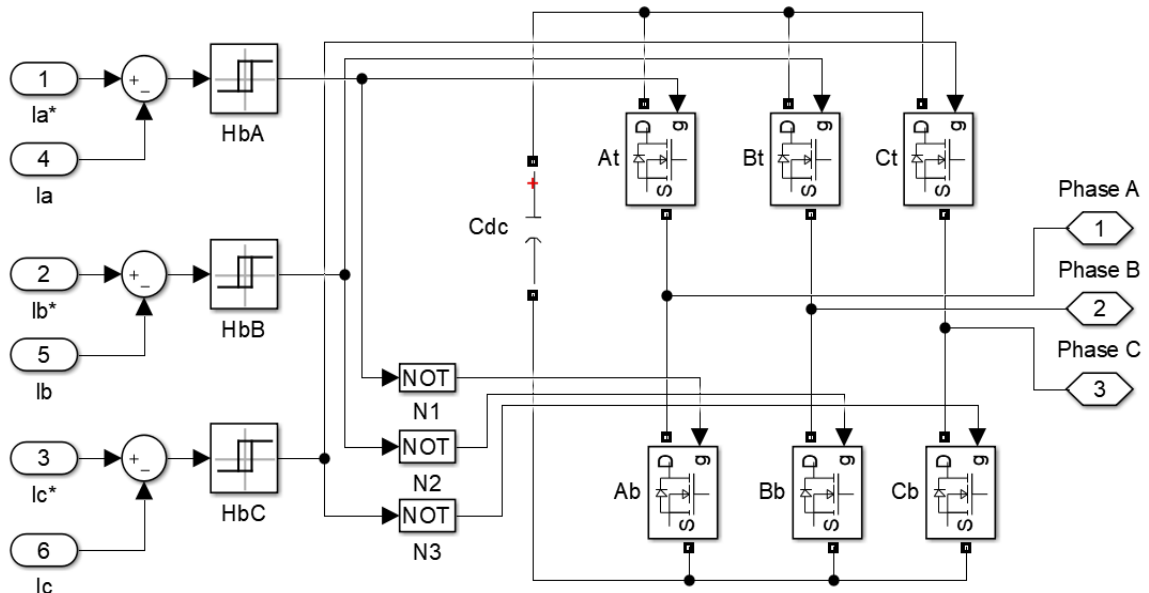
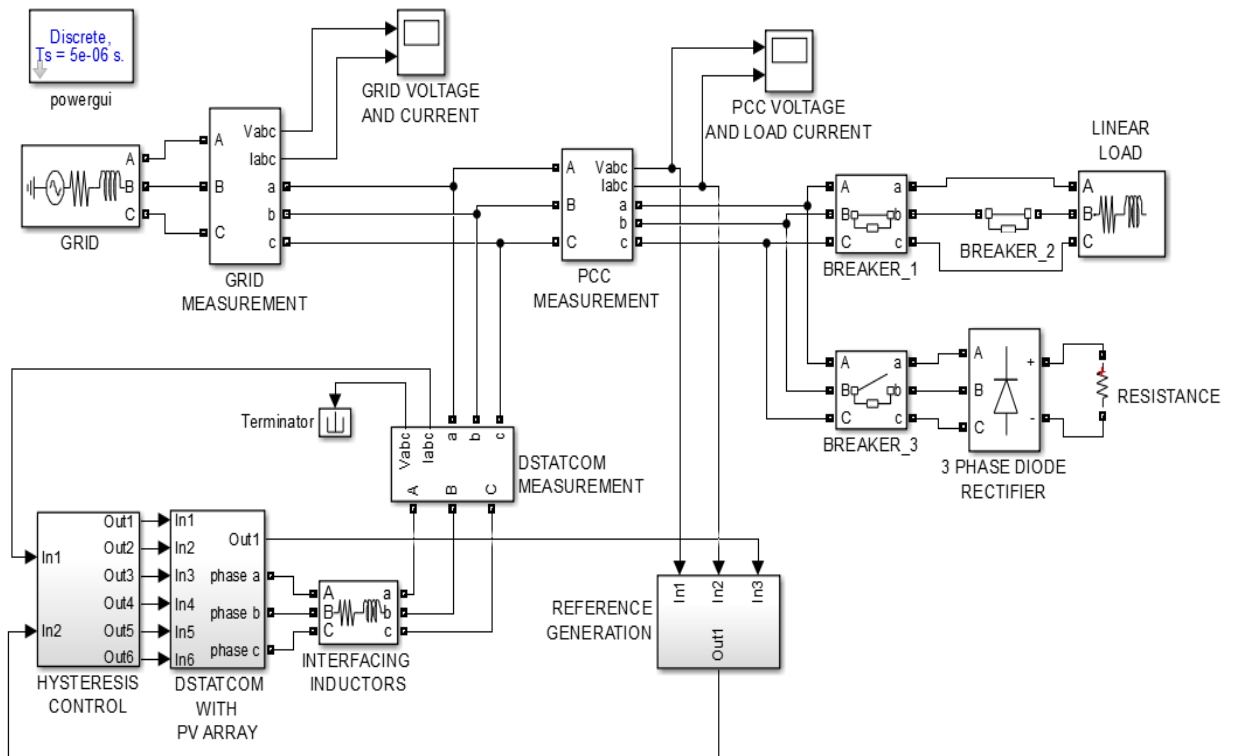


Figure 4-7. Hysteresis current controller

#### 4.7 MATLAB Simulation of Grid Connected Two-Stage PV System

A MATLAB-SIMULINK model is developed for grid connected two-stage PV system according to the design discussed in previous section. MATLAB-SIMULINK model is shown in figure 4.8. and system specifications are given in table 4.2.



**Figure 4-8. MATLAB-SIMULINK model for grid connected two-stage PV system**

**Table 4-2. Specification of MATLAB model for grid connected two-stage PV system**

3-phase AC Source	415 V, $R_S = 0.03 \Omega$ , $L_S = 0.1 \text{ mH}$
Load	i) 415 V, 5 kW, 0.8 pf, 3-phase linear load ii) 3-phase diode rectifier, $R_{dc} = 100 \Omega$ .
Interfacing Inductor ( $L_r$ )	7 mH
Reference DC-link Voltage ( $V_{dc}$ )	800 V
DC-link Capacitor ( $C_{dc}$ )	3 mF
Switching Frequency of Boost Converter ( $F_{sw}$ )	20 kHz
Inductor ( $L_b$ ) for Boost Converter	5 mH
PV Array	$P_{MPP} = 12.789 \text{ kW}$ , $V_{MPP} = 580 \text{ V}$ , $I_{MPP} = 22.05 \text{ A @ STC}$



The model is run with INC control for MPPT and different control techniques discussed for VSI. The waveforms of PCC voltage, grid current, load current, inverter current, dc-link voltage, PV output power, PV output voltage, PV current and THD (total harmonic distortion) analysis are obtained and presented for each control algorithm. System performance with all control algorithm is tested for four different cases given below:

i) Dynamic switching of linear load

In this case there is a 3-phase 5 kW, 0.8 power factor balanced linear load connected to grid and PV array is supplying maximum power of 12.789 kW at solar irradiance = 1000 W/m<sup>2</sup> initially. At 0.3 seconds additional linear load is switched in parallel to the existing load. The real power load demand increases to 20 kW and reactive power load demand increases to 6 kVAR. This case will test the system performance to track MPP in the PV array and dc-link voltage stability of the system under dynamic load switching. Additional results showing real and reactive power of grid (Pgrid, Qgrid), load (Pload, Qload) and VSI (Pvsi, Qvsi) respectively are included for this case.

ii) Linear load with change in solar irradiance:

In this case there is a 3-phase 5 kW, 0.8 power factor balanced linear load connected to grid and PV array is supplying maximum power of 12.789 kW at solar irradiance = 1000 W/m<sup>2</sup> initially. At 0.25 seconds solar irradiance starts reducing up to 500 W/m<sup>2</sup> as shown in figure 4.9. This case will test the system performance to track MPP in the PV array and dc-link voltage stability of the system under changing solar irradiance.

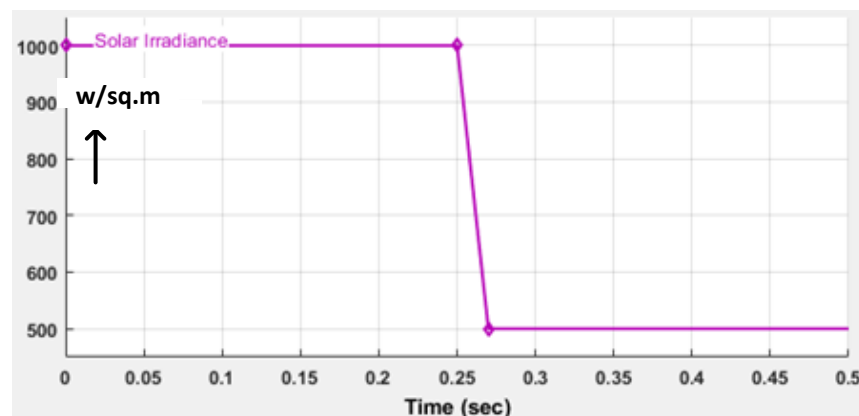


**Figure 4-9. Solar irradiance input to PV array**

iii) Unbalanced load:

In this case there is a 3-phase 5 kW, 0.8 power factor balanced linear load connected to grid and PV array is supplying maximum power of 12.789 kW at solar irradiance = 1000 W/m<sup>2</sup> initially. At 0.25 second one out of 3-phases of the load is removed. This case will test the system performance to compensate for unbalance in load and dc-link voltage stability under dynamic load change.

iv) Non-Linear load:

In this case the system is supplying a 3-phase diode rectifier with resistance  $R_{dc}$  of 100  $\Omega$  connected at its dc side. This case will test the performance of the system to compensate for non-linearity in load.

## 4.8 Simulation Results for Grid Connected Two-Stage PV System

### 4.8.1 Results for Unit Template control

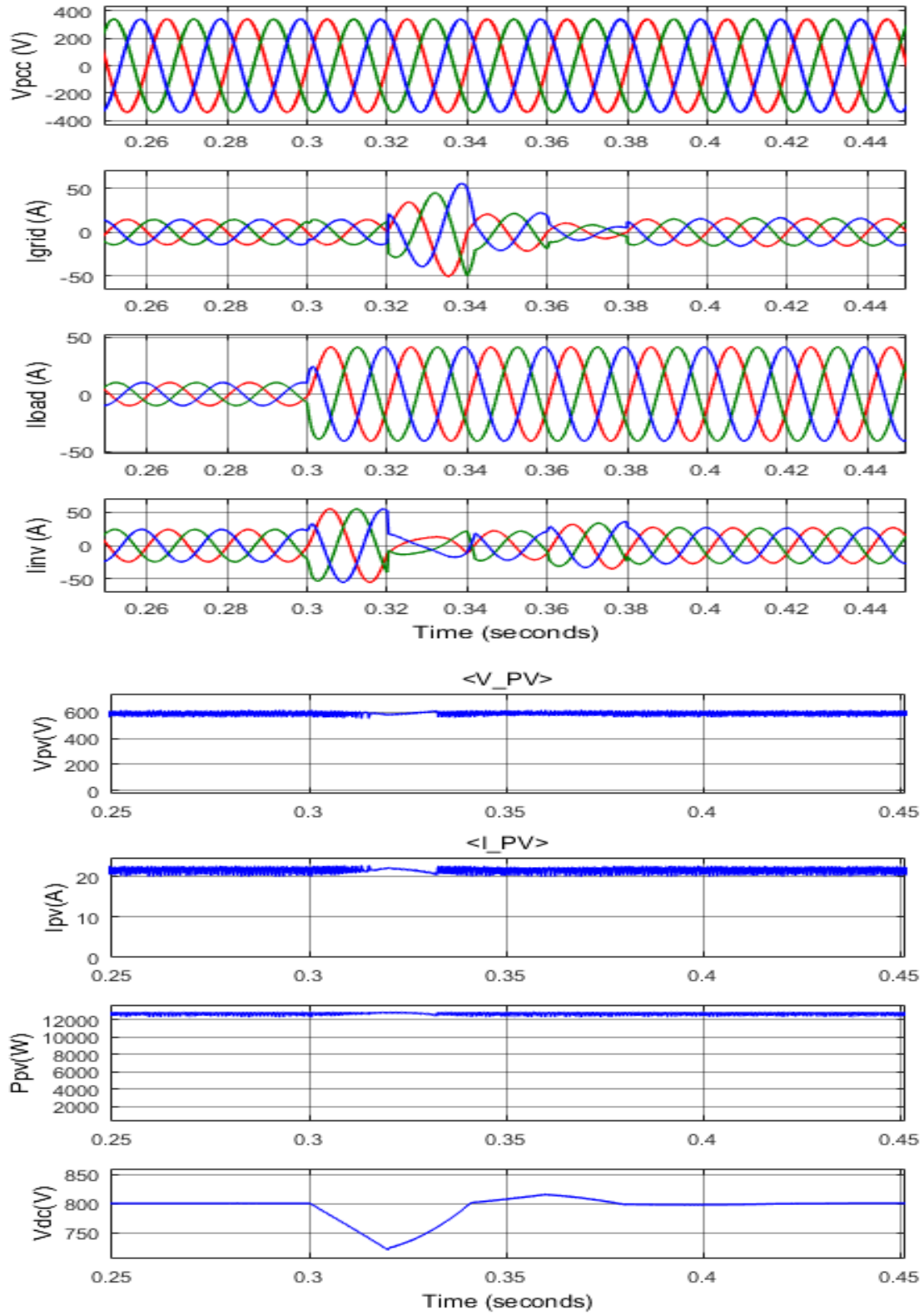
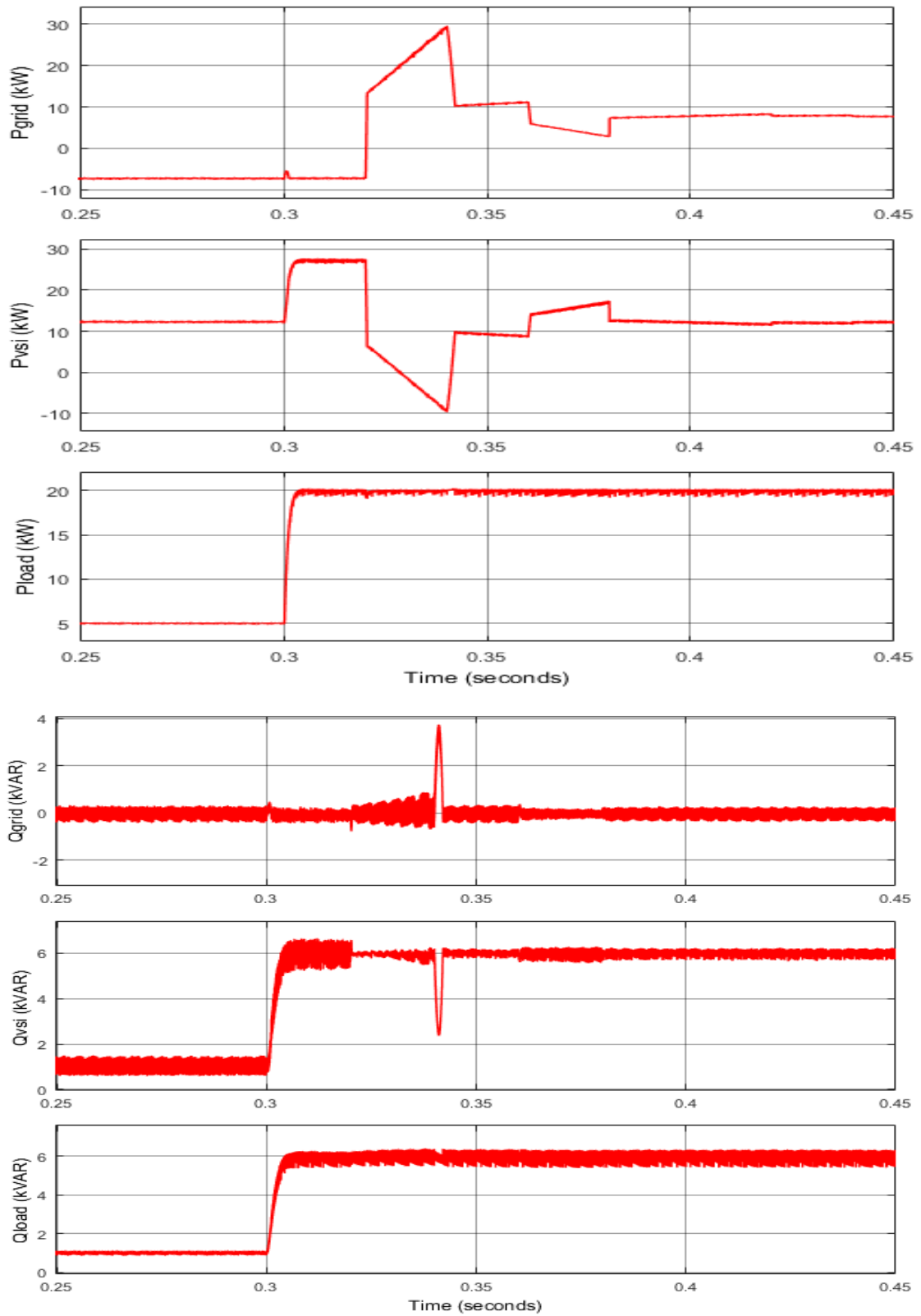
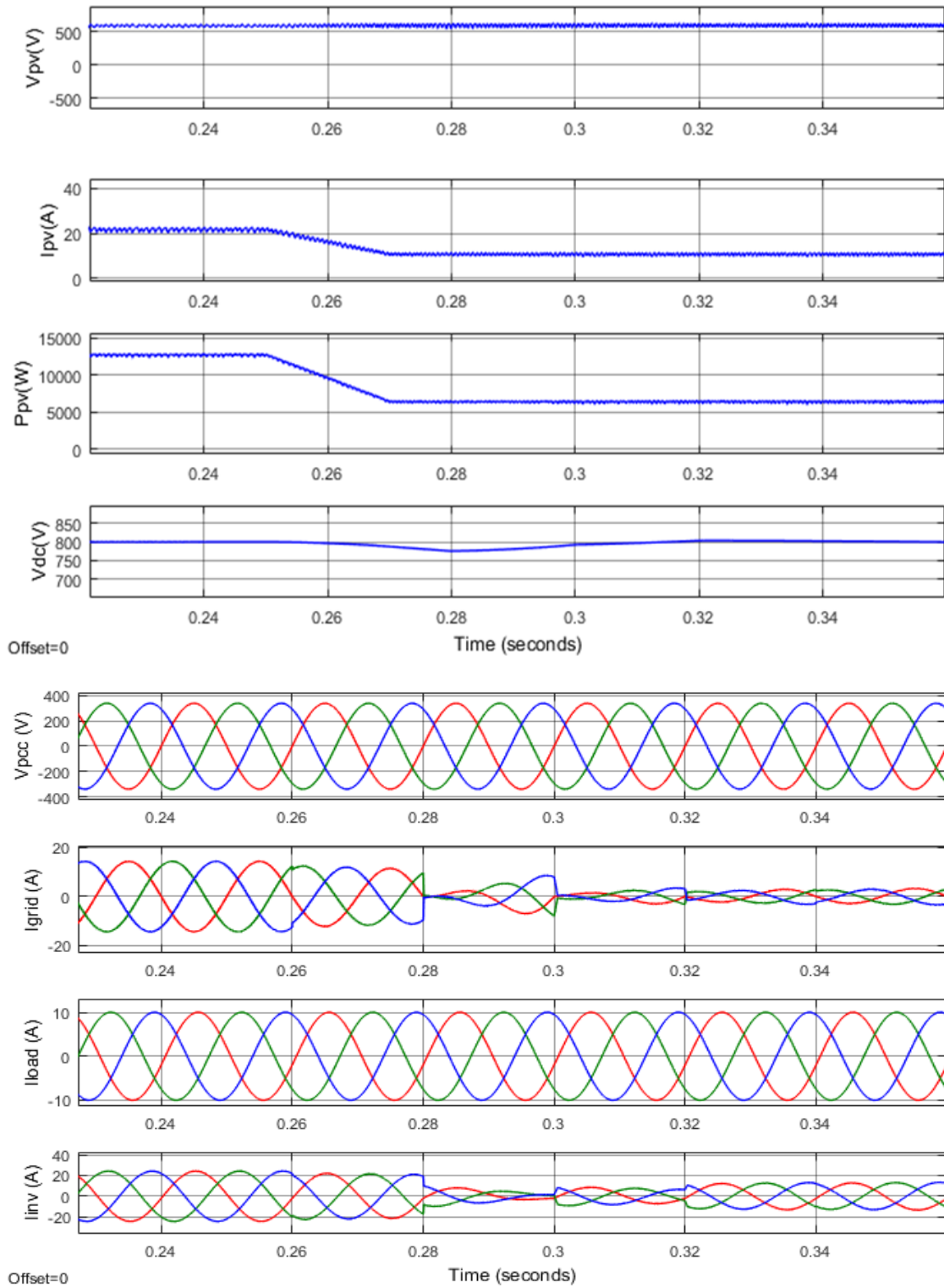


Figure 4-10. Results of Unit template control for dynamic switching of linear load



**Figure 4-11. Results of Unit template control for dynamic switching of linear load showing real and reactive power of grid, VSI and load respectively**



**Figure 4-12. Results of Unit template control with linear load and change in solar irradiance**

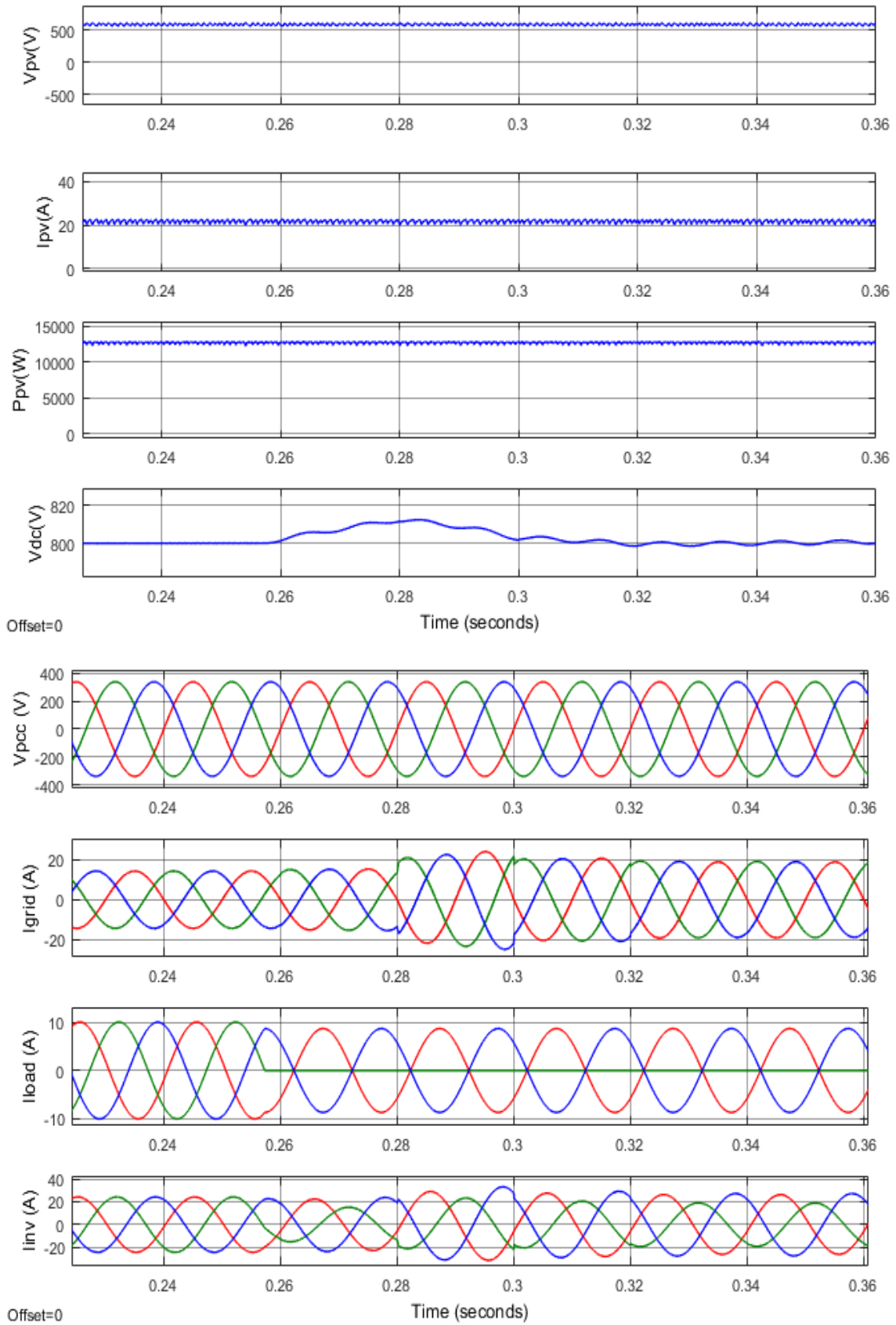


**Figure 4-13. Results of Unit template control with unbalanced load**

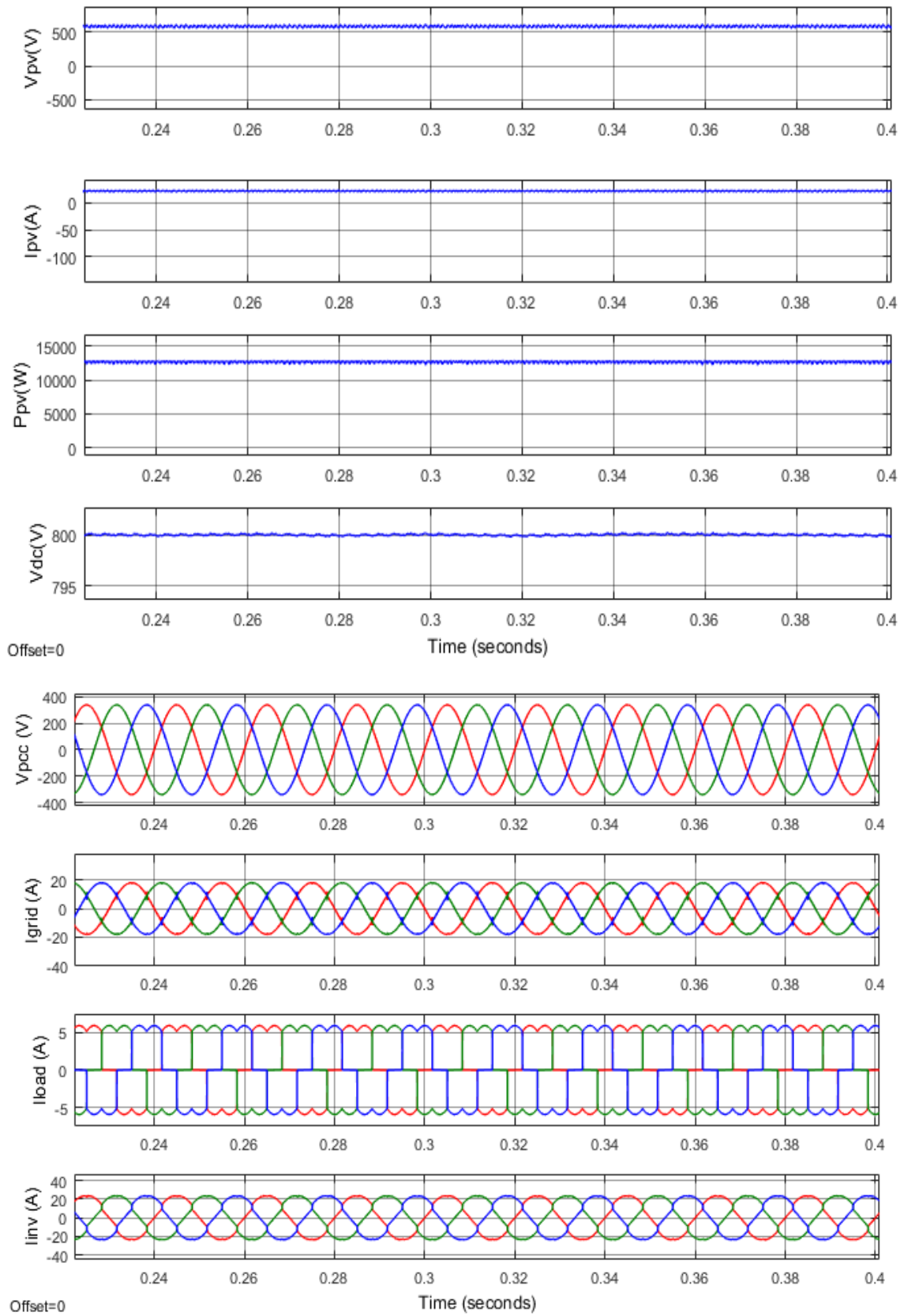


**Figure 4-14. Results of Unit template control with non-linear load**

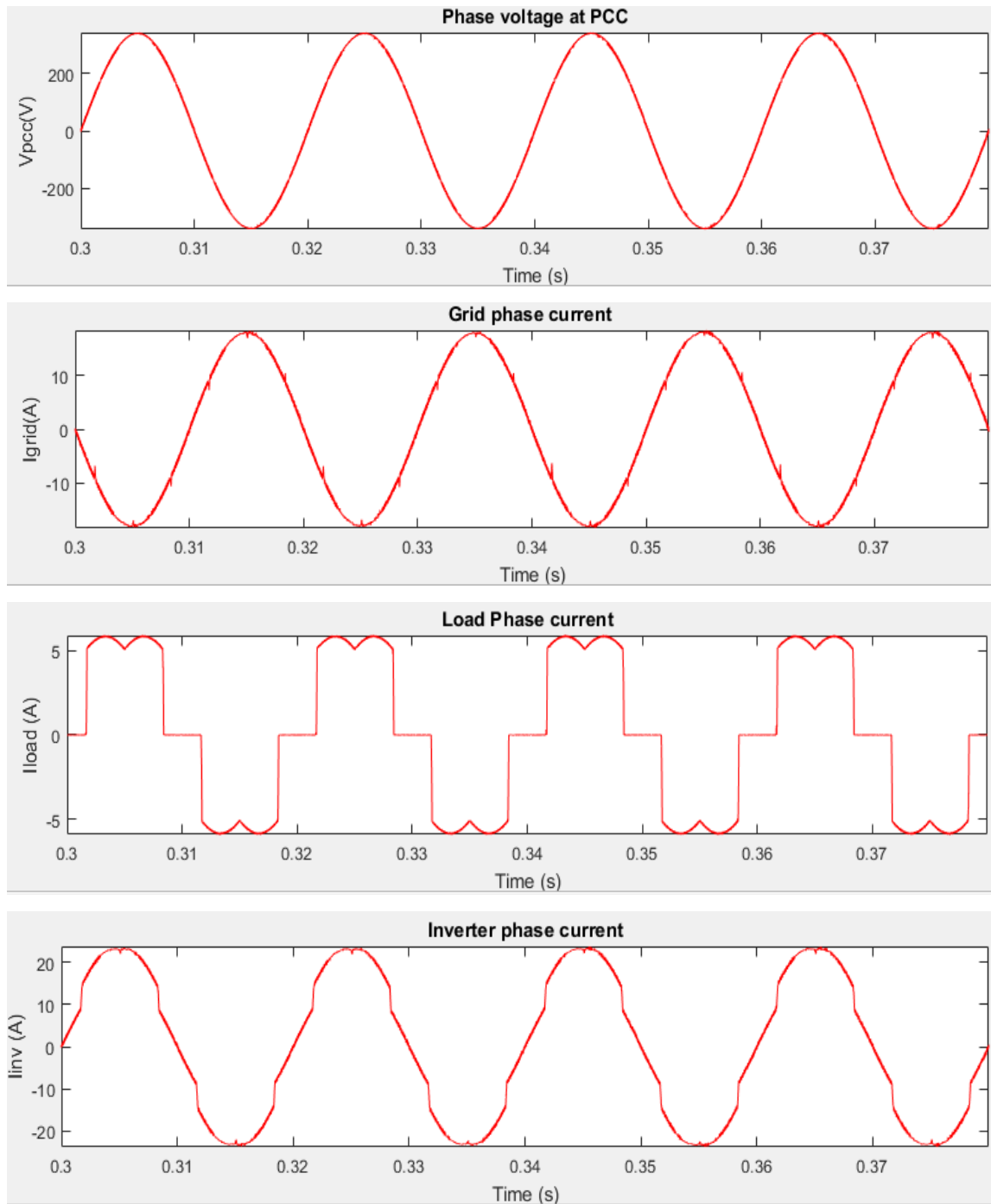
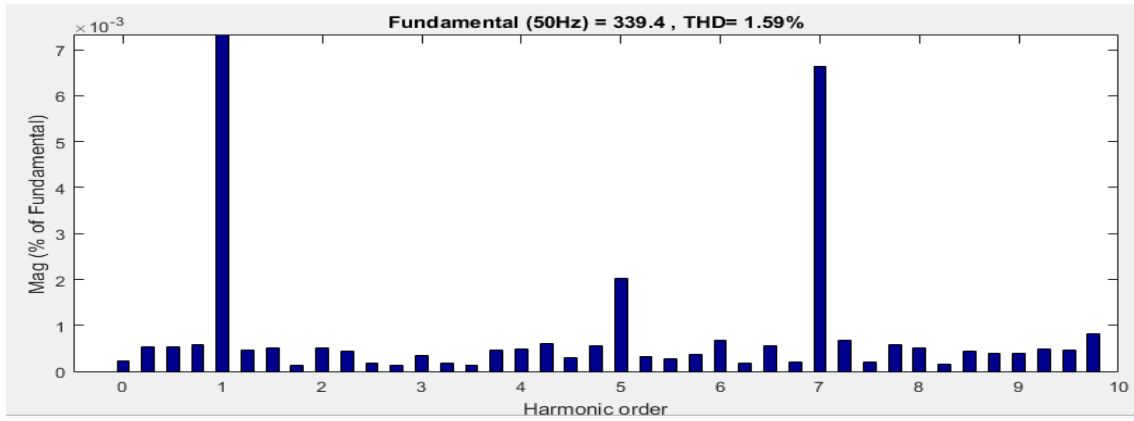
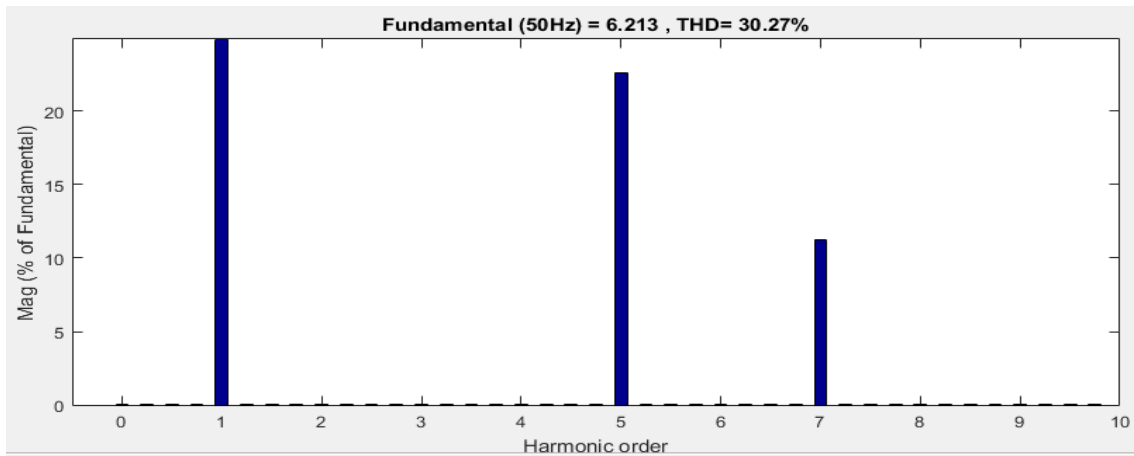


**Figure 4-15. Current profiles in unit template control for non-linear load**

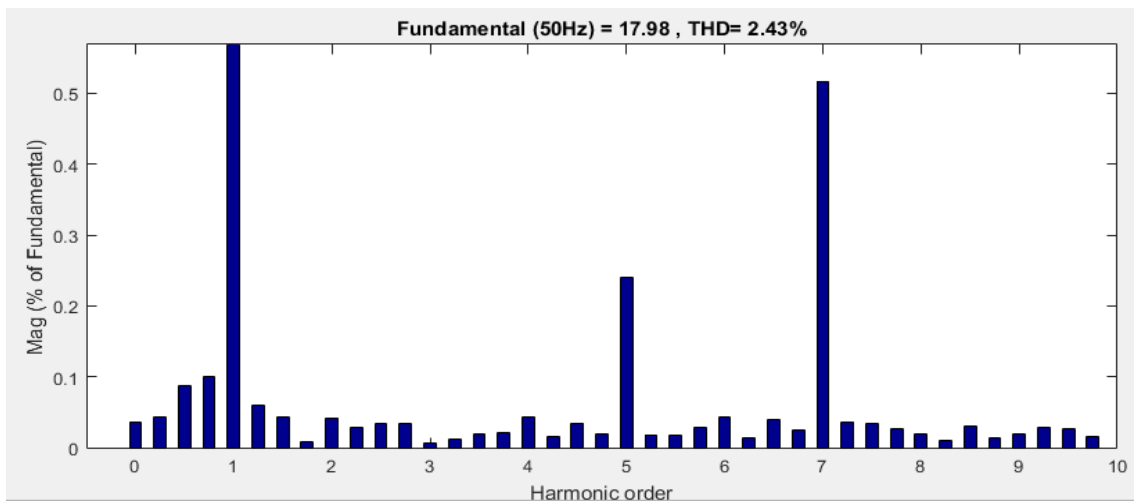




(a) PCC voltage



(b) Load current



(c) Grid current

**Figure 4-16. Harmonic profile in Unit template for non-linear load**

## 4.8.2 Results for IRPT Control

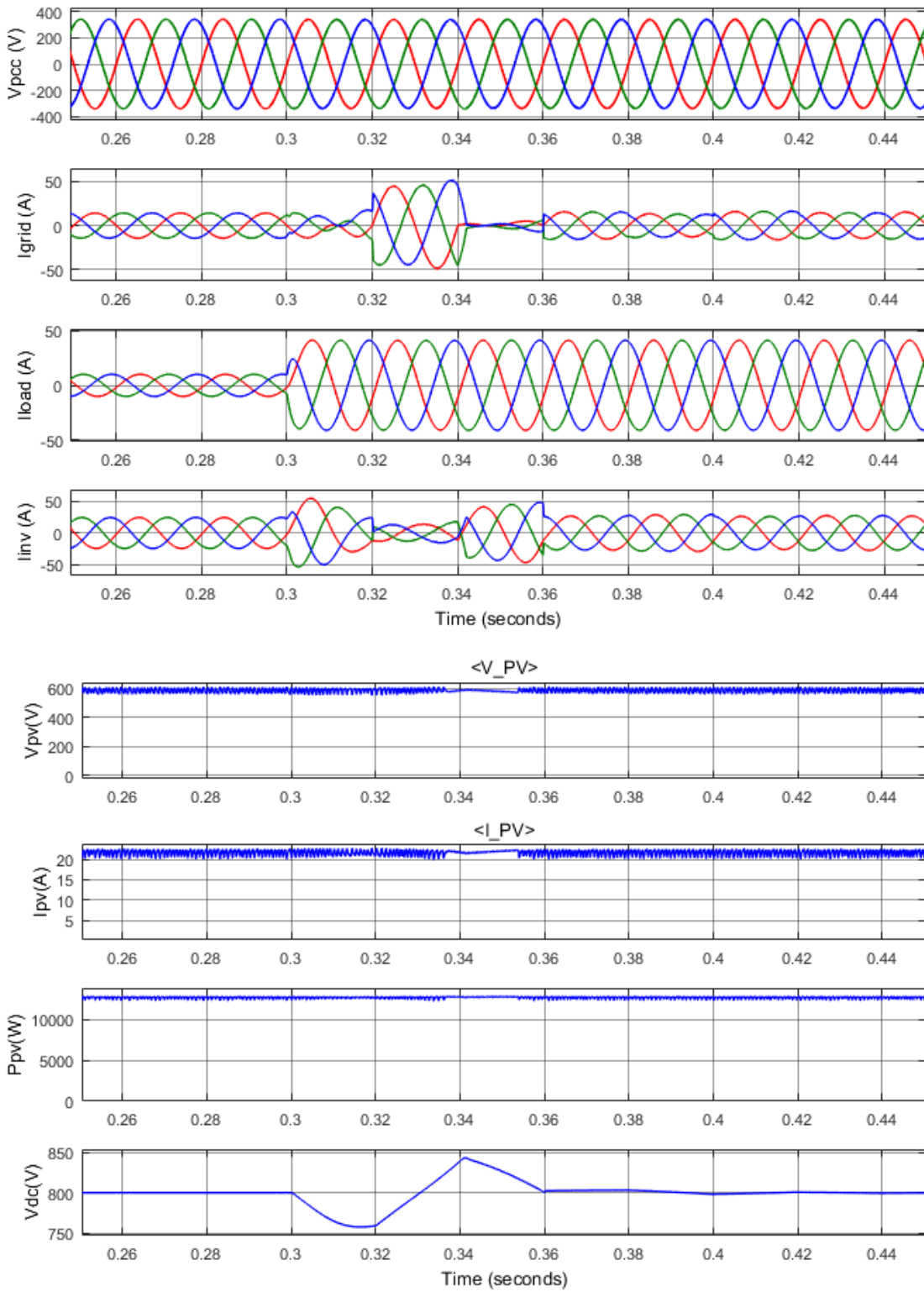
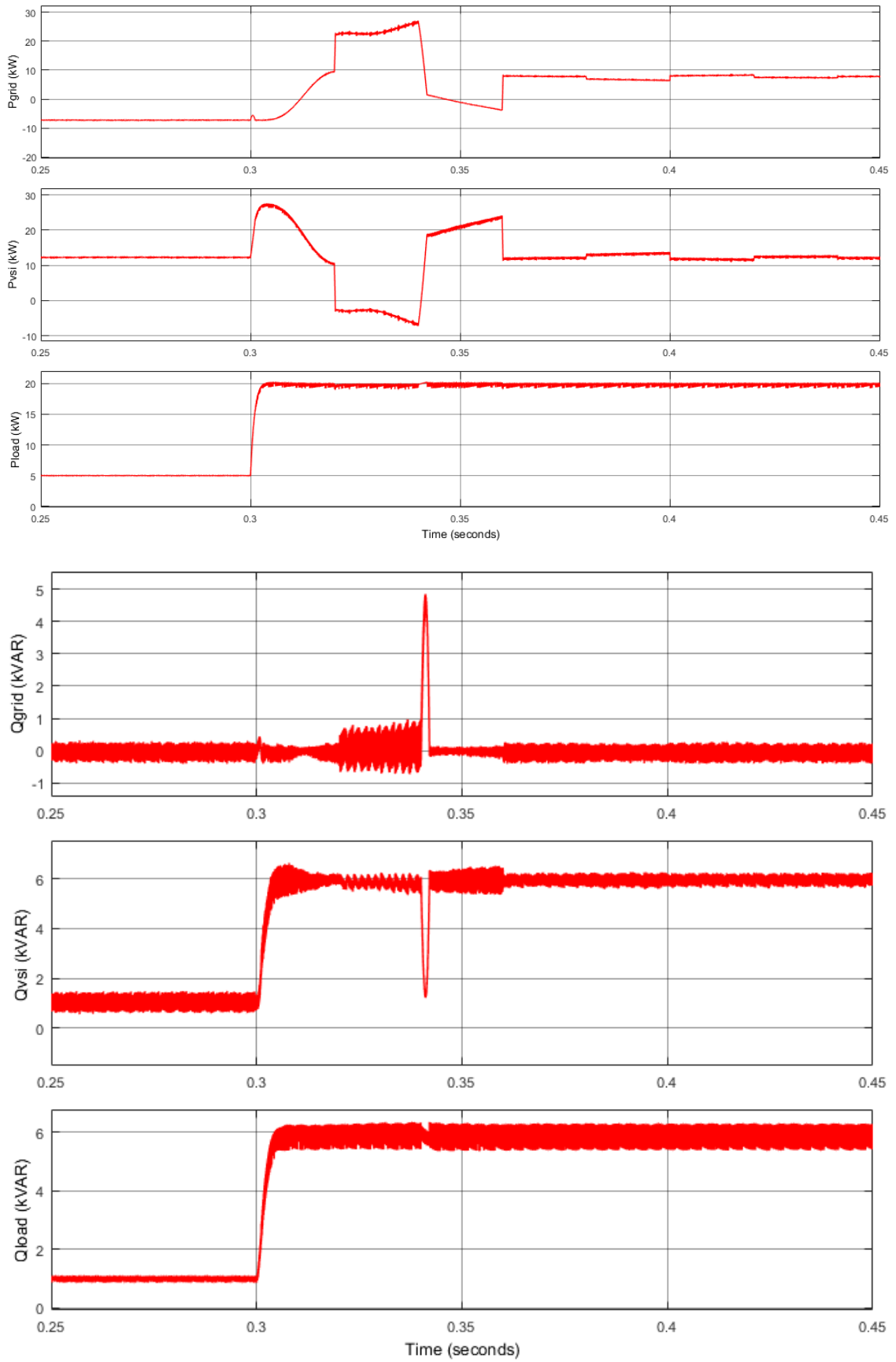
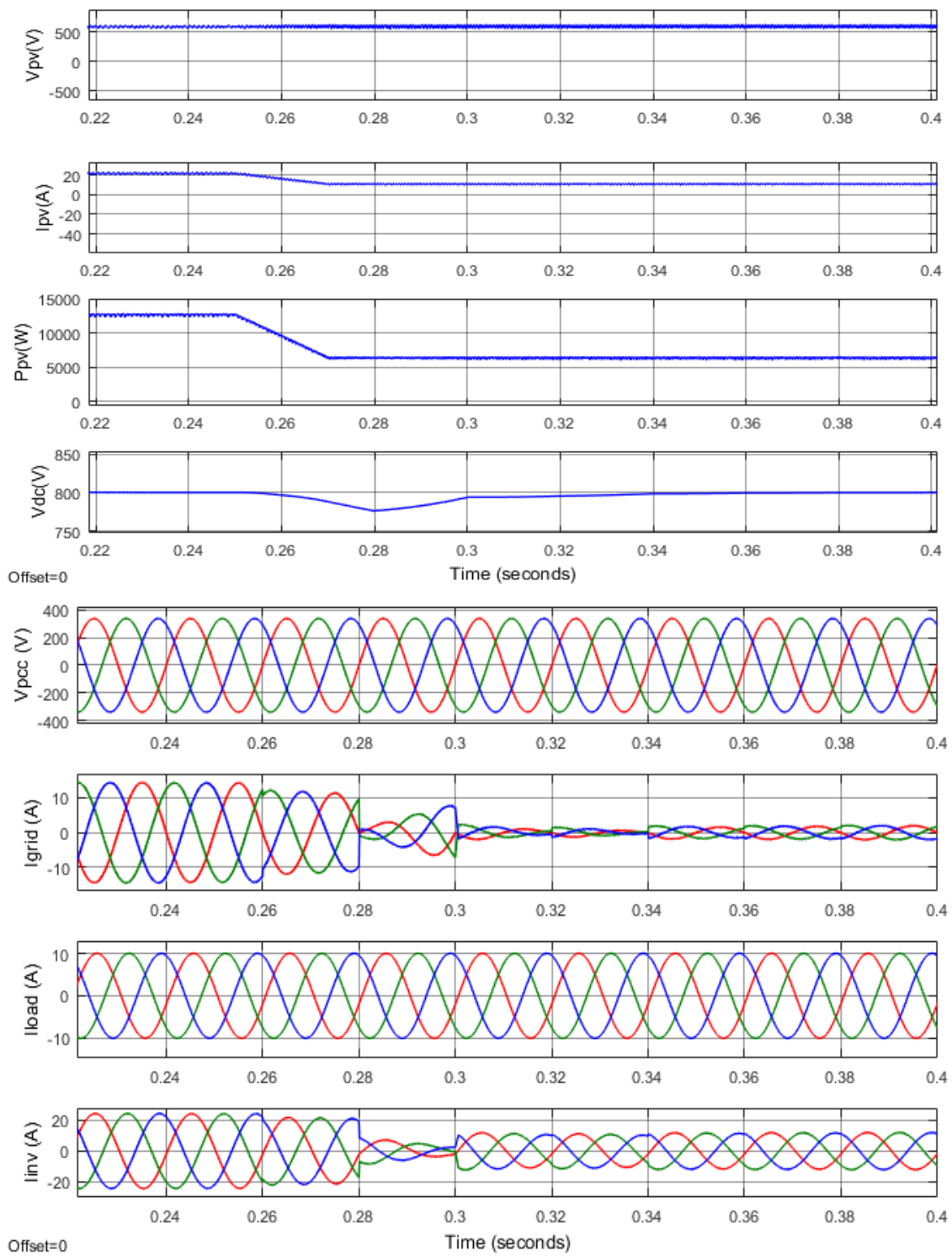


Figure 4-17. Results of IRPT control for dynamic switching of linear load



**Figure 4-18. Results of IRPT control for dynamic switching of linear load showing real and reactive power of grid, VSI and load respectively**



**Figure 4-19. Results of IRPT control with linear load and change in solar irradiance**

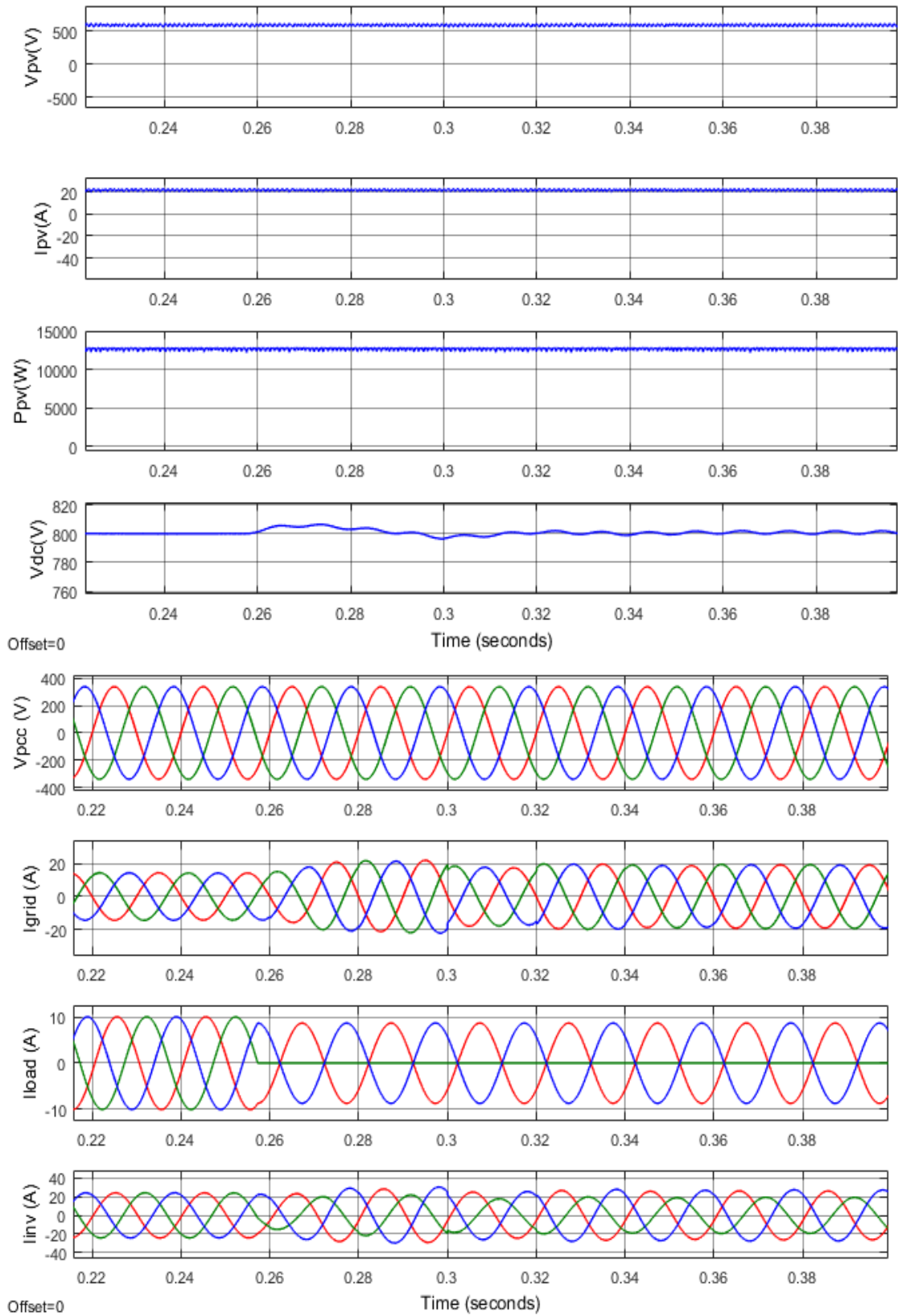


**Figure 4-20. Results of IRPT control with unbalanced load**

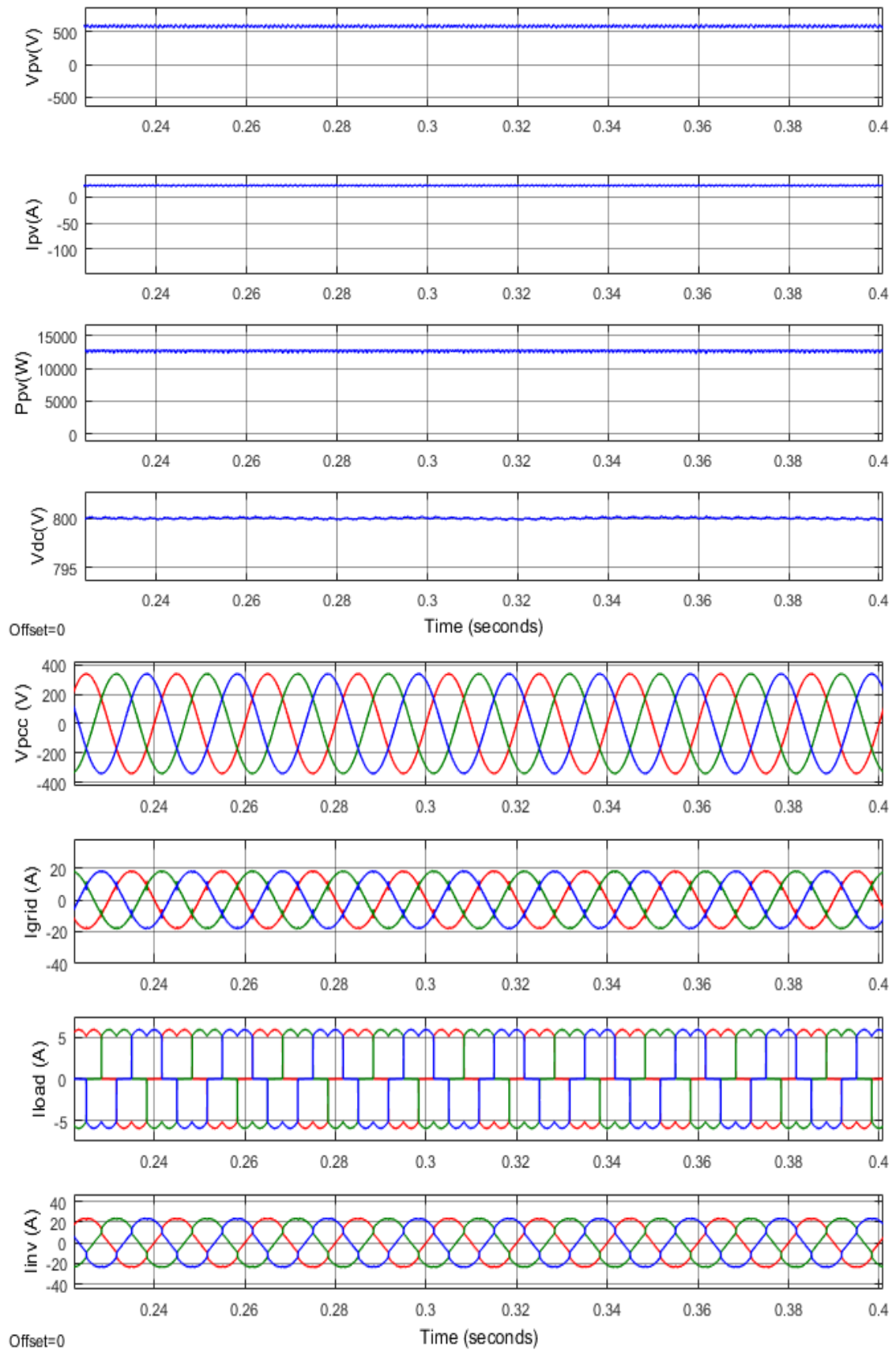


**Figure 4-21. Results of IRPT control with non-linear load**

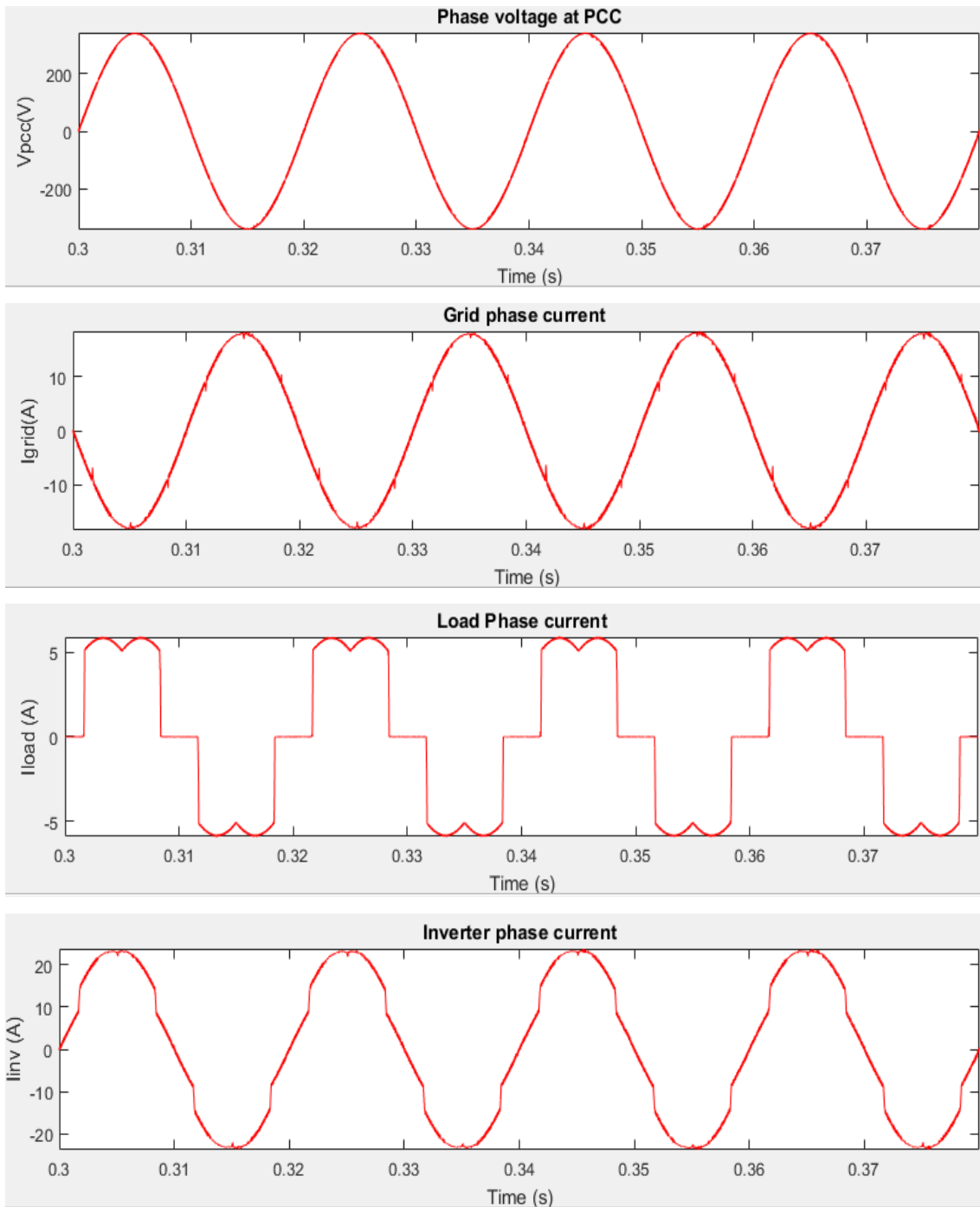
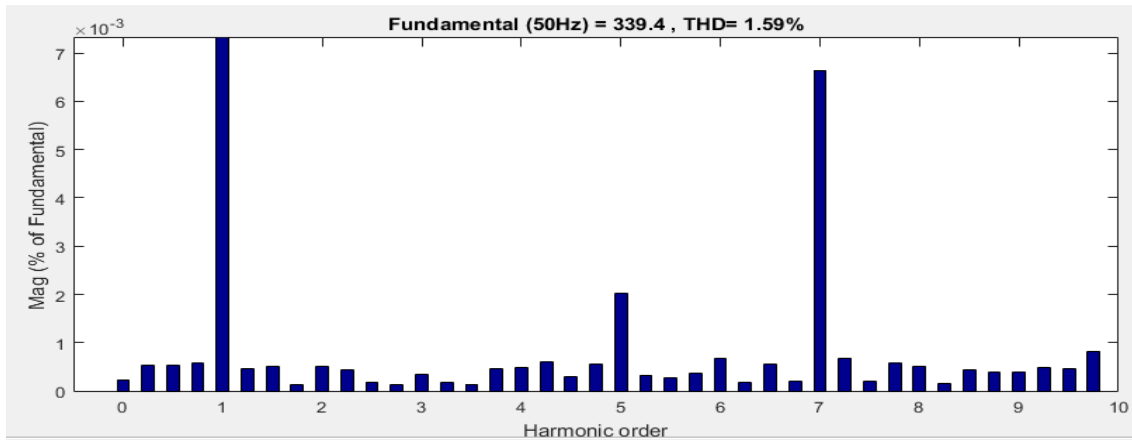
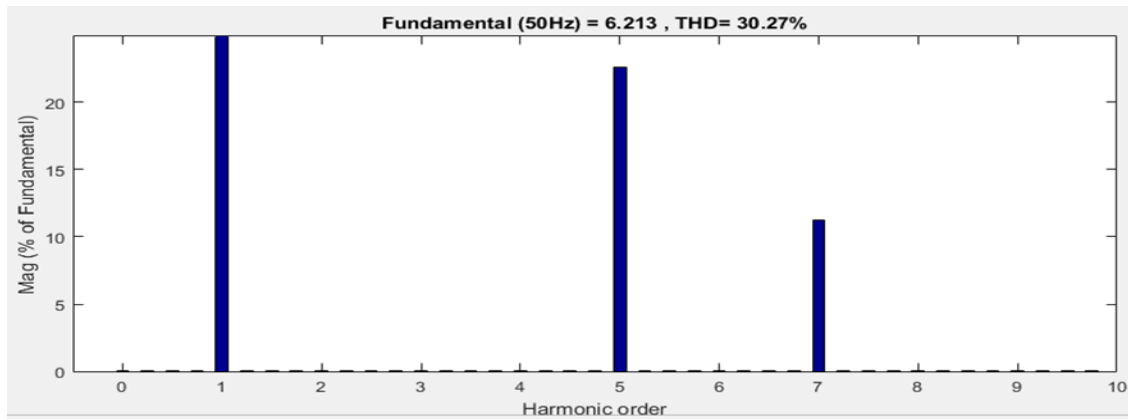


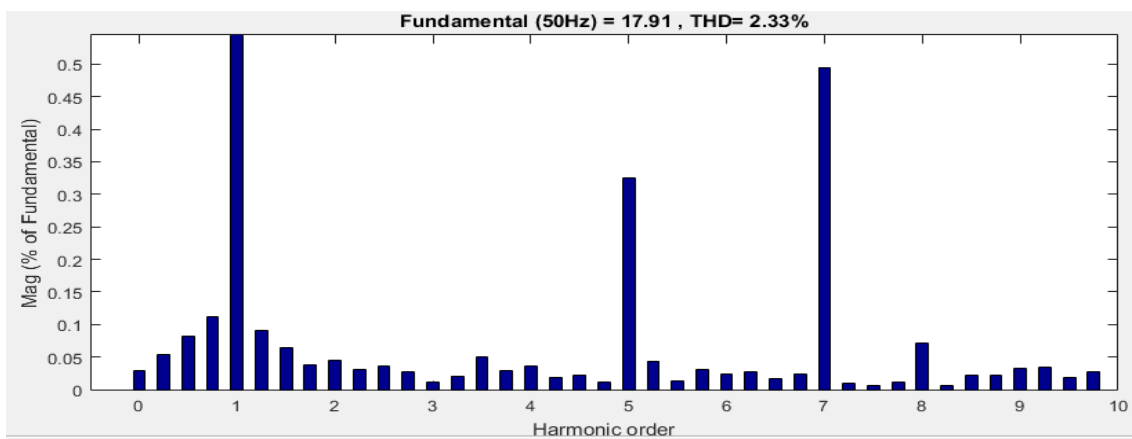
**Figure 4-22. Current profile in IRPT control for non-linear load**



(a) Voltage at PCC



(b) Load current



(c) Grid current

Figure 4-23. Harmonic profile in IRPT control for nonlinear load



### 4.8.3 Results for SRFT Control

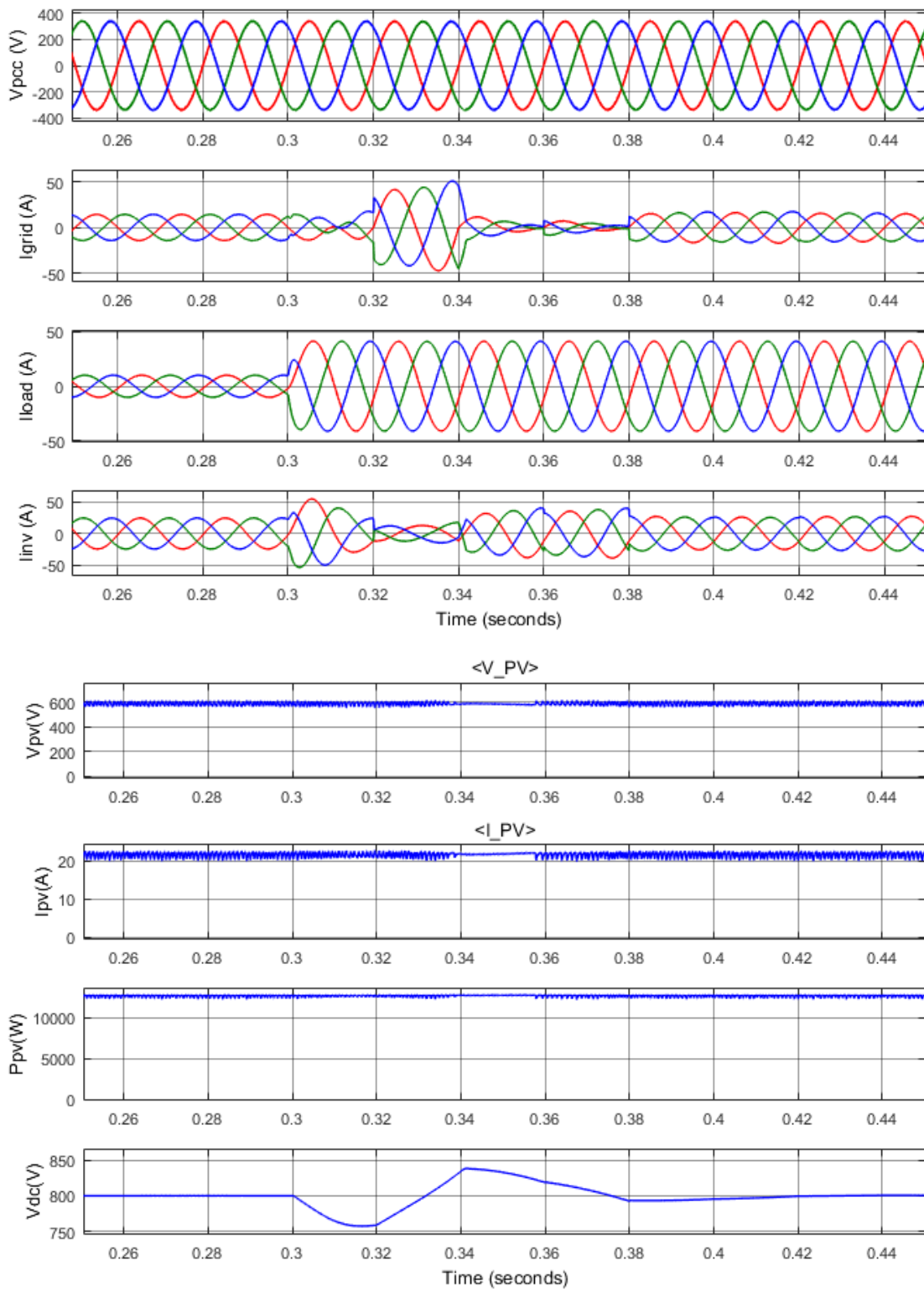
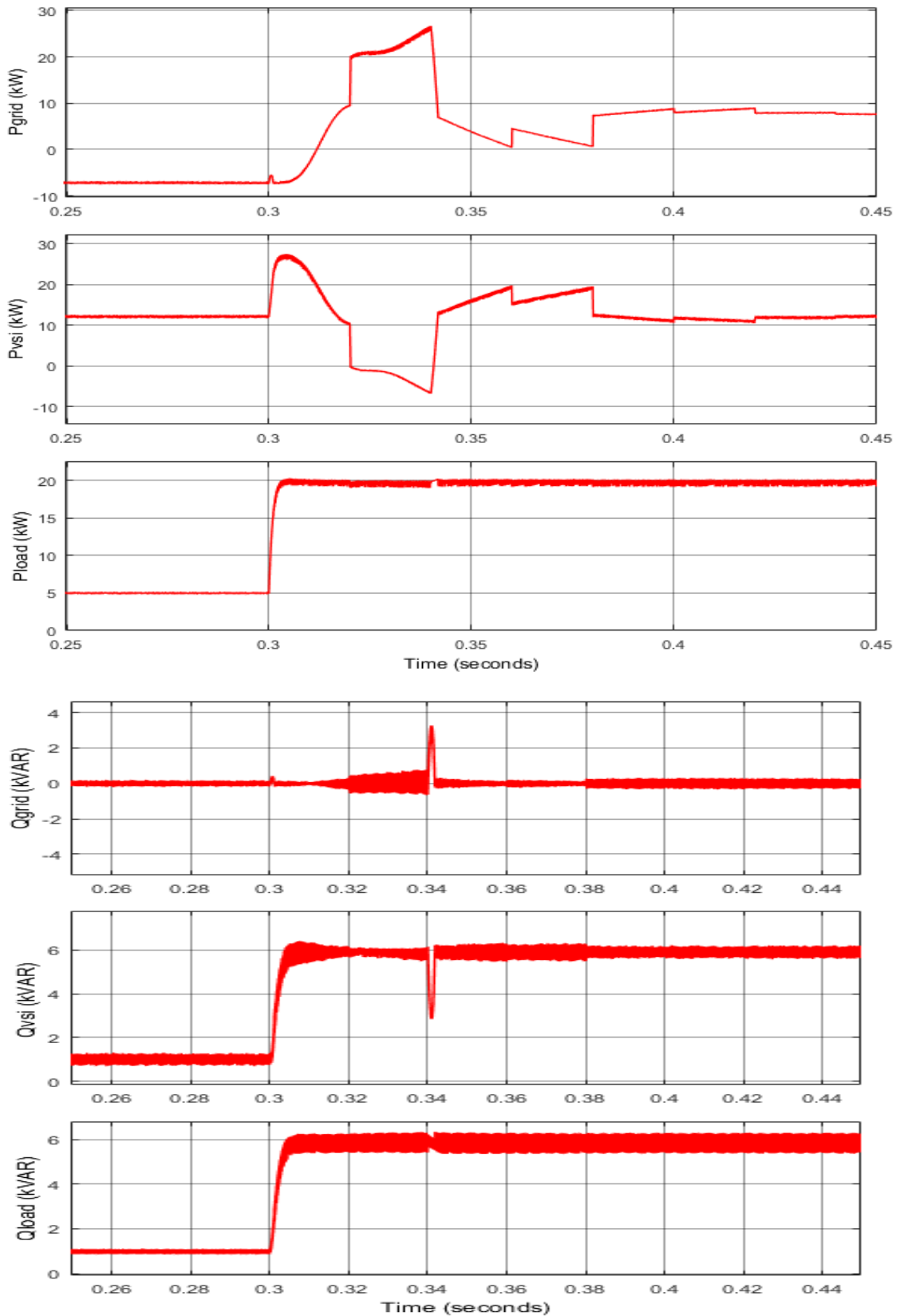
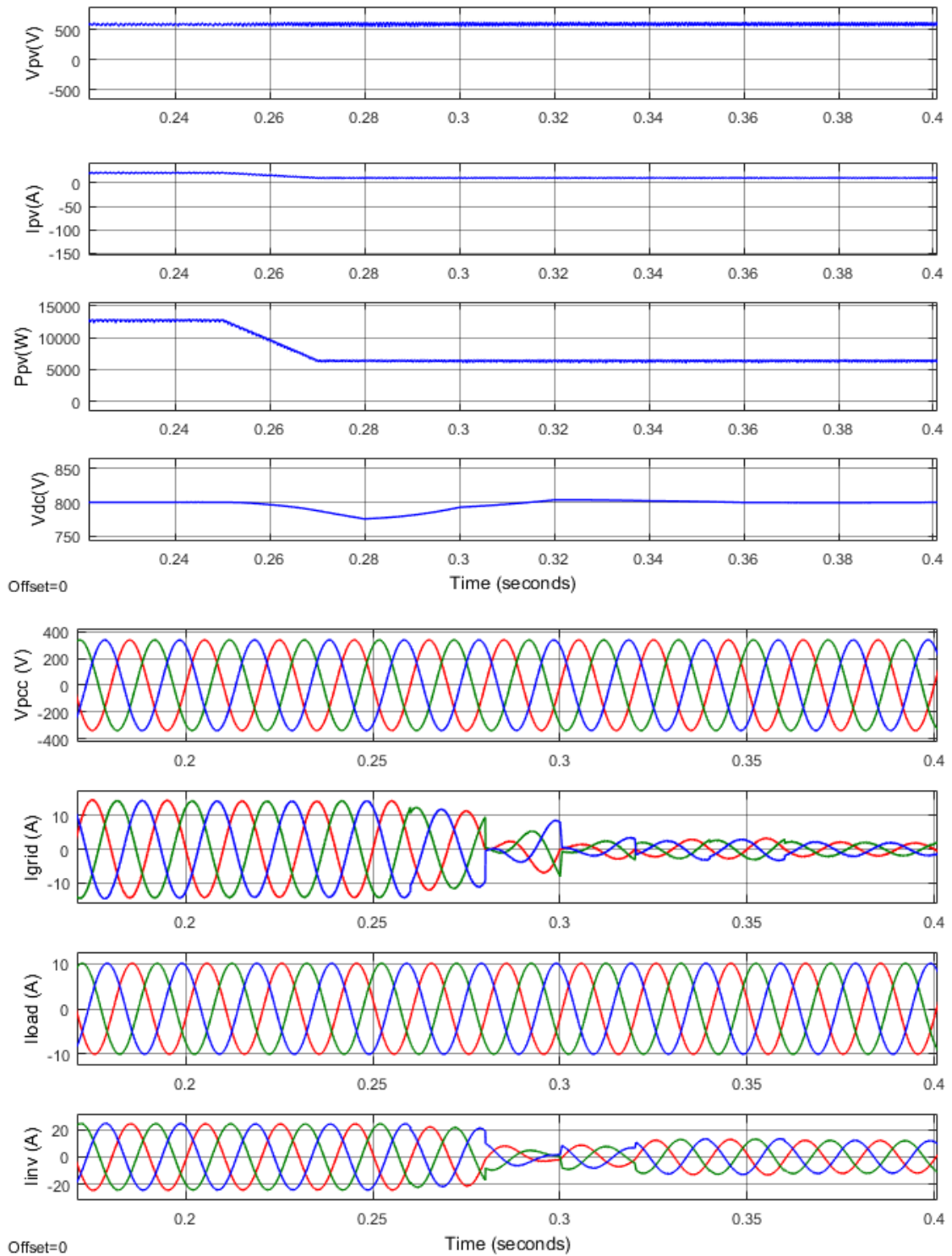


Figure 4-24. Results of SRFT control for dynamic switching of linear load



**Figure 4-25. Results of SRFT control for dynamic switching of linear load showing real and reactive power of grid, VSI and load respectively**



**Figure 4-26. Results of SRFT control with linear load and change in solar irradiance**

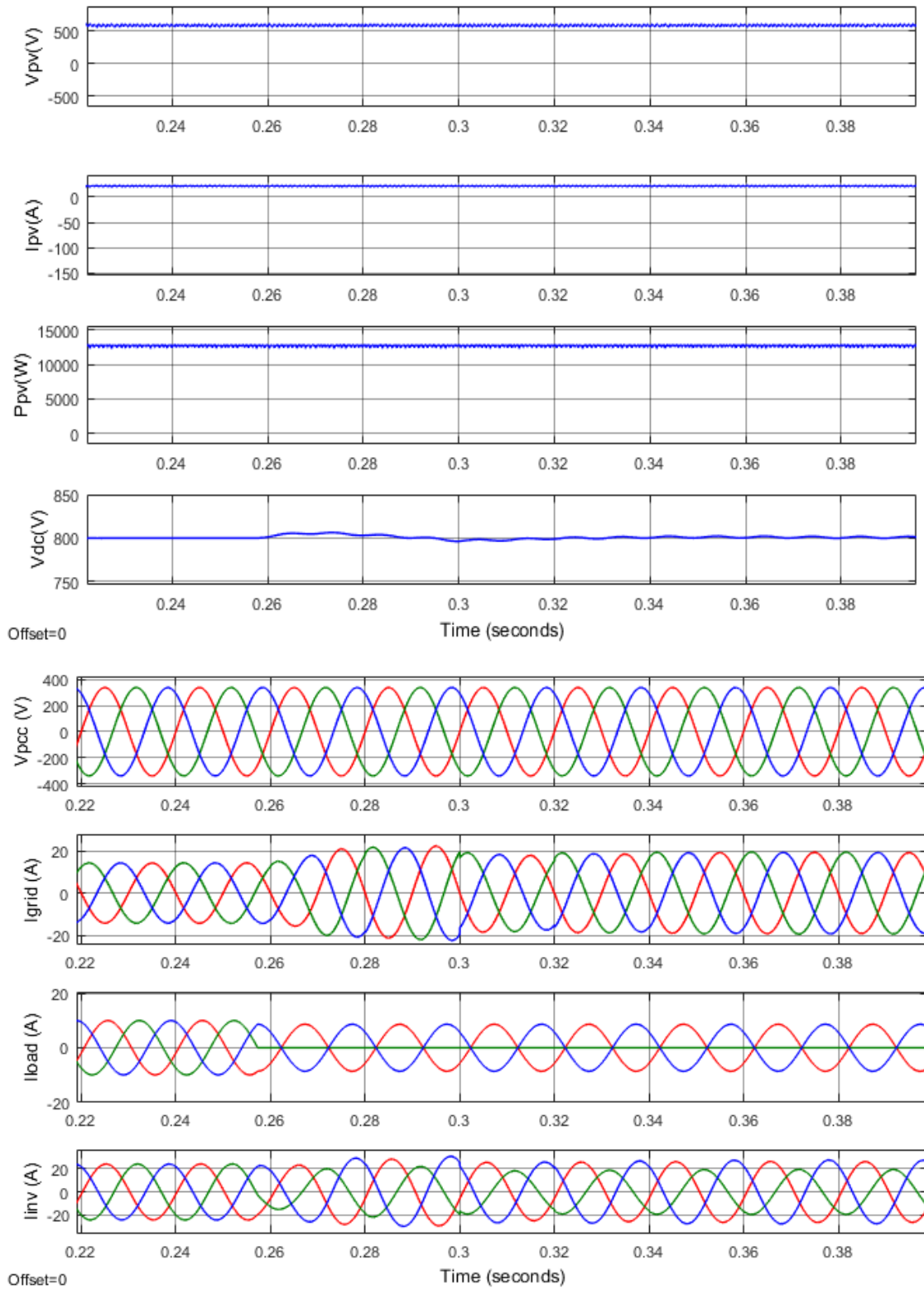


**Figure 4-27. Results of SRFT control with unbalanced load**

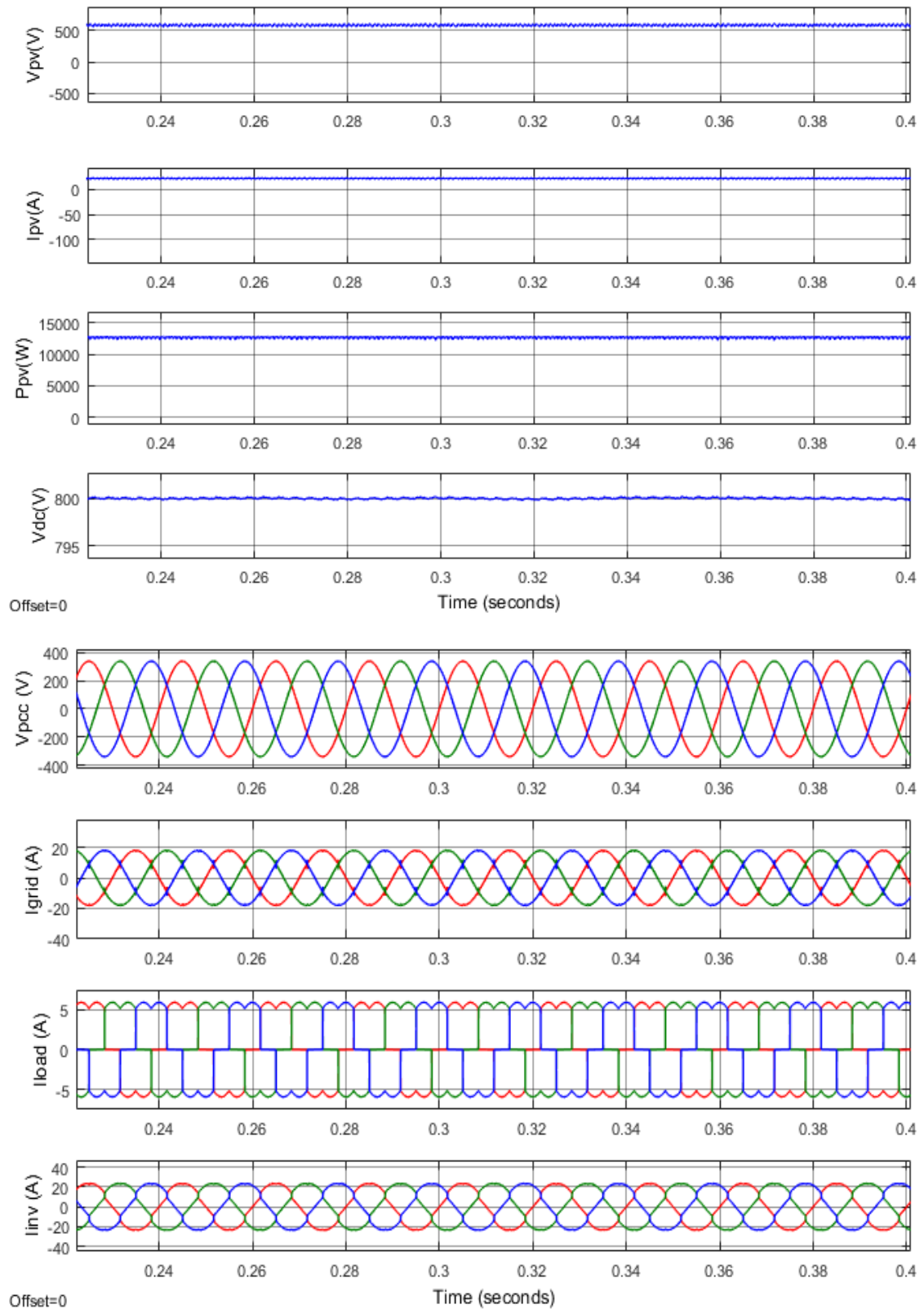


**Figure 4-28. Results of SRFT control with nonlinear load**

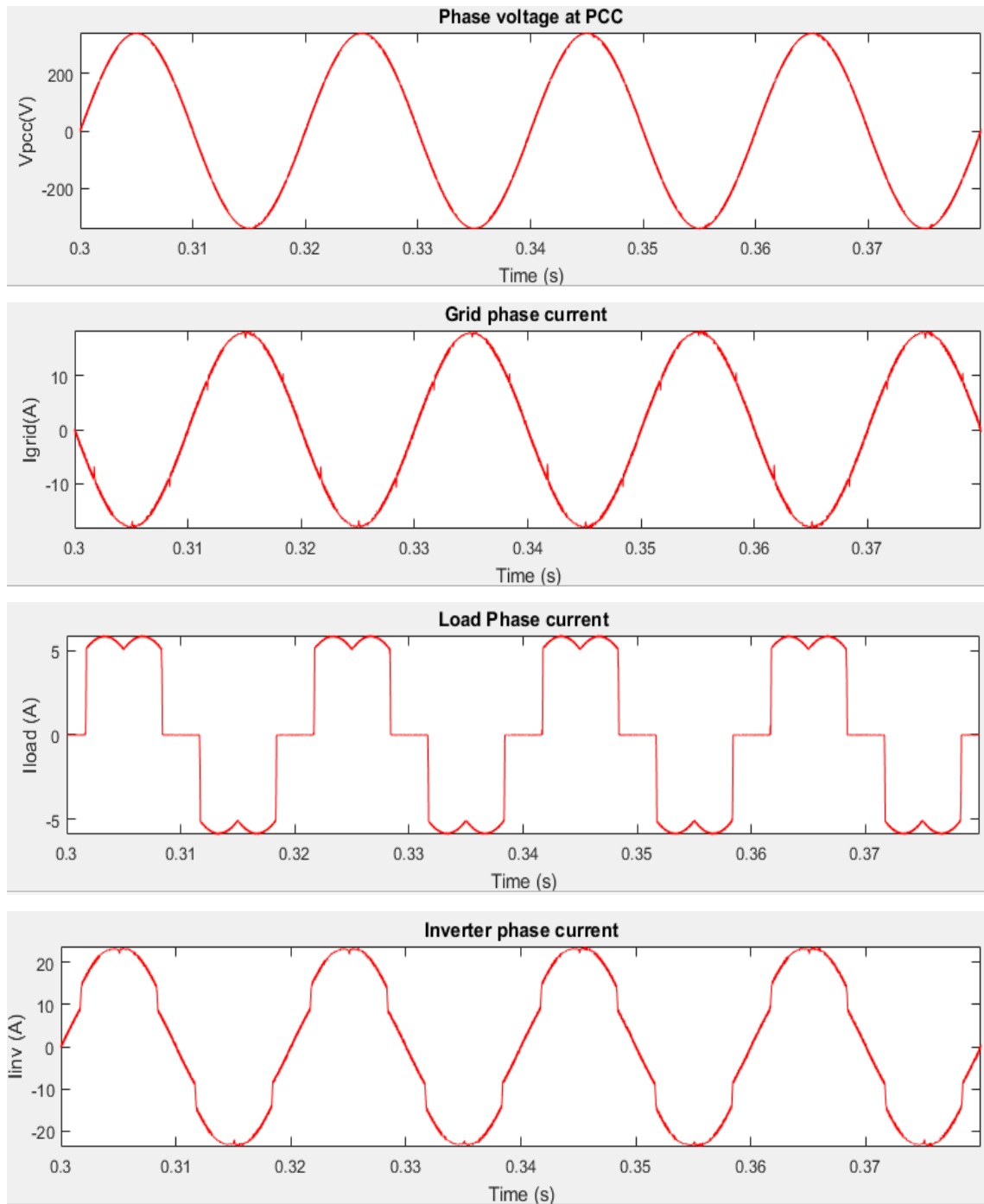
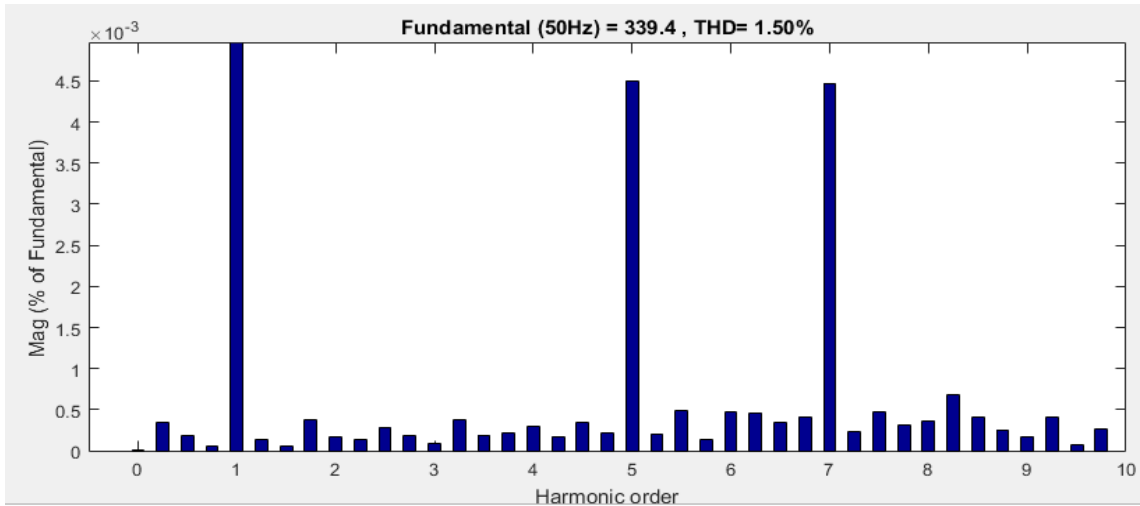
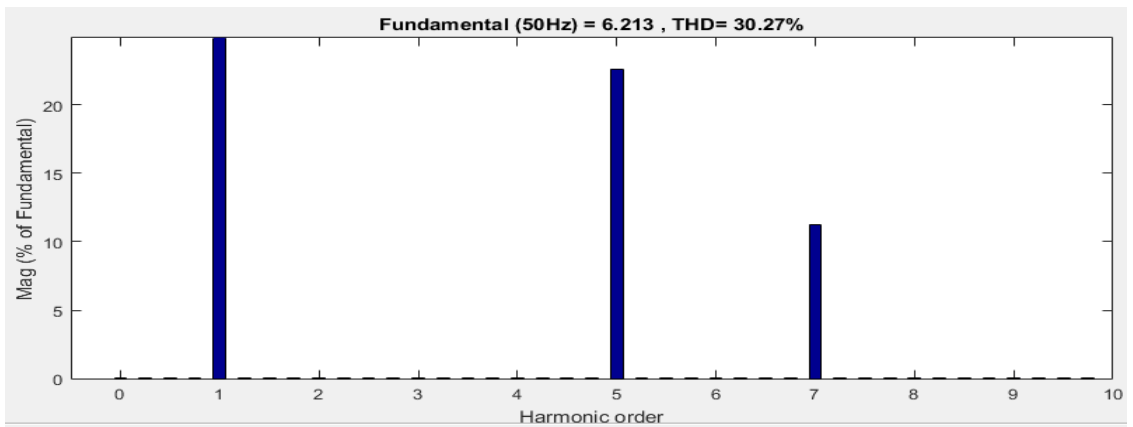


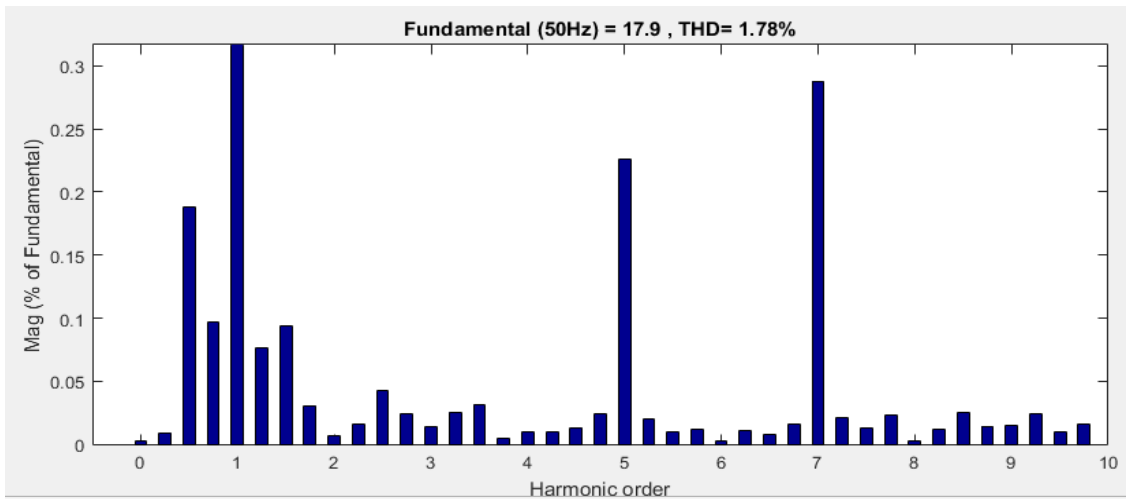
**Figure 4-29. Current profile in SRFT control for non-linear load**



(a) Voltage at PCC



(b) Load current



(c) Grid current

**Figure 4-30. Harmonic profile in SRFT control for non-linear load**

#### 4.8.4 Results for Indirect SRFT Control

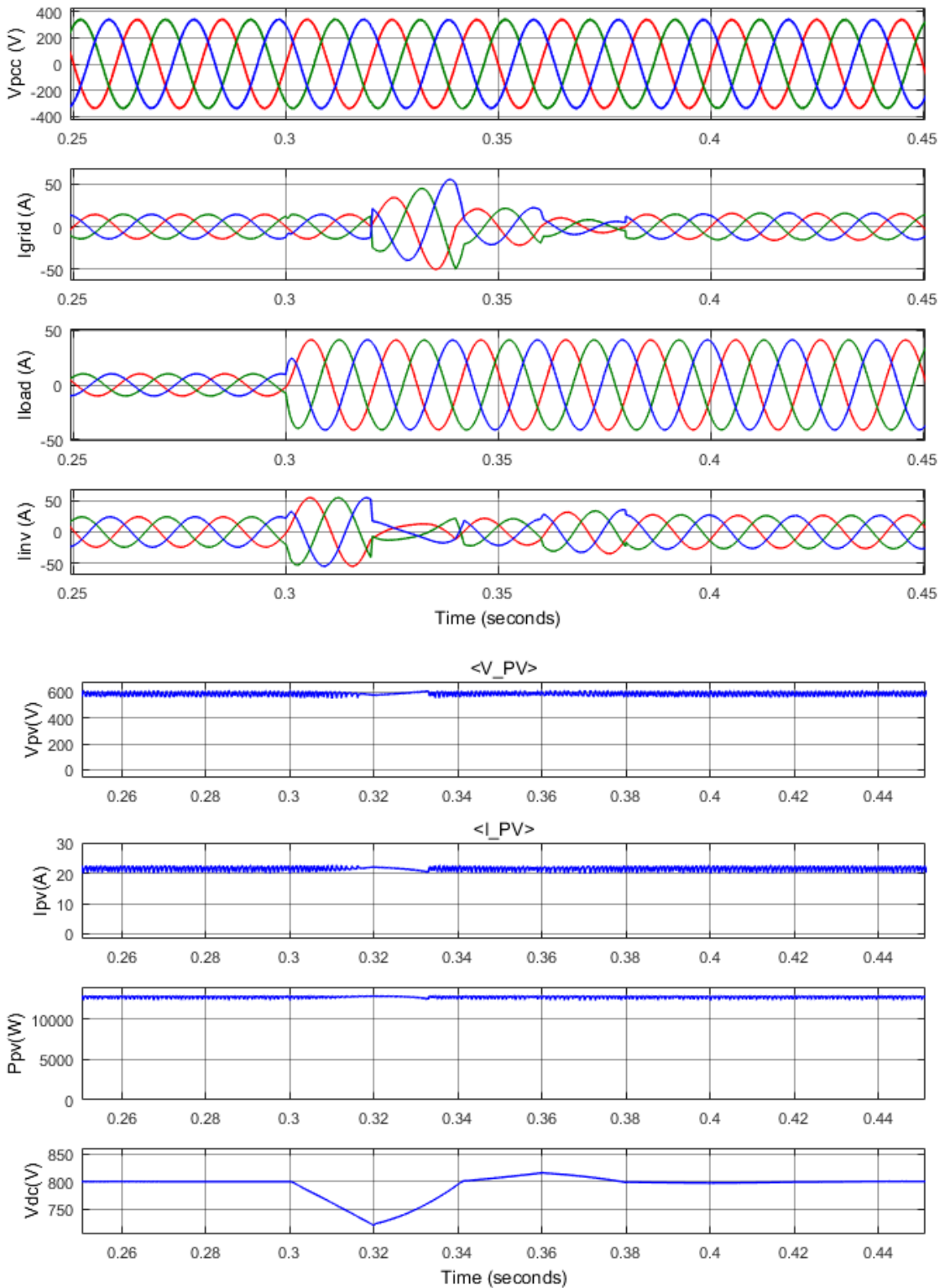
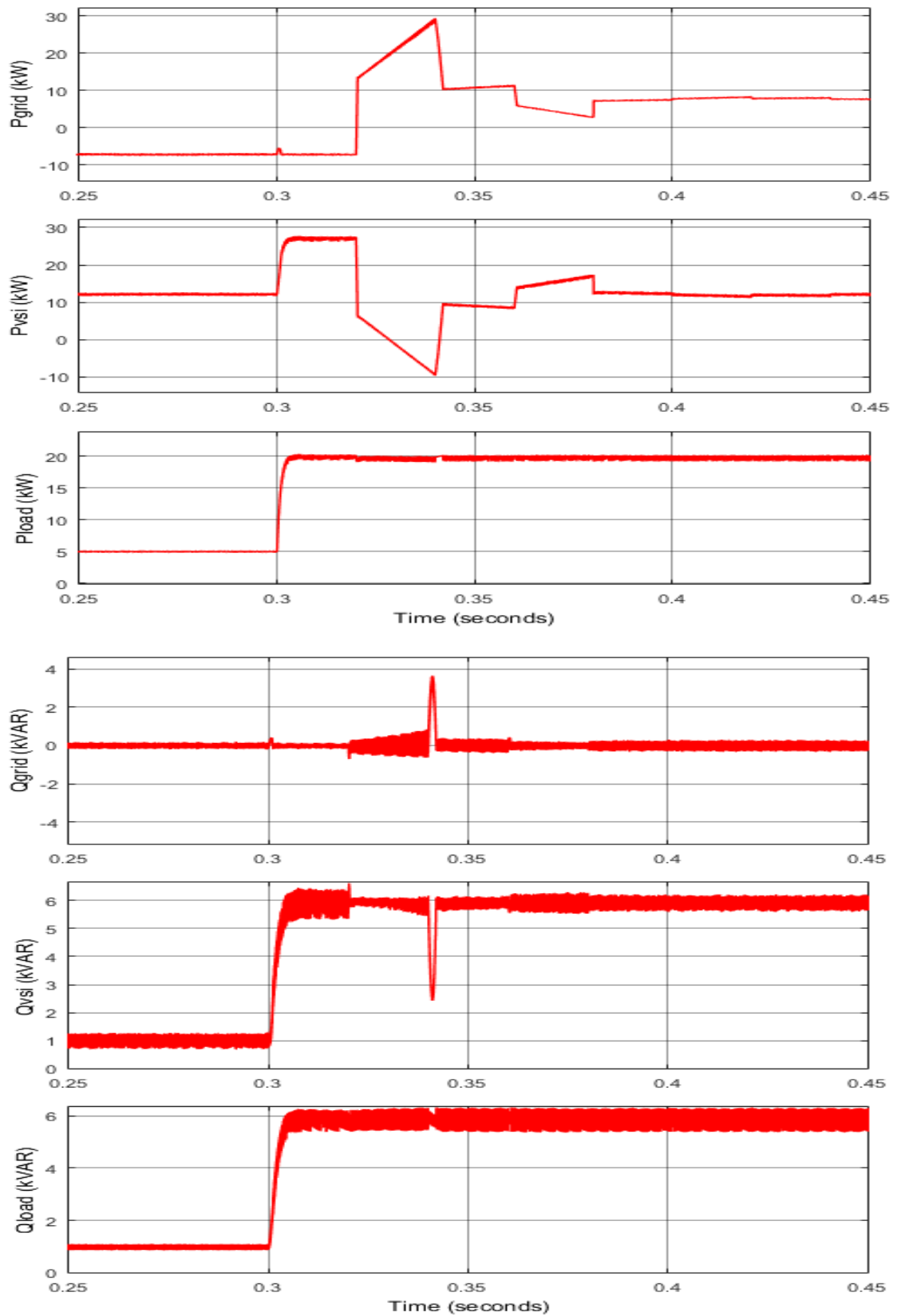
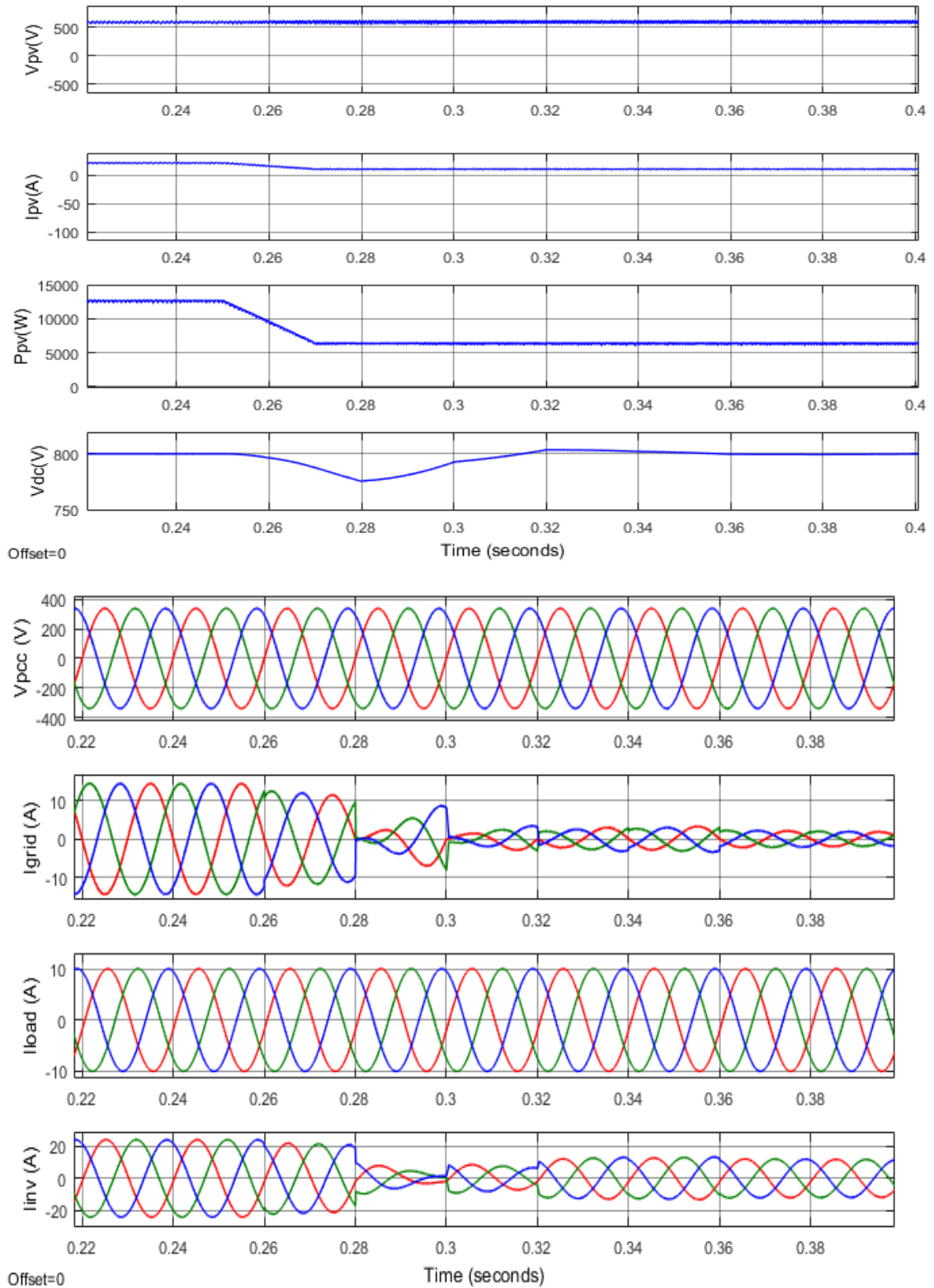


Figure 4-31. Results of Indirect SRFT control for dynamic switching of linear load





**Figure 4-32. Results of Indirect SRFT control for dynamic switching of linear load showing real and reactive power of grid, VSI and load respectively**



**Figure 4-33. Results of Indirect SRFT control with linear load and change in solar irradiance**

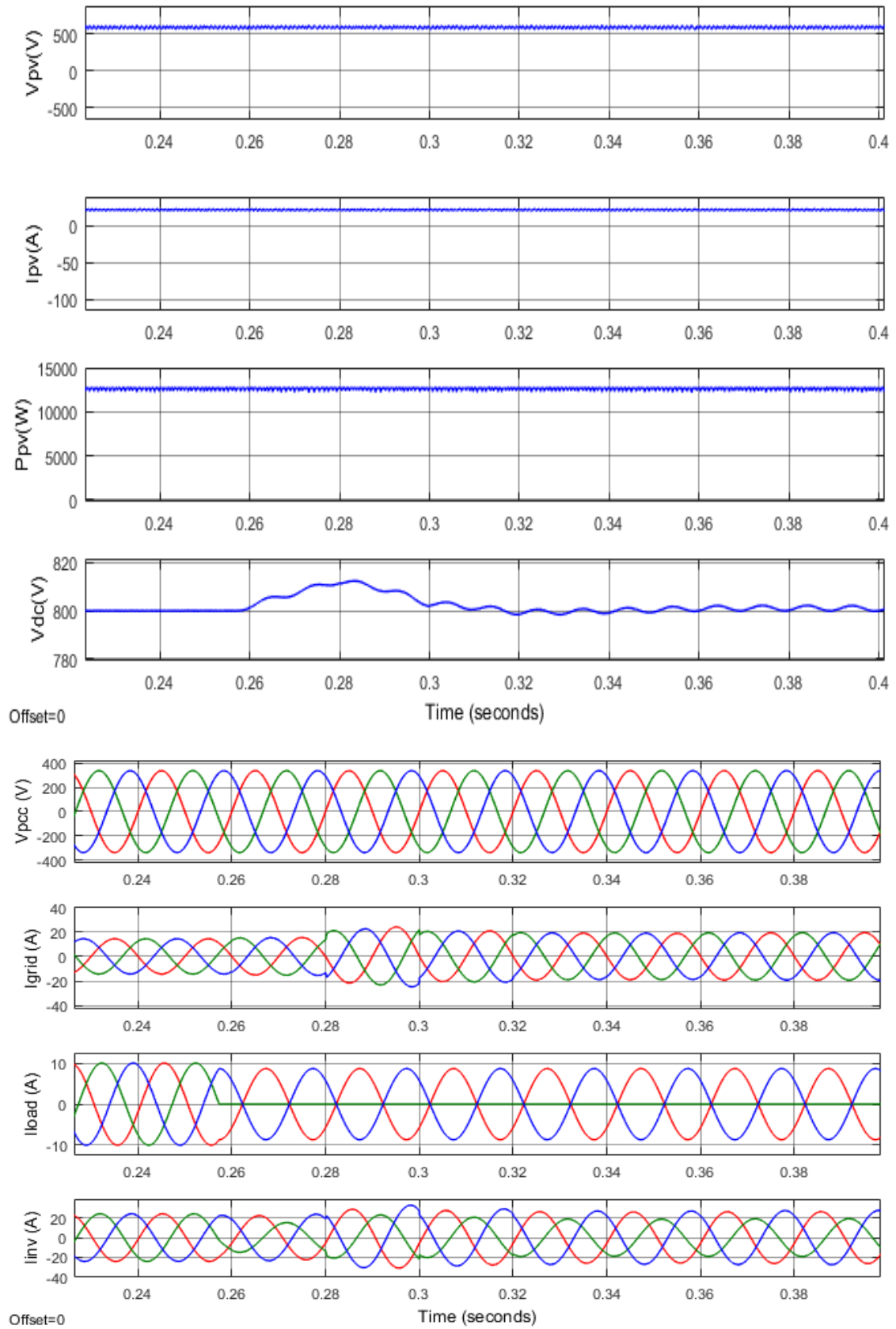


**Figure 4-34. Results of Indirect SRFT control with unbalanced load**

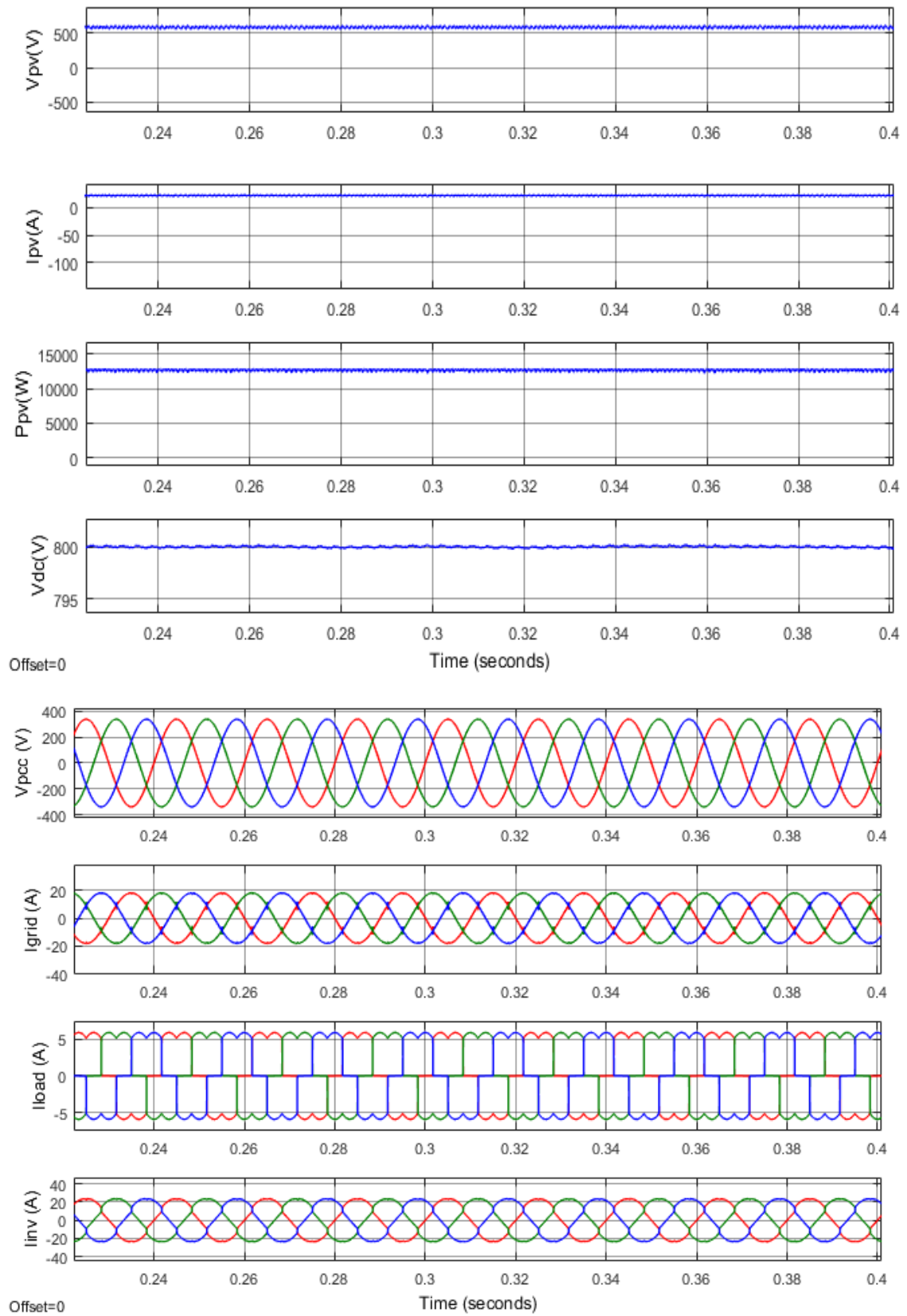


**Figure 4-35. Results of Indirect SRFT control with nonlinear load**

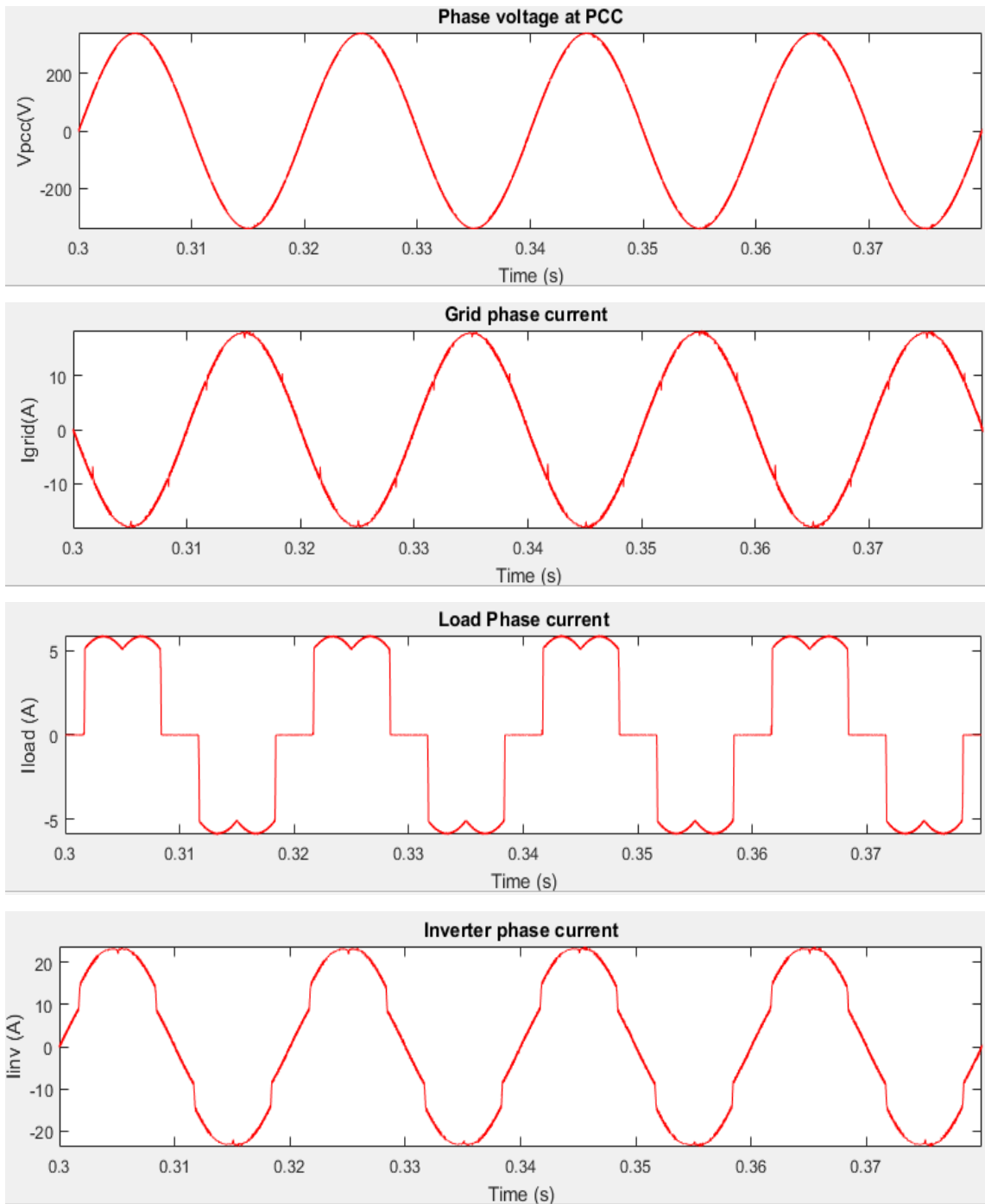
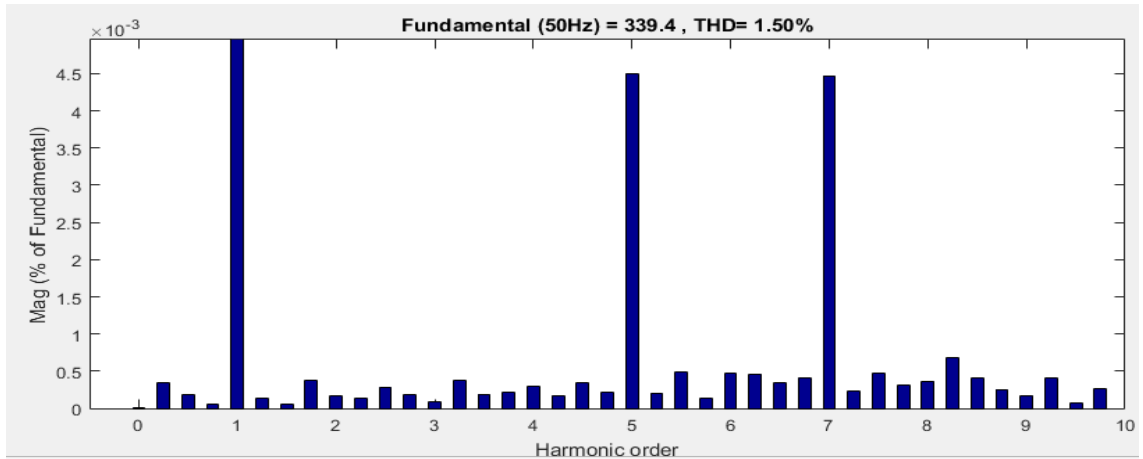
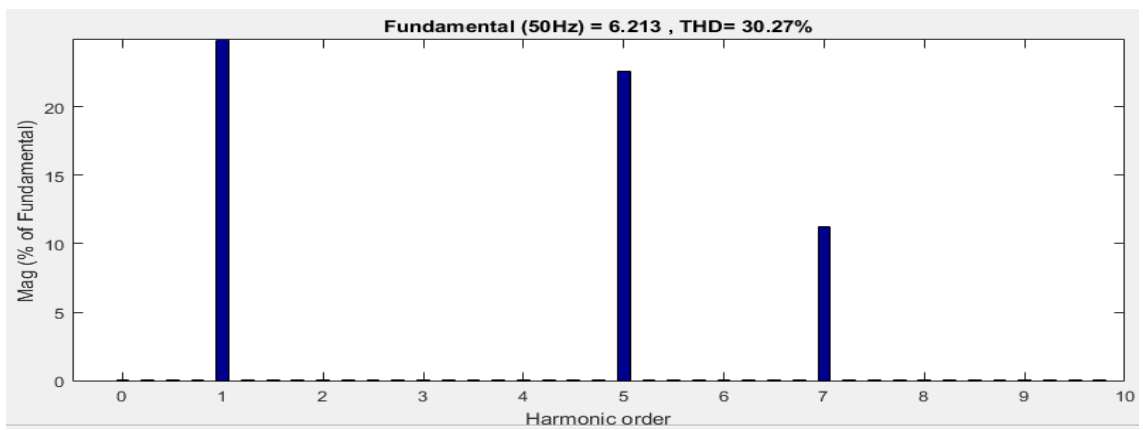


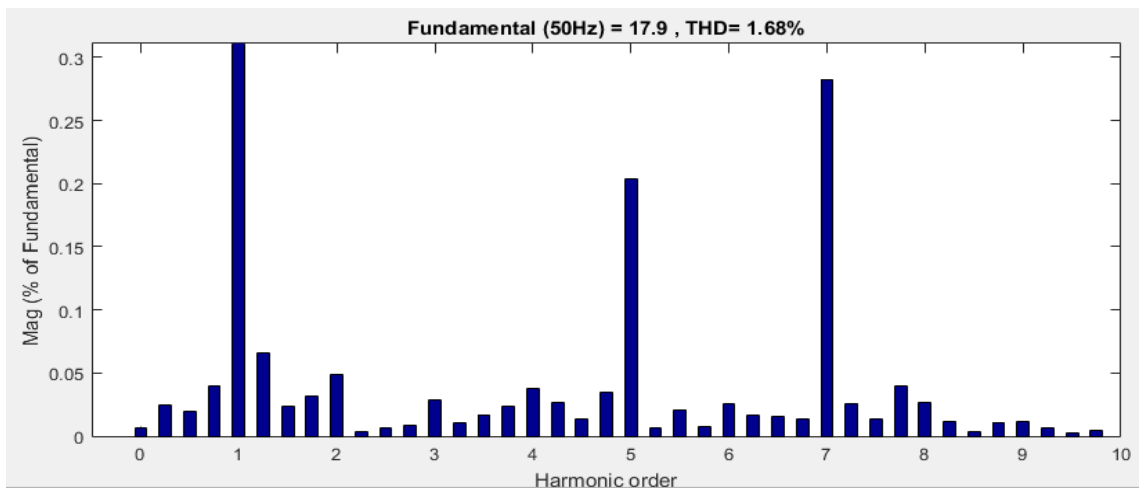
**Figure 4-36. Current profile for Indirect SRFT control for non-linear load**



(a) Voltage at PCC



(b) Load current



(c) Grid current

Figure 4-37. Harmonic spectrum in Indirect SRFT control for non-linear load

## 4.9 Observations

### Dynamic switching of linear load:

It is observed that all the control algorithm gives satisfactory performance for this case. The MPPT control is tracking maximum power of 12.789 kW from PV array at standard irradiance and temperature and this power is injected into the grid. 5 kW out of 12.789 kW is absorbed by the load and remaining 7.789 kW is injected into the grid as it can be seen in the results that grid current is  $180^\circ$  out of phase with grid voltage. Also, the reactive power of the load is supplied by the VSI. The dc-link voltage remains stable at 800 volts. It is seen at 0.3 seconds when an additional linear load is switched in parallel to the existing load. The real power load demand increases to 20 kW and reactive power load demand increases to 6 kVAR. As now the connected load kW is greater than that generated by PV therefore grid starts supplies the balance power of 7.211 kW. It can also be observed that the reactive power supplied by VSI increases from 1 kVAR to 6 kVAR to cater complete load reactive power demand and thus the grid operates at approximately unity power factor.

### Linear load with change in solar irradiance:

It is observed that all the control algorithm gives satisfactory performance for this case. The MPPT control is tracking maximum power of 12.789 kW from PV array at standard irradiance and temperature and this power is injected into the grid. 5 kW out of 12.789 kW is absorbed by the load and remaining 7.789 kW is injected into the grid as it can be seen in the results that grid current is  $180^\circ$  out of phase with grid voltage. Also, the reactive power of the load is supplied by the VSI. The dc-link voltage remains stable at 800 volts. At 0.25 seconds solar irradiance starts reducing up to  $500 \text{ W/m}^2$ , the output of PV array also reduces to 6.3 kW with little transients in dc-link voltage settling back at 800 Volt. As a result of reduced PV output there is less power injected into the grid hence, we see a reduction in grid current.

### Unbalanced load:

It is observed that all the control algorithm gives satisfactory performance for this case . Initially the MPPT control is tracking maximum power of 12.789 kW from PV array at standard irradiance and temperature and this power is injected into the grid. The dc-link voltage remains stable at 800 volts. At 0.25 second one out of 3-phases of the load is removed which can be seen in 3-phase load current waveform as a result load power is reduced. There is a small transient in dc-link but it settles back to 800 volts, the MPPT

continues to track 12.789 kW of power from PV array, with load power reduced more amount of PV power is now injected into the grid therefore there is increase in grid current value which is out of phase with the grid voltage hence absorbing power. The grid current is still balanced despite of unbalanced load, this proves compensation ability in case of unbalanced load.

Non-Linear load:

It is observed that all the control algorithm gives satisfactory performance for this case. In this case the system is supplying a 3-phase diode rectifier with resistance  $R_{dc}$  of 100  $\Omega$  connected at its dc side. The 3-phase load current is non-linear with 30.7 % THD, however the 3-phase grid current waveform is close to sinusoidal in nature proving harmonic compensation ability of the two-stage system. The MPPT continues to track 12.789 kW of power from PV array and dc-link is settled at 800 V. However, with different control techniques there is a difference in grid current THD and grid voltage THD given in table 4.3. It can be seen in table 4.3 that the grid current THD without compensation is 30.27 %, there is a tremendous improvement in grid current THD when two-stage system is connected.

**Table 4-3. Grid current and voltage THD in case of non-linear load with different control techniques**

Control Technique	Voltage THD (%)	Current THD (%)
Unit template	1.59	2.43
IRPT	1.59	2.33
SRF	1.50	1.78
Indirect SRF	1.5	1.68

**4.10 Conclusion**

In this chapter the design of a grid connected two-stage system was discussed. Conventional VSI control techniques were discussed. A MATLAB-SIMULINK model for the grid connected two-stage system was developed and its performance was analyzed under dynamic load switching, varying solar input, unbalanced load and non-linear load conditions. The results obtained in MATLAB-SIIMULINK for different control techniques are presented and it is observed that the designed system performs satisfactorily with all control techniques. The system is able to track MPP in PV array and transfer it into the grid and simultaneously compensate for load reactive power, load unbalance and load harmonics.



## CHAPTER 5 HARDWARE IMPLEMENTATION OF DSTATCOM

### 5.1 General

In this chapter a hardware model of DSTATCOM is presented. The design of components of a DSTATCOM is explained. MicroLabBox (dSPACE product) is used for controlling DSTATCOM. The performance of DSTATCOM is analysed for different control algorithms and the results are recorded using FLUKE 435 Series II 3-phase power quality and energy analyzer.

### 5.2 DSTATCOM

A DSTATCOM is a custom power device used at distribution level to compensate for load reactive power, load unbalance, and load harmonics. Figure 5.1 shows the block diagram of the hardware setup of DSTATCOM. The DSTATCOM consists of a two level VSI which is connected in shunt to the grid at point of common coupling (PCC). The PCC voltages, load currents and output current of VSI are sensed and given as input to the MicroLabBox. MicroLabBox based on sensed inputs and programmed control algorithm generates gate pulses for the VSI and thus controls the compensating current injected into the grid such that grid current is sinusoidal, balanced and in phase with grid voltage.

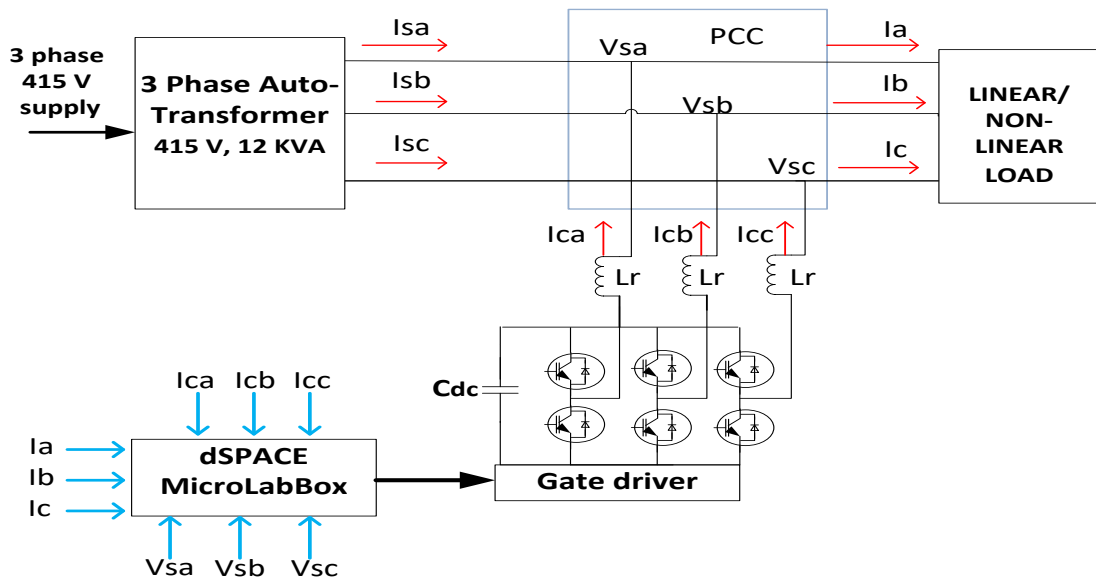


Figure 5-1. Block diagram for hardware setup of DSTATCOM

There are several control techniques available for DSTATCOM like Instantaneous reactive power theory (IRPT), Synchronous reference frame theory (SRF), Power balance theory, Conductance based current algorithm, etc.

### 5.3 Hardware Setup of DSTATCOM

Figure 5.2 shows the hardware setup developed for DSTATCOM. The DSTATCOM is developed for 3-phase, 3 wire system with system voltage equal to 110 V. The available 3-phase, 415 V is stepped down to 3-phase,110 V using a 3-phase auto transformer.

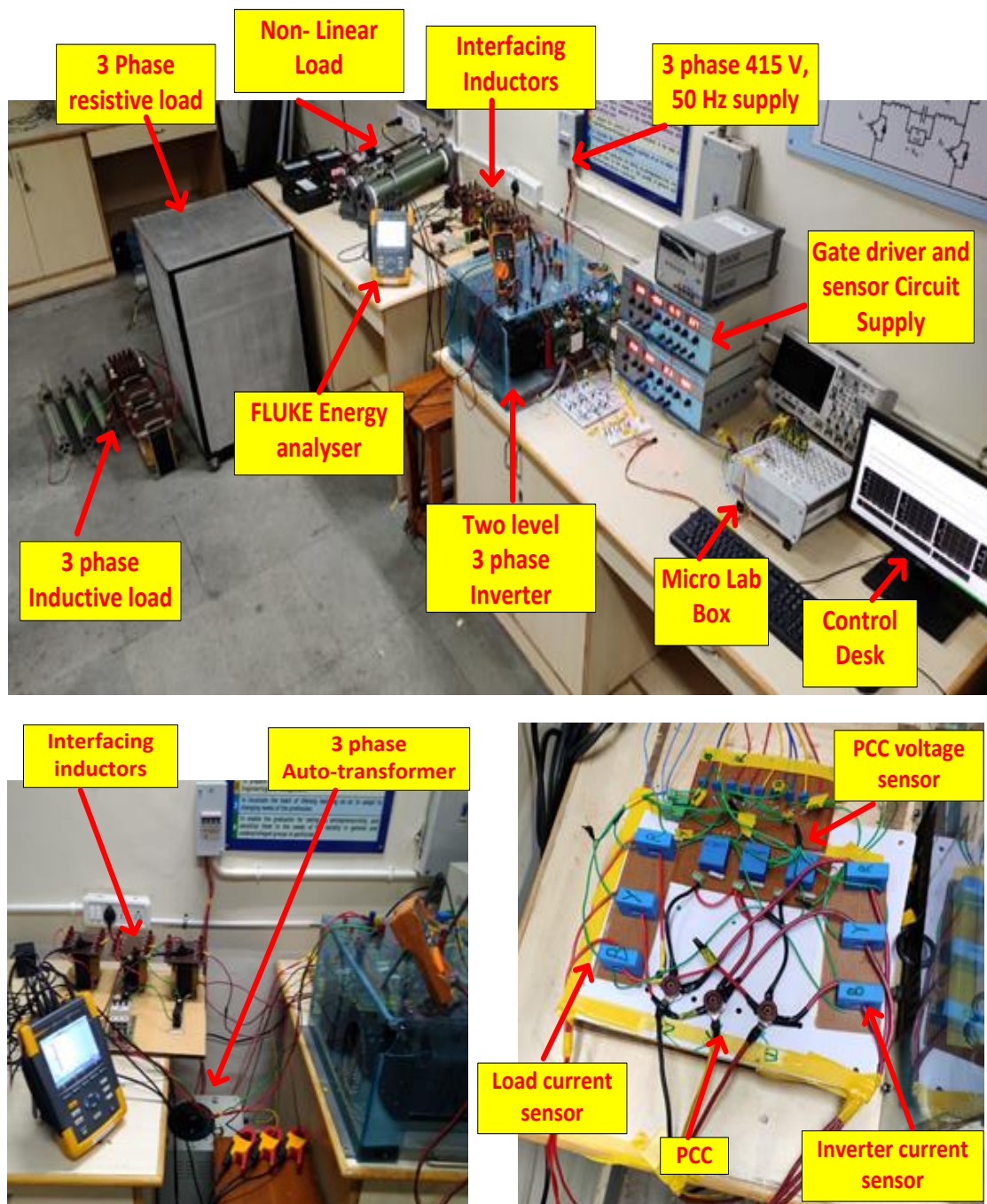


Figure 5-2. Hardware setup of DSTATCOM

### 5.3.1 Choice of DC-link voltage ( $V_{dc}$ )

In order to achieve proper operation of the VSI, the minimum dc-link voltage of  $V_{dc}$  should be greater than twice the peak phase voltage on the ac side of the VSI [36].

$$.V_{dc} \geq (2 * \sqrt{2} * V_{LL})/\sqrt{3} \quad (5.1)$$

Here  $V_{LL}$  is ac side line voltage = 110 V. The calculated value of the  $V_{dc}$  from equation 5.1 is 179.63 V, selected value of  $V_{dc}$  is = 200 V.

### 5.3.2 Sizing of DC-Link capacitor ( $C_{dc}$ )

The dc-link capacitor shown in figure 5.1 is designed to ensure a stable dc-link voltage with minimum voltage ripple. The value of dc-link capacitor value can be calculated using equation 5.2 [37]:

$$C_{dc} = 6 * k * I_{ph} * V_{ph} * a * t / (V_{dc1}^2 - V_{dc2}^2) \quad (5.2)$$

Here  $V_{ph}$  is phase voltage = 63.5 V,  $I_{ph}$  is phase current of inverter = 4A,  $k$  is constant = 0.1,  $a$  is overload factor = 1.2,  $t$  is time by which dc voltage recovers to its standard voltage = 0.015 sec,  $V_{dc1}$  is reference voltage = 200V,  $V_{dc2}$  is minimum dc-link voltage = 195 V. The calculated value of dc-link capacitor from equation 5.2 is  $C_{dc} = 1.38$  mF, A

### 5.3.3 Interfacing Inductor ( $L_r$ )

Interfacing inductor  $L_r$  shown in figure 5.1 is designed to minimise the ripple in ac side output current of VSI [35]. The basic equation governing dynamics between VSI and PCC is given by equation 5.3:

$$L_r \frac{di_c}{dt} = V_f - V_S \quad (5.3)$$

Here  $V_f$  is the instantaneous inverter pole voltage of any phase and  $V_S$  is the instantaneous PCC voltage of the corresponding phase. The ripple in current through interfacing inductor will be maximum when  $V_S$  is at its peak equal to  $V_{Sm}$ , at this instant the average value of inverter pole can be considered equal to  $1.1 * V_{Sm}$  assuming a 10% voltage drop across interfacing inductor. Thus equation 5.3 can be now modified into equation 5.4:

$$L_r \frac{di_c}{dt} = 1.1V_{Sm} - V_{Sm} \quad (5.4)$$

$$L_r \frac{di_c}{dt} = 0.1V_{Sm} \quad (5.5)$$

In equation 5.5 is simplified version of equation 5.4, here  $V_{Sm}$  is phase voltage = 63.5 V,  $di_c$  is the ripple in inductor current taken to be 0.2 A (at maximum),  $dt$  is the switching time interval taken to be 0.1 ms. The calculated value of  $L_r$  comes out to be 3.175 mH. A higher value of inductor  $L_r = 5$  mH, 10 A is used.

### **5.3.4 Voltage Source Inverter**

A 3-phase two level VSI is used as shown in figure 5.1. VSI has three legs, each leg is made of two IGBT switches called the top switch (connected to positive of dc-link) and bottom switch (connected to negative of dc-link) of the leg. The midpoint of each leg is connected to ac output of VSI. IGBT switches have inbuilt reverse conducting diodes. Each IGBT switch should be capable of blocking complete dc-link voltage therefore the voltage rating of IGBT switches should be selected accordingly, in our design we have  $V_{dc}$  equal to 200V therefore with safety factor of 1.5 IGBT voltage rating should be 300 V. The current rating of each switch depends on the current that will flow through the switch, this current is composed of the load reactive power, load balancing and harmonic compensating currents. Thus, the current rating depends on the load compensation required. The IGBT switches used in the model have a voltage rating of 1200 V and current rating of 75 A which are much higher ratings than required in this model.

### **5.3.5 Gate Driver Circuit**

Three SKYPER 32 R IGBT module drivers are used to drive each leg of VSI. These drivers require a 15 V dc supply and also the gate pulse input should be at 15 V level. However, the gate pulse output from MicroLabBox is at 5 V level only. Therefore, the gate driver circuit discussed in chapter 4 which steps up 5 V gate pulse to 15 V is used as intermediate stage to interface the MicroLabBox gate pulse output to the SKYPER 32 R IGBT module drivers.

### **5.3.6 Sensor Circuit**

The sensor circuit described in chapter 3 is used in this model for measurement of 3-phase grid voltage, 3-phase load currents, 3-phase grid currents and 3-phase inverter currents.

## **5.4 Control of DSTATCOM Using MicroLabBox**

The techniques used for control of DSTATCOM are:

1. Unit template based current control algorithm
2. IRPT based current control algorithm
3. SRFT based current control algorithm
4. SRFT based indirect current control algorithm

The MATLAB-SIMULINK model for all the above techniques was presented in the previous chapter. MicroLabBox is compatible with MATLAB-SIMULINK and models built in MATLAB-SIMULINK can be built into program and fed into MicroLabBox.

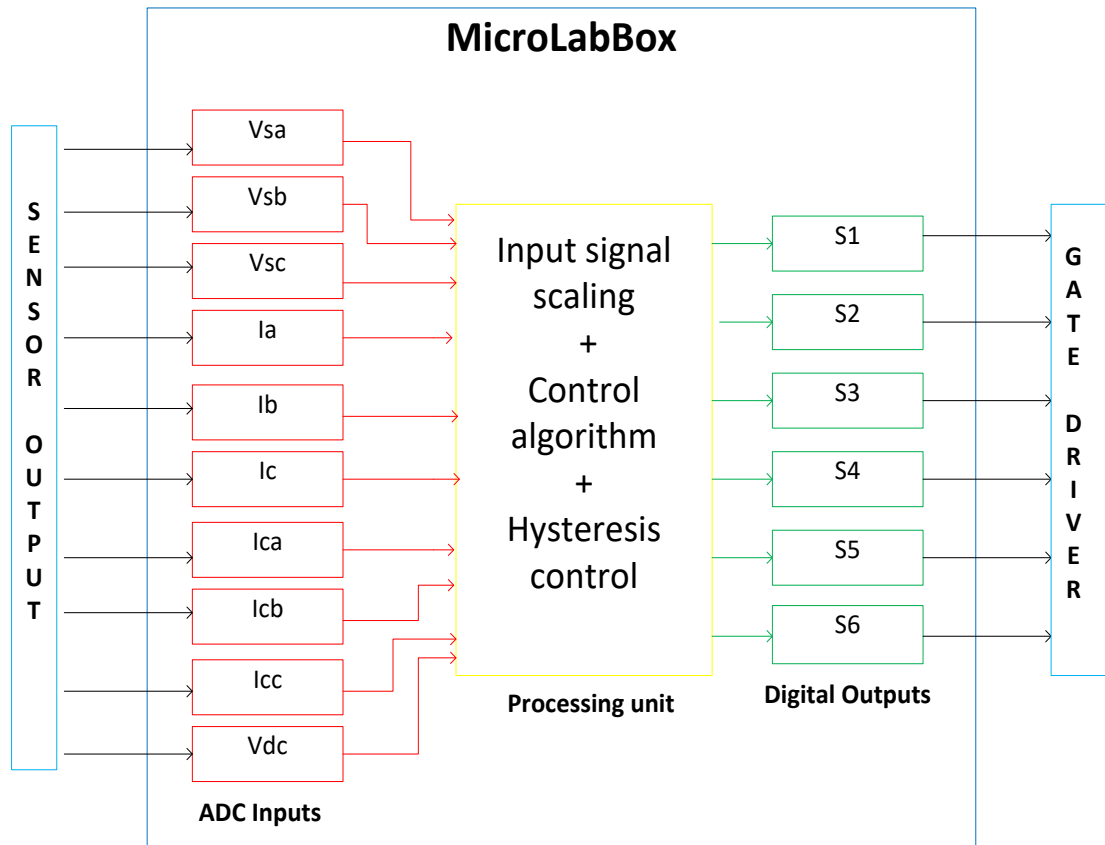


**Figure 5-3. Block diagram for control of DSTATCOM using MicroLabBox**

Figure 5.3 shows the block diagram for control of DSTATCOM, the outputs of the sensor circuit which are PCC voltage, load current, inverter output current/grid current and dc-link voltage respectively are given as input to the ADC channel of MicroLabBox. These signals are processed and reference inverter/grid currents are generated based on the control algorithm used. The switching signals are generated through hysteresis current control at digital output pins of the MicroLabBox. These digital outputs are connected to gate driver circuits for switching VSI.

## 5.5 Specifications of Hardware Model for DSTATCOM

Table 5.1 gives specifications of the hardware model developed for DSTATCOM.

**Table 5.1. Specifications for hardware model for DSTATCOM**

3-phase autotransformer	415 V, 12 KVA
System voltage	110 V (line-line)
Controller	Micro Lab Box
DC-Link Reference voltage	200 V
DC-Link capacitor	1.5 mF, 1200 V
Interfacing Inductors	5 mH, 10 A
IGBT module	1200 V, 75 A
Gate driver	SKYPER 32 R, IGBT module driver
Voltage sensor	LV25-P
Current sensor	LA25-P
Loads	Linear Load: 3phase resistive bank (415 V, 5 kW), three Inductors (20 mH, 25 A), 5 rheostats (5A, 50Ω), Non-Linear Load: 3-phase diode rectifier (35 A)

## 5.6 Hardware Results for DSTATCOM

The hardware setup was tested for compensation of reactive power of load, load harmonics and load unbalance with different control techniques. The results were recorded through FLUKE 435 Series II 3-phase power quality and energy analyzer and are presented for each case in the following sections.

### 5.6.1 Grid Voltage and Current Profile for Different Types of Load without Compensation

This section compiles the waveforms, THD profiles, phasor analysis, power and energy details of grid currents and PCC voltages for different loadings when DSTATCOM was not connected.

#### 1) Linear Load

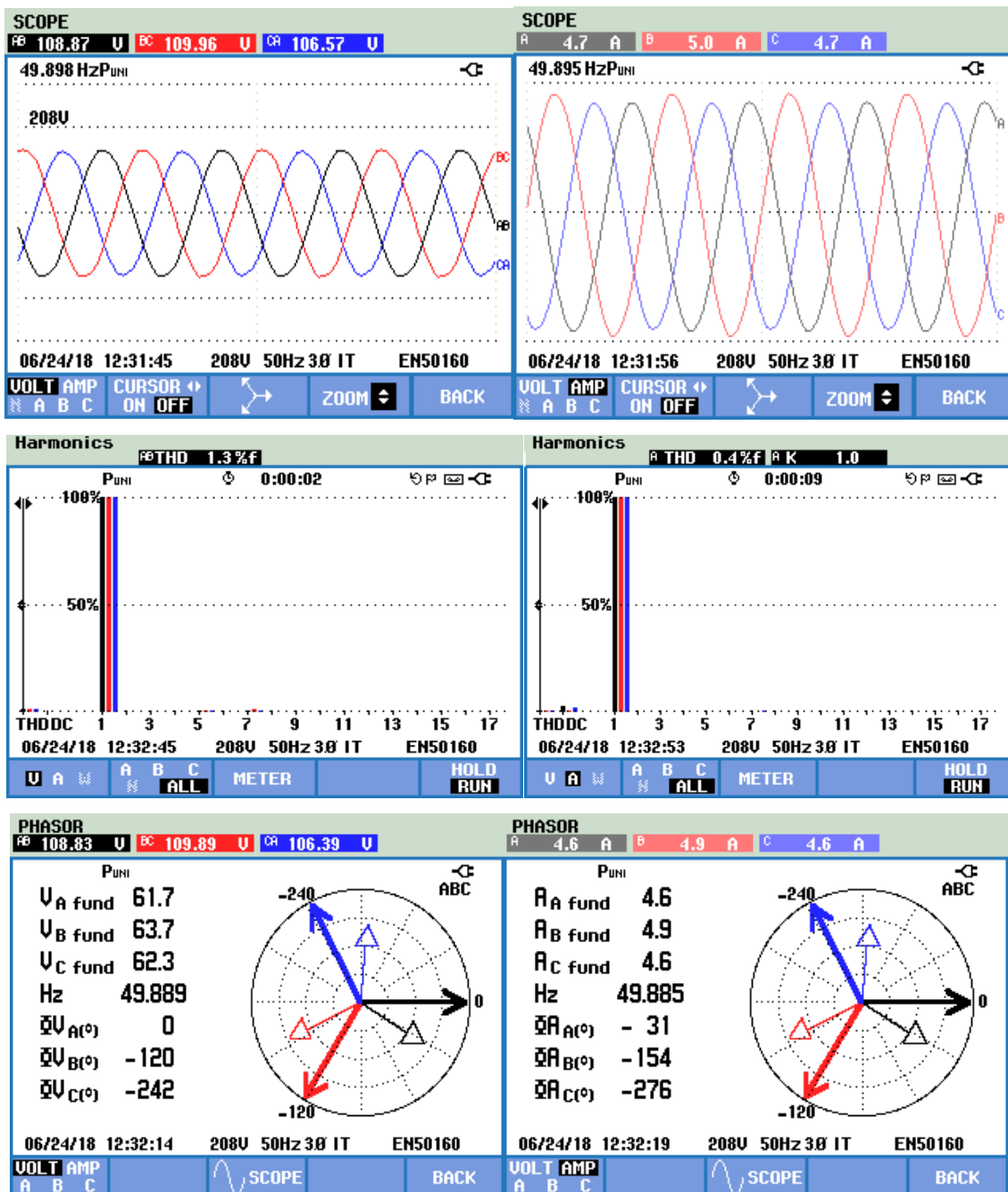


Figure 5-4. Grid voltage and current respectively in case of linear load without compensation

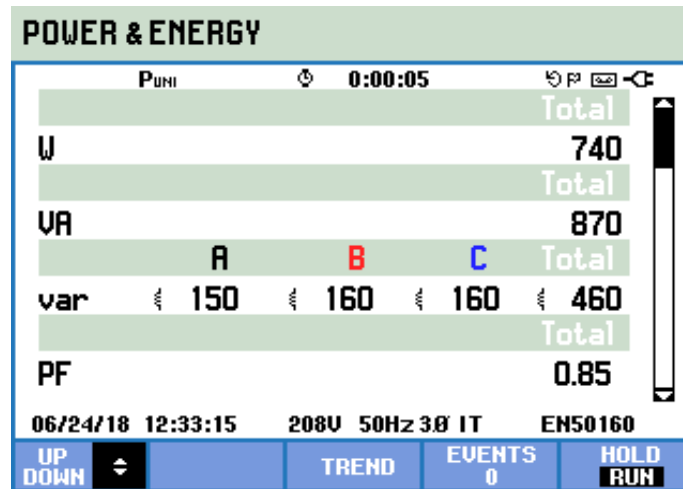


Figure 5-5. Grid Power analysis in case of linear load without compensation

## 2) Non-Linear Load

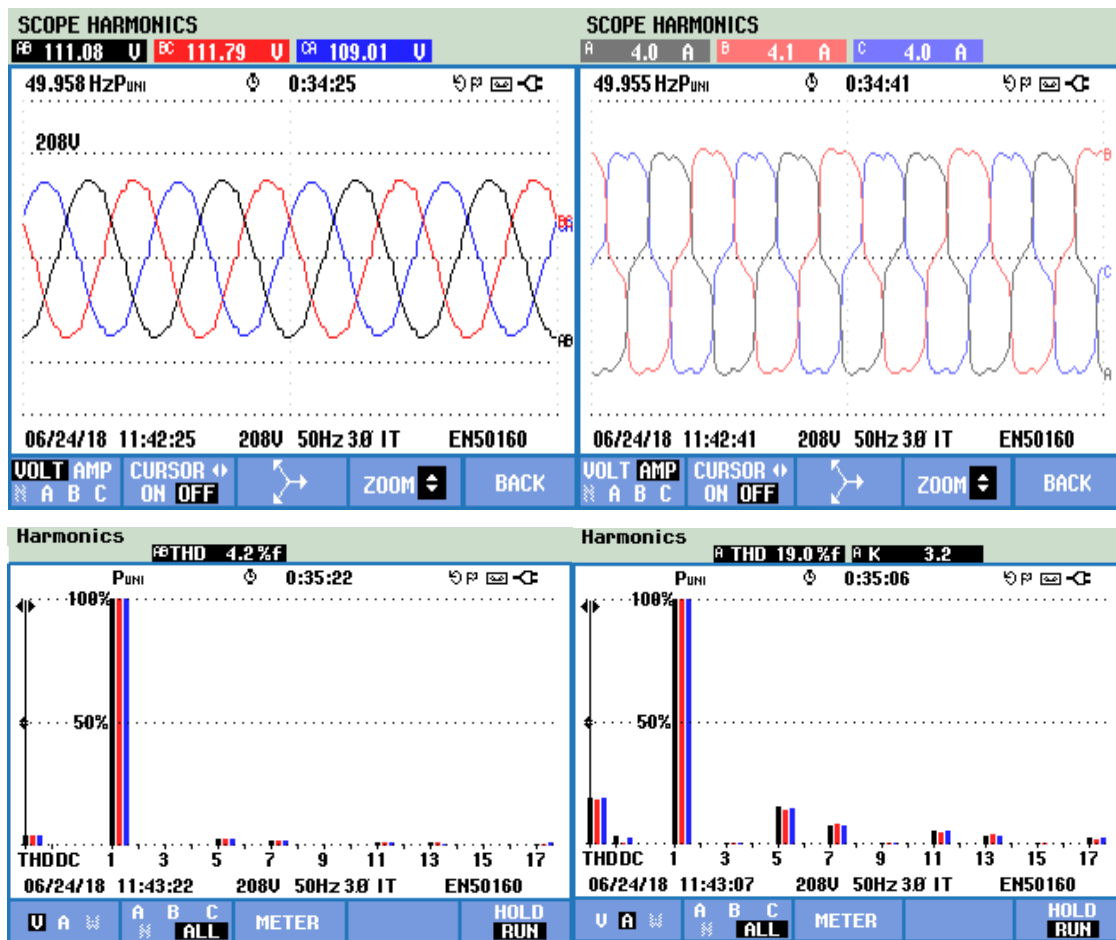


Figure 5-6. Grid voltage and current respectively in case of non-linear load without compensation



### 5.6.2 Results for Unit Template Control

This section compiles the waveforms, THD profiles, phasor analysis, power and energy details of grid currents and PCC voltages for different loadings when DSTATCOM is connected and unit template control algorithm is used.

#### 1) Linear Load

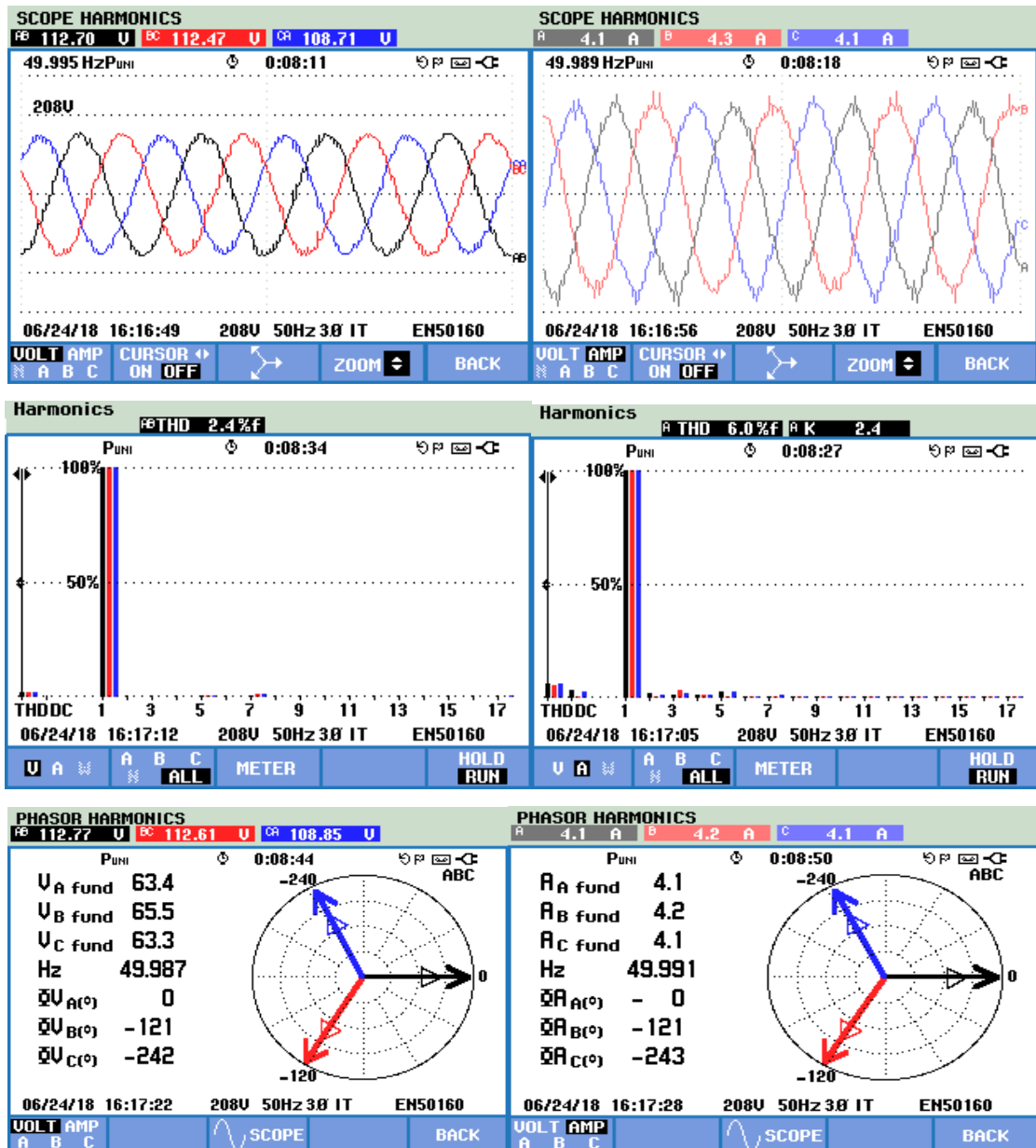
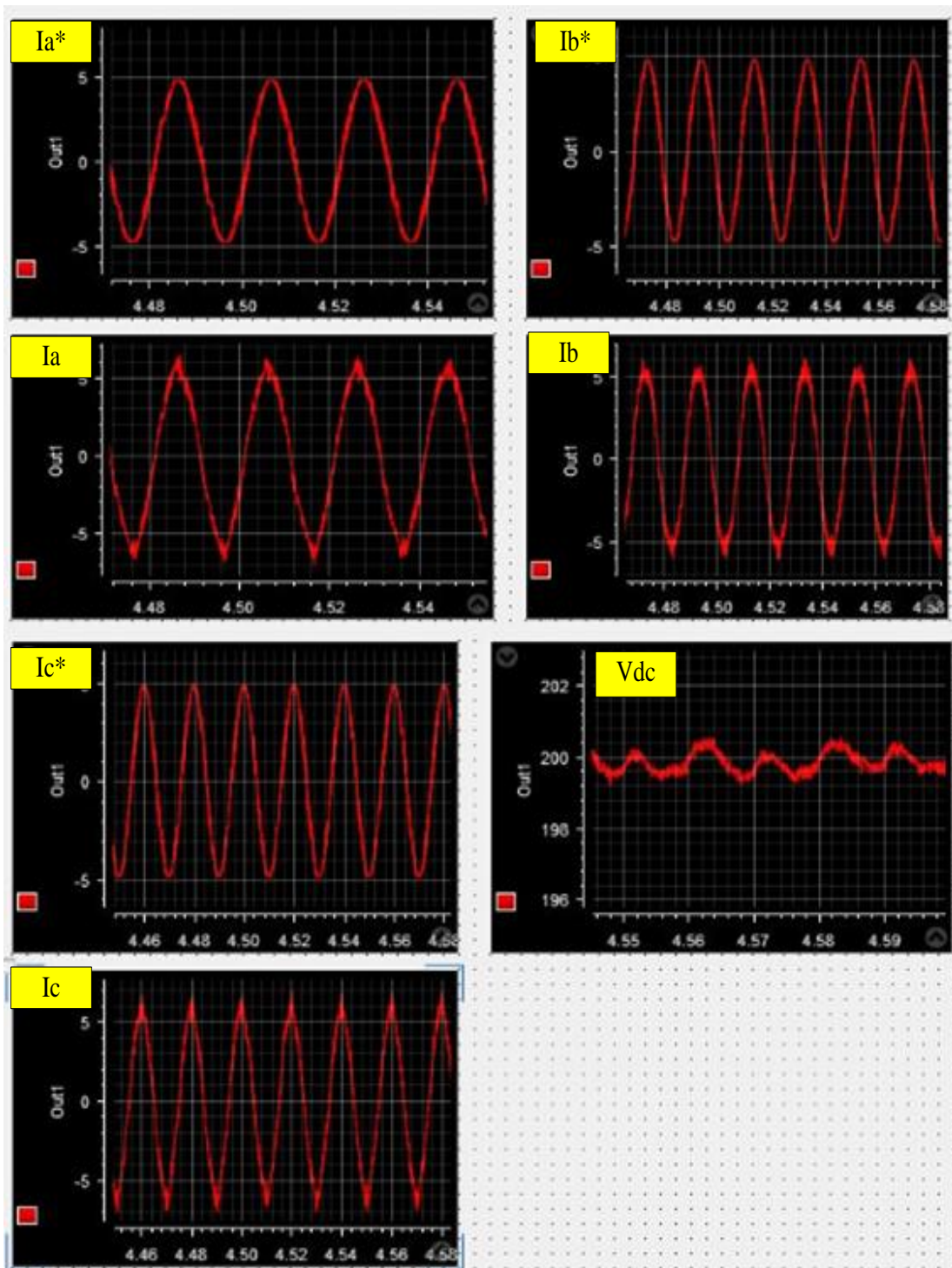


Figure 5-7. Compensated grid voltage and current in case of linear load with Unit template control



**Figure 5-8. Reference grid currents, actual grid currents and dc-link voltage in case of linear load with unit template control**

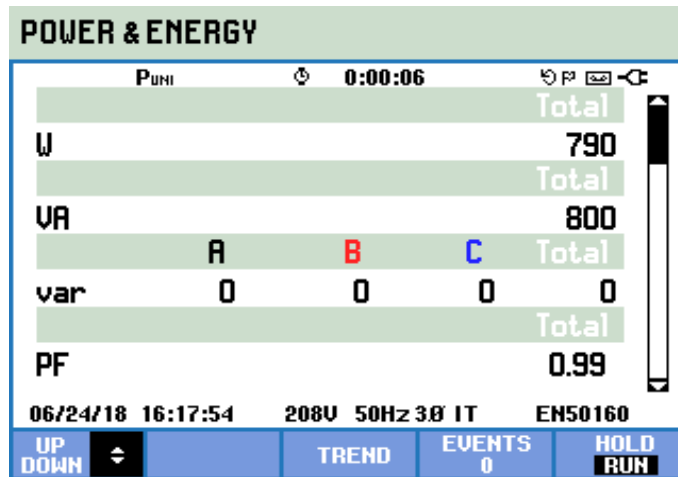


Figure 5-9. Grid power analysis in case of linear load with unit template control

## 2) Non-Linear Load

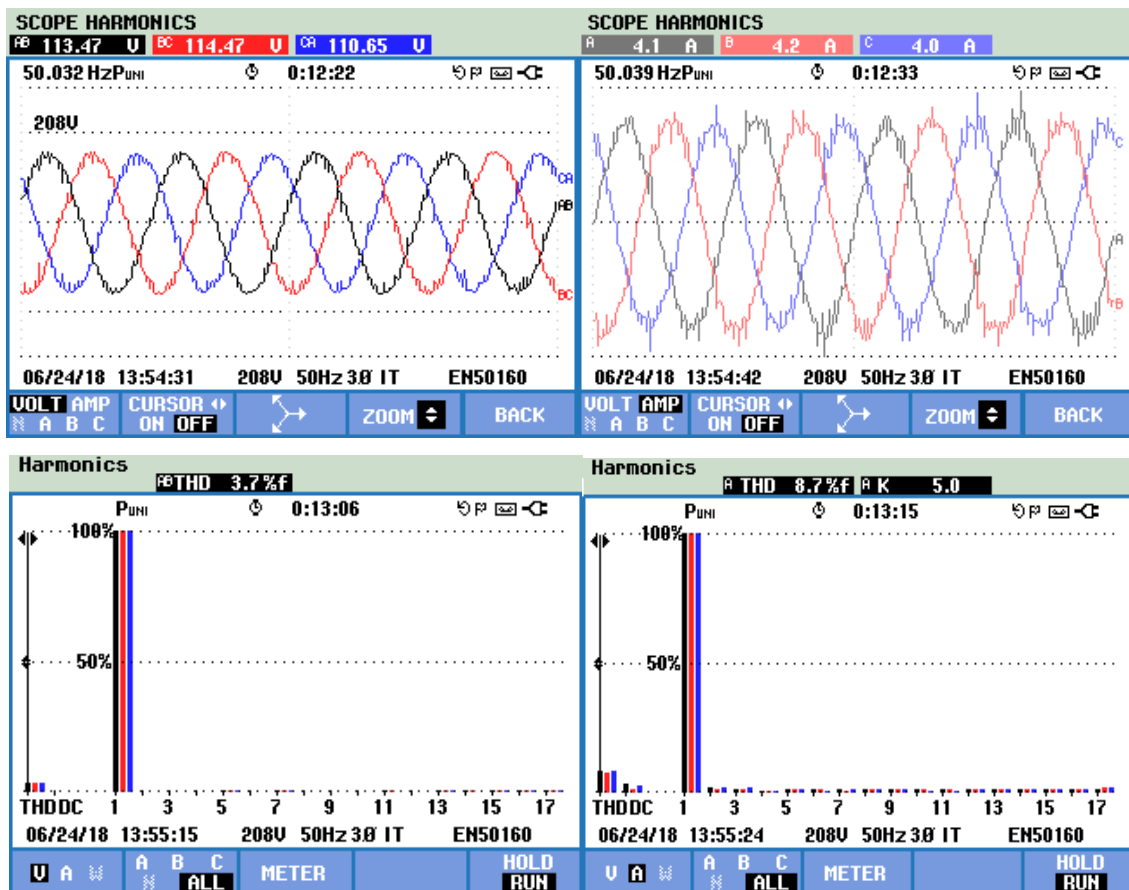


Figure 5-10. Compensated grid voltage and current in case of non-linear load with Unit template control

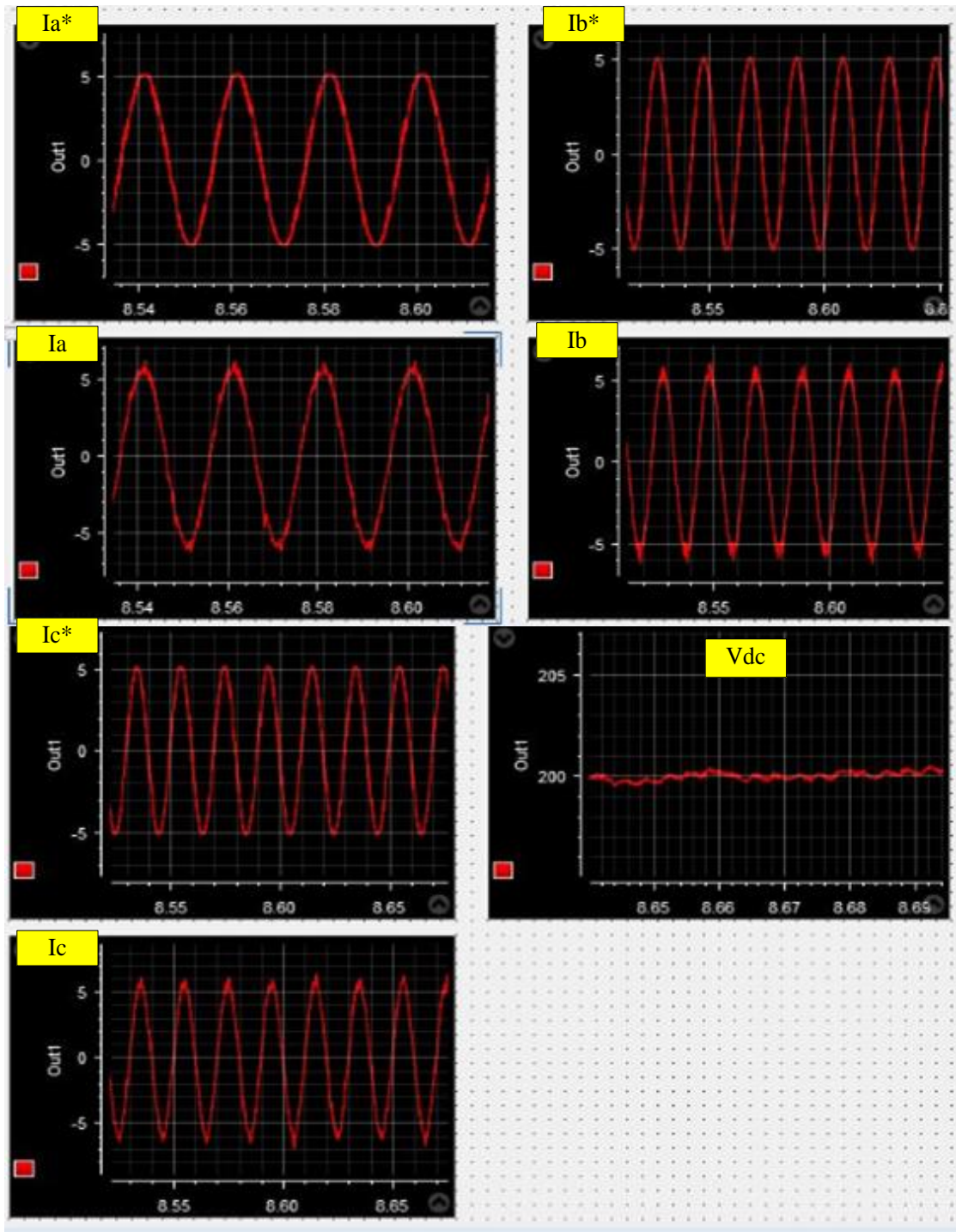


Figure 5-11. Reference grid currents, actual grid currents and dc-link voltage in case of non-linear load with unit template control

### 5.6.3 Results for IRPT Control

This section compiles the waveforms, THD profiles, phasor analysis, power and energy details of grid currents and PCC voltages for different loadings when DSTATCOM is connected and IRPT control algorithm is used.

#### 1) Linear Load

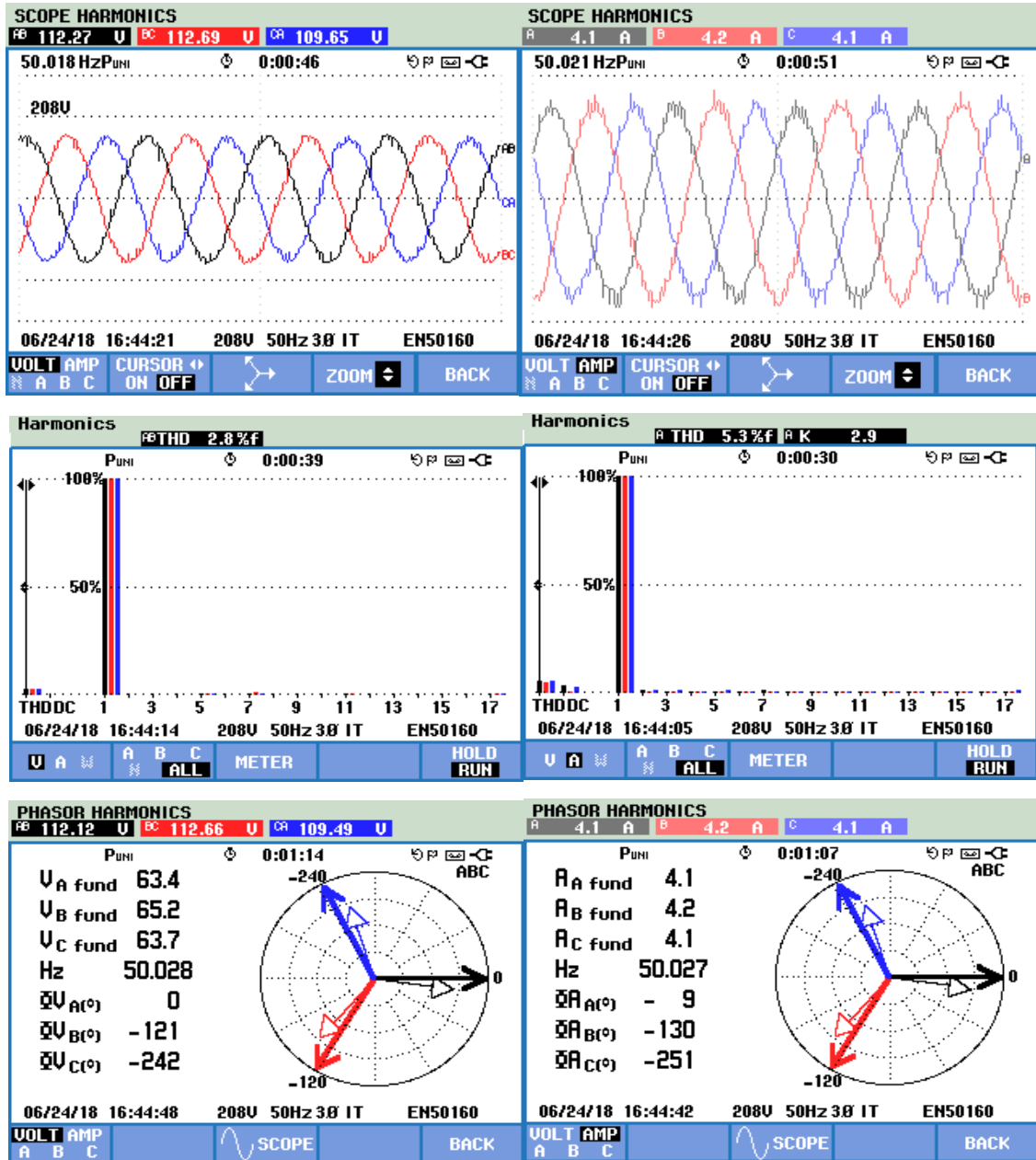
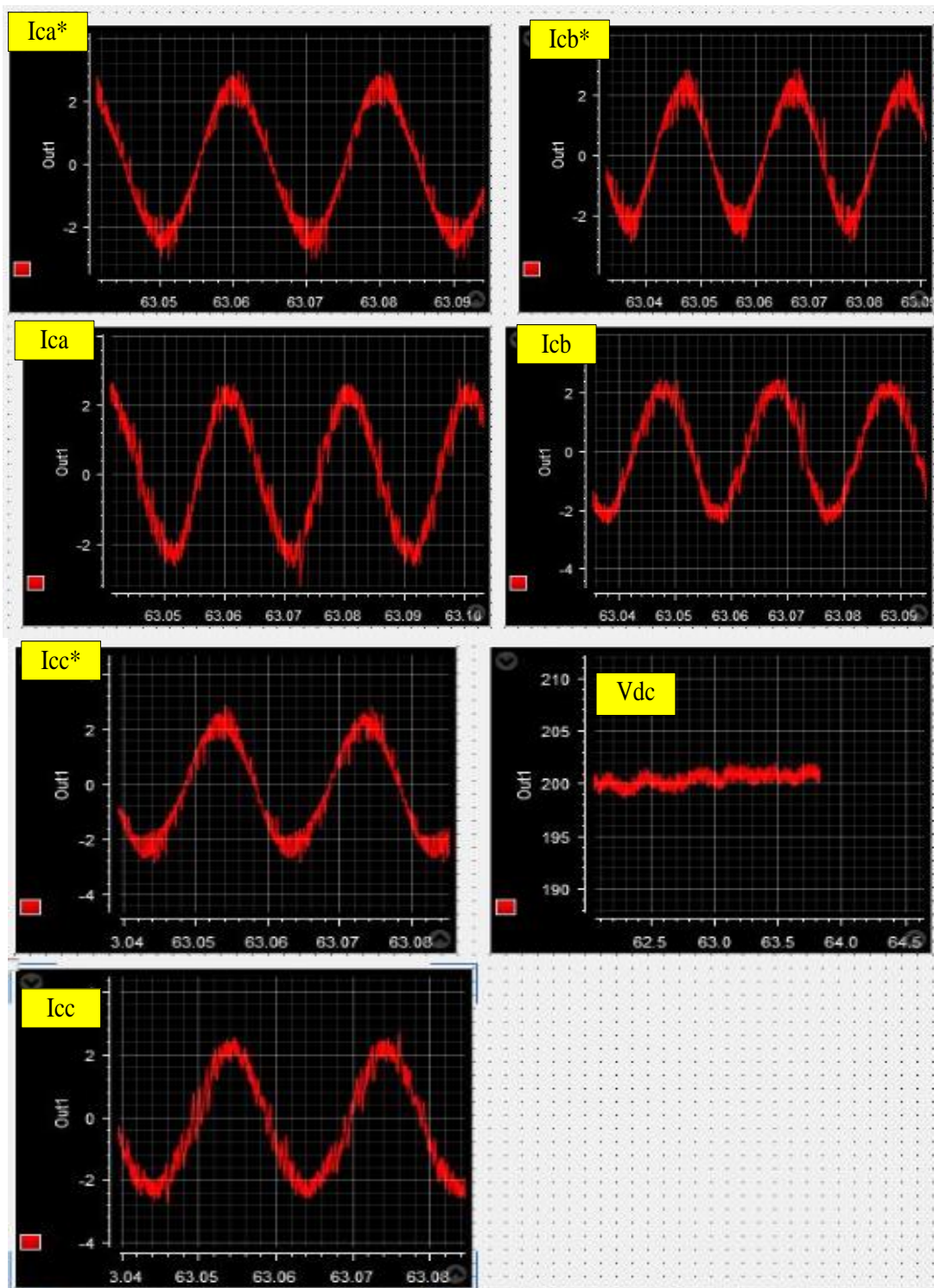


Figure 5-12. Compensated grid voltage and current in case of linear load with IRPT control





**Figure 5-13. Reference VSI currents, actual VSI currents and dc-link voltage in case of linear load with IRPT control**

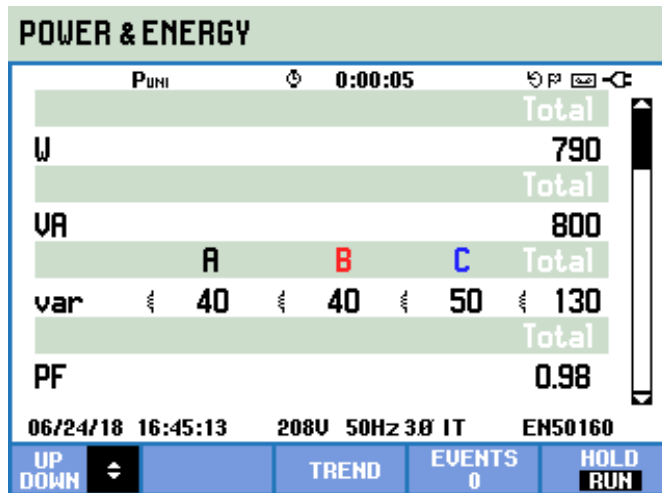


Figure 5-14. Grid power analysis in case of linear load with IRPT control

## 2) Non-Linear Load

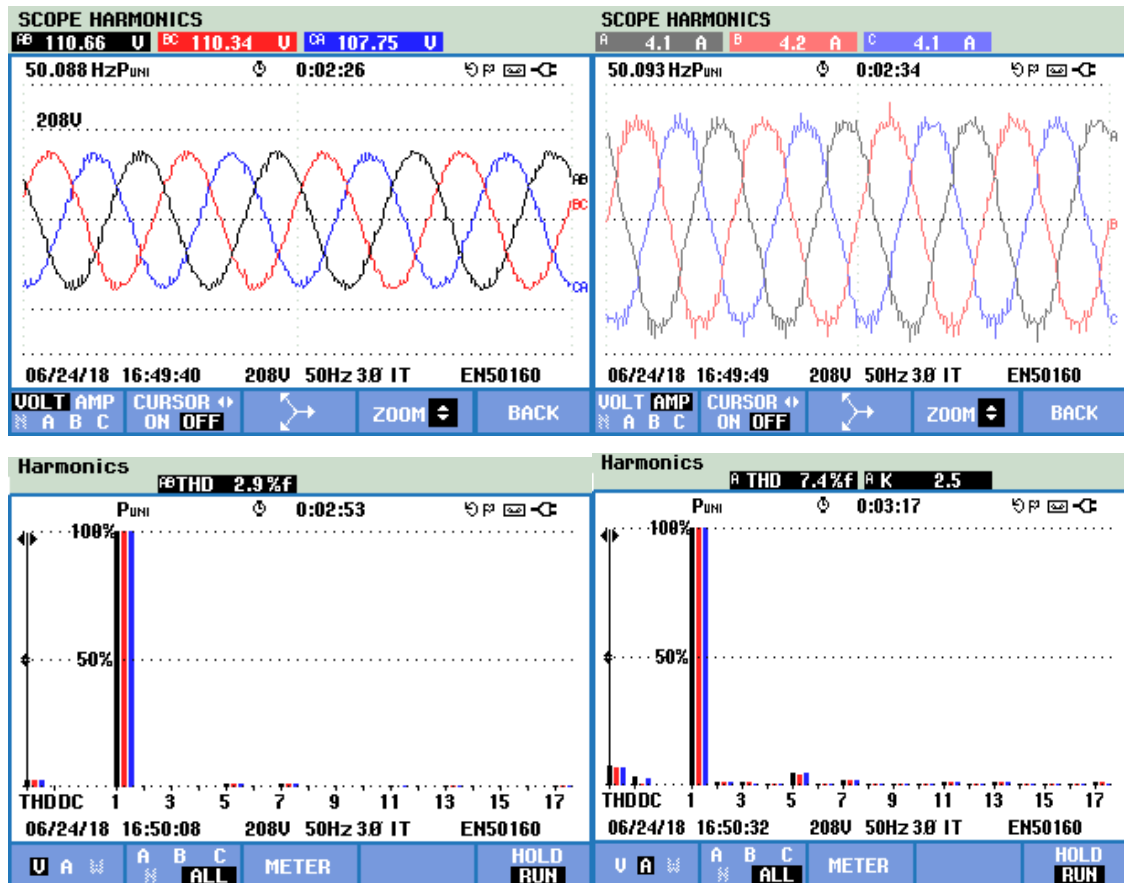
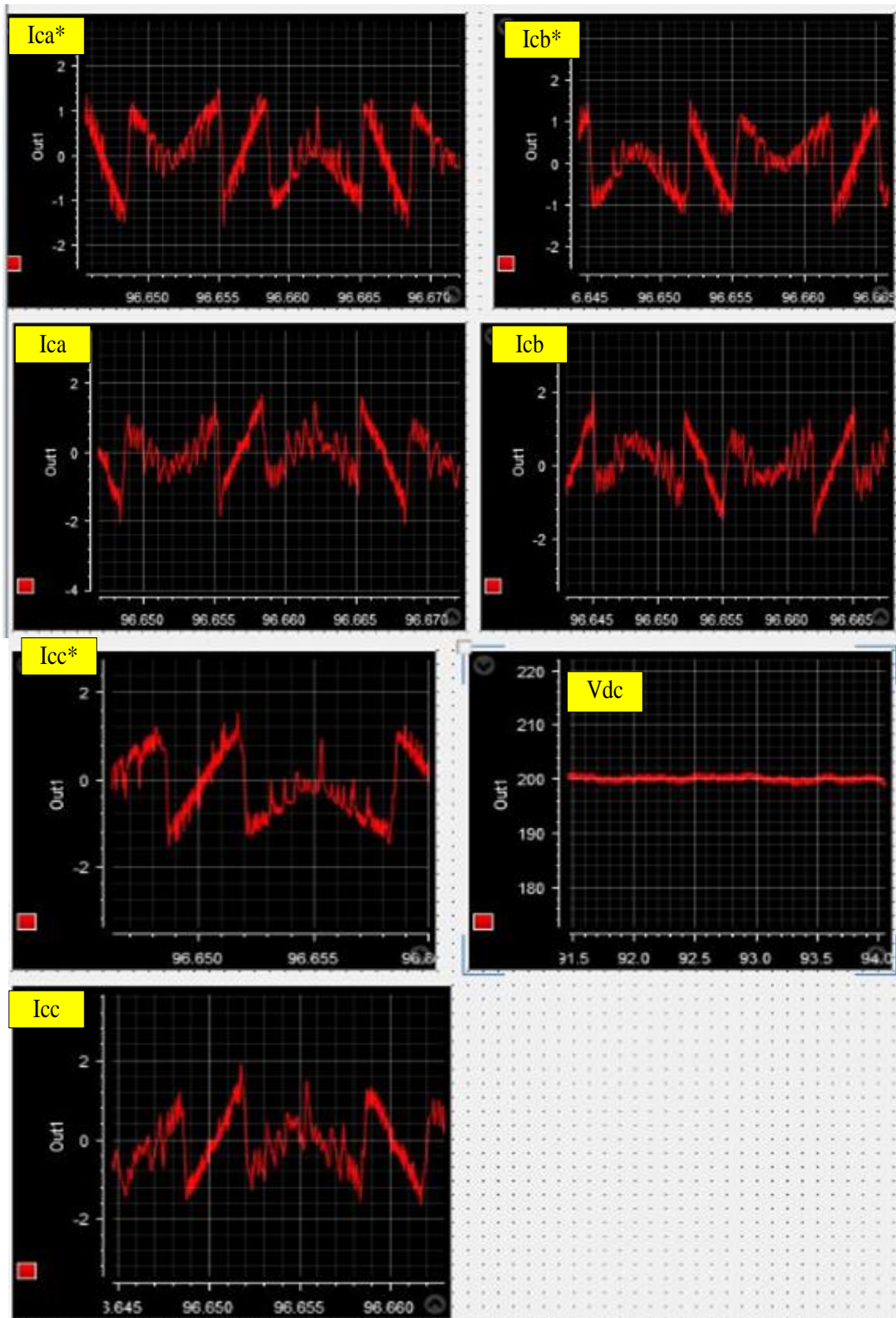


Figure 5-15. Compensated grid voltage and current in case of non-linear load with IRPT control



**Figure 5-16. Reference VSI currents, actual VSI currents and dc-link voltage in case of non-linear load with IRPT control**



### 5.6.4 Results for SRFT Control

This section compiles the waveforms, THD profiles, phasor analysis, power and energy details of grid currents and PCC voltages for different loadings when DSTATCOM is connected and SRFT control algorithm is used.

#### 1) Linear Load

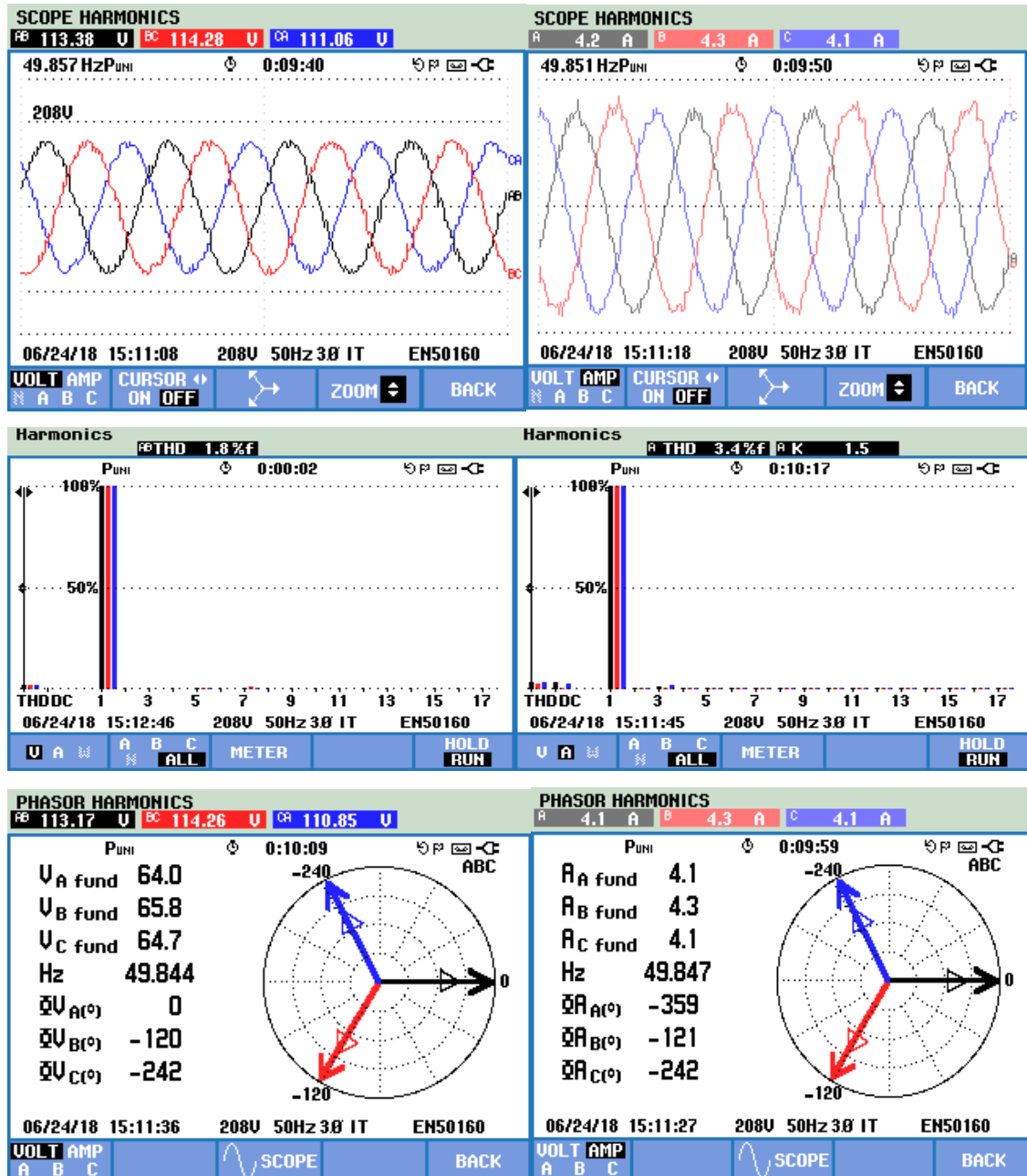
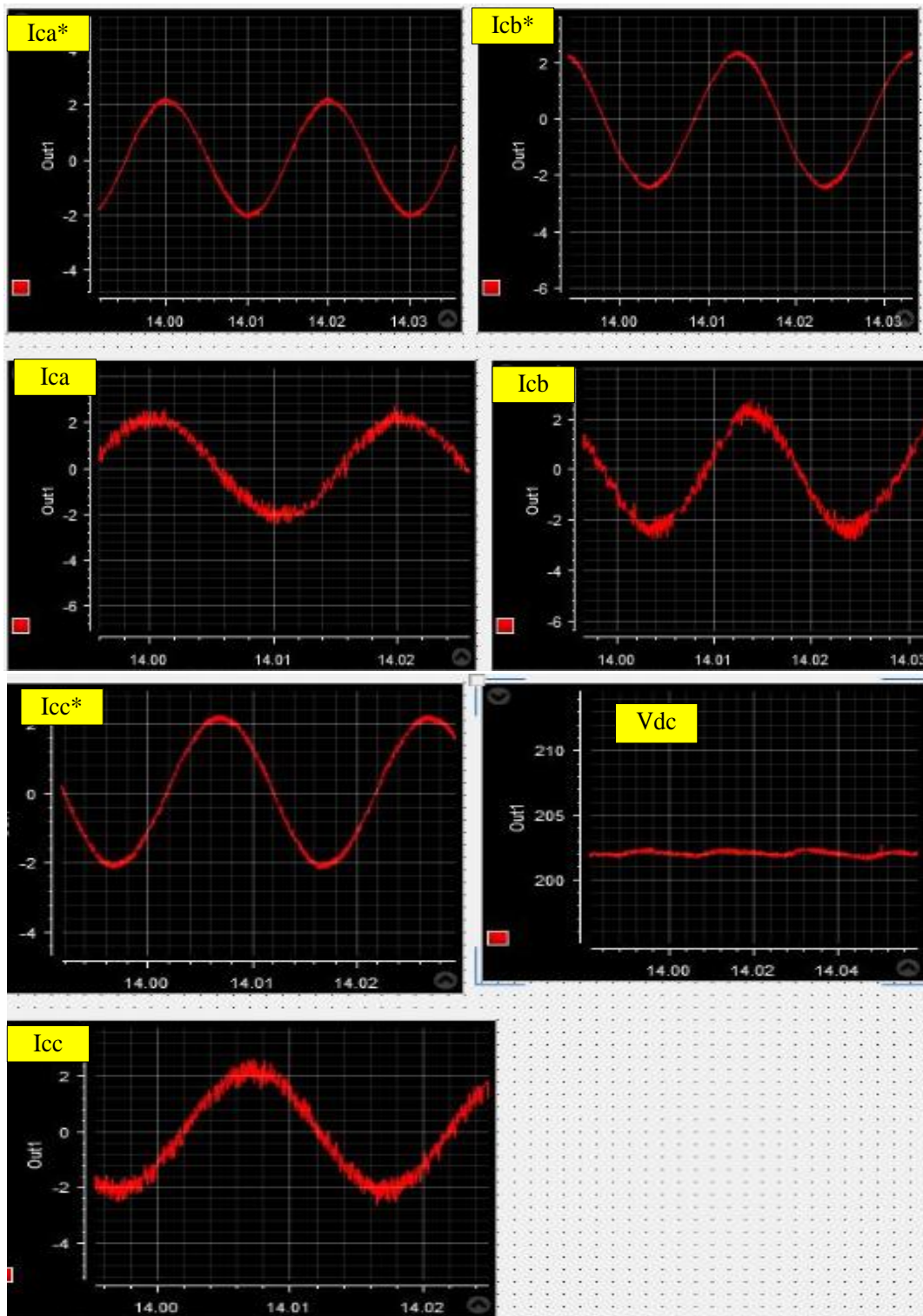


Figure 5-17. Compensated grid voltage and current in case of linear load with SRFT control



**Figure 5-18. Reference VSI currents, actual VSI currents and dc-link voltage in case of linear load with SRFT control**

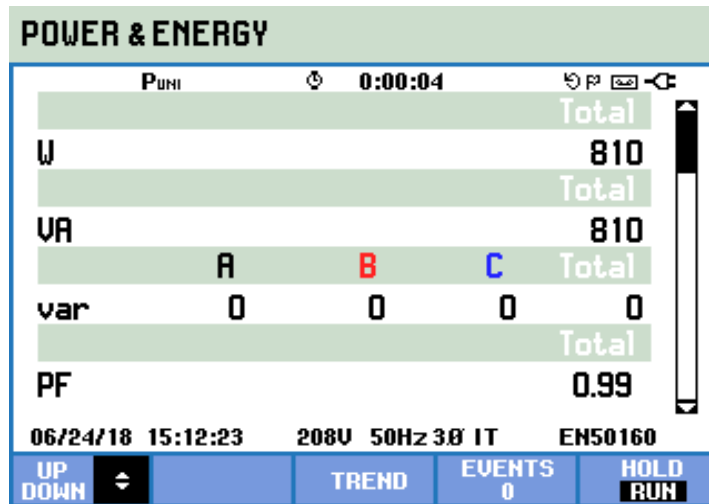


Figure 5-19. Grid power analysis in case of linear load with SRFT control

## 2) Non-Linear Load

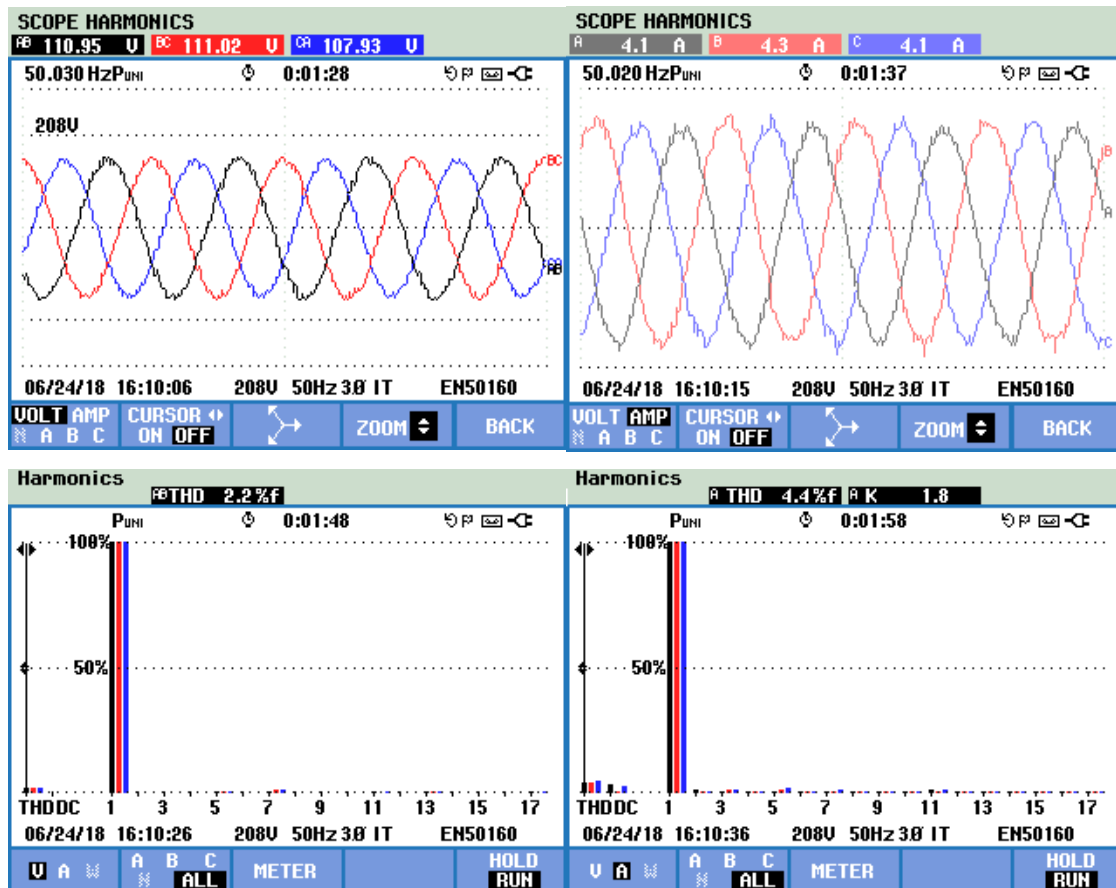
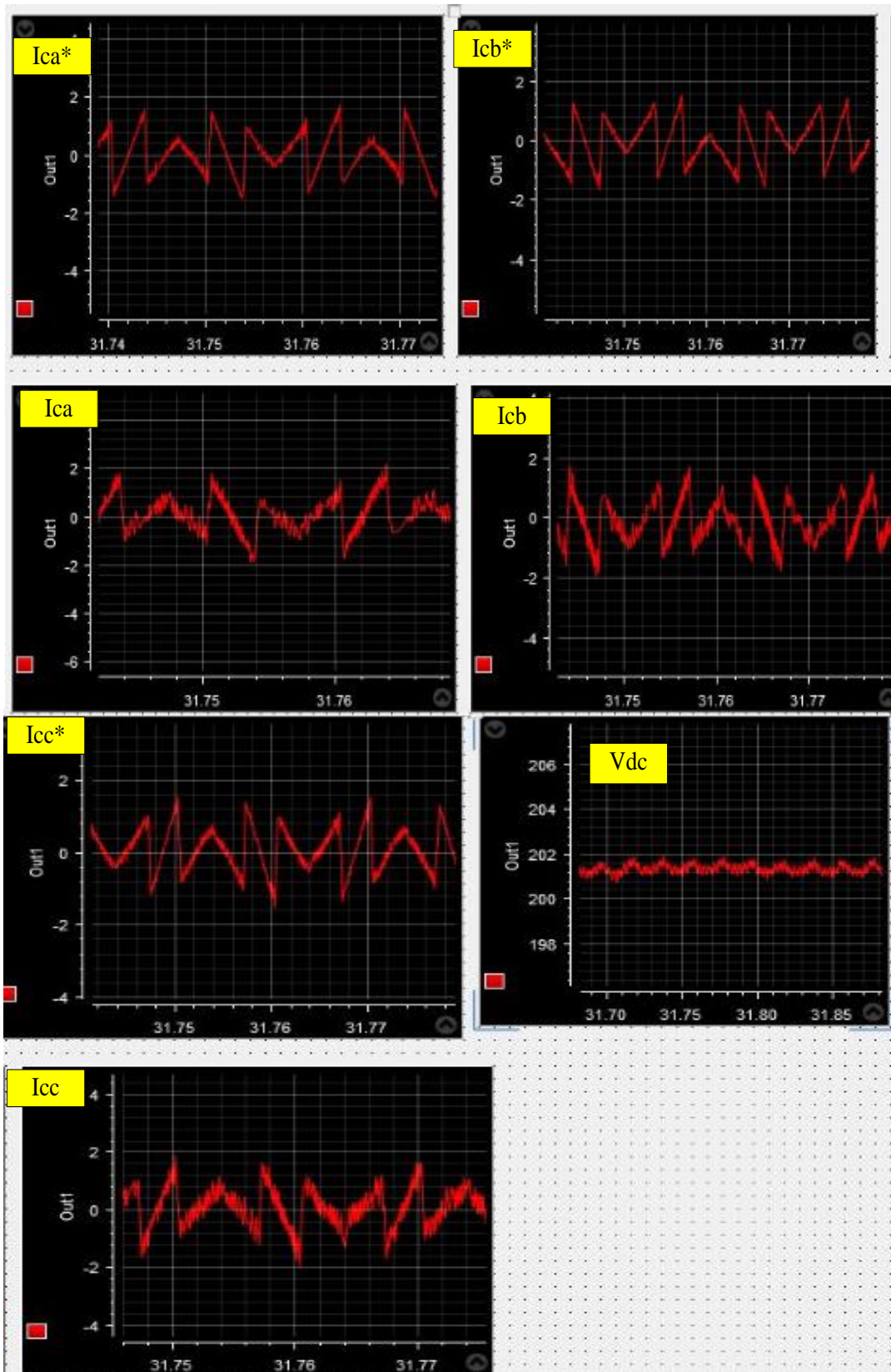


Figure 5-20. Compensated grid voltage and current in case of non-linear load with SRFT control



**Figure 5-21. Reference VSI currents, actual VSI currents and dc-link voltage in case of non-linear load with SRFT control**

### 5.6.5 Results for Indirect SRFT Control:

This section compiles the waveforms, THD profiles, phasor analysis, power and energy details of grid currents and PCC voltages for different loadings when DSTATCOM is connected and Indirect SRFT control algorithm is used.

#### 1) Linear Load

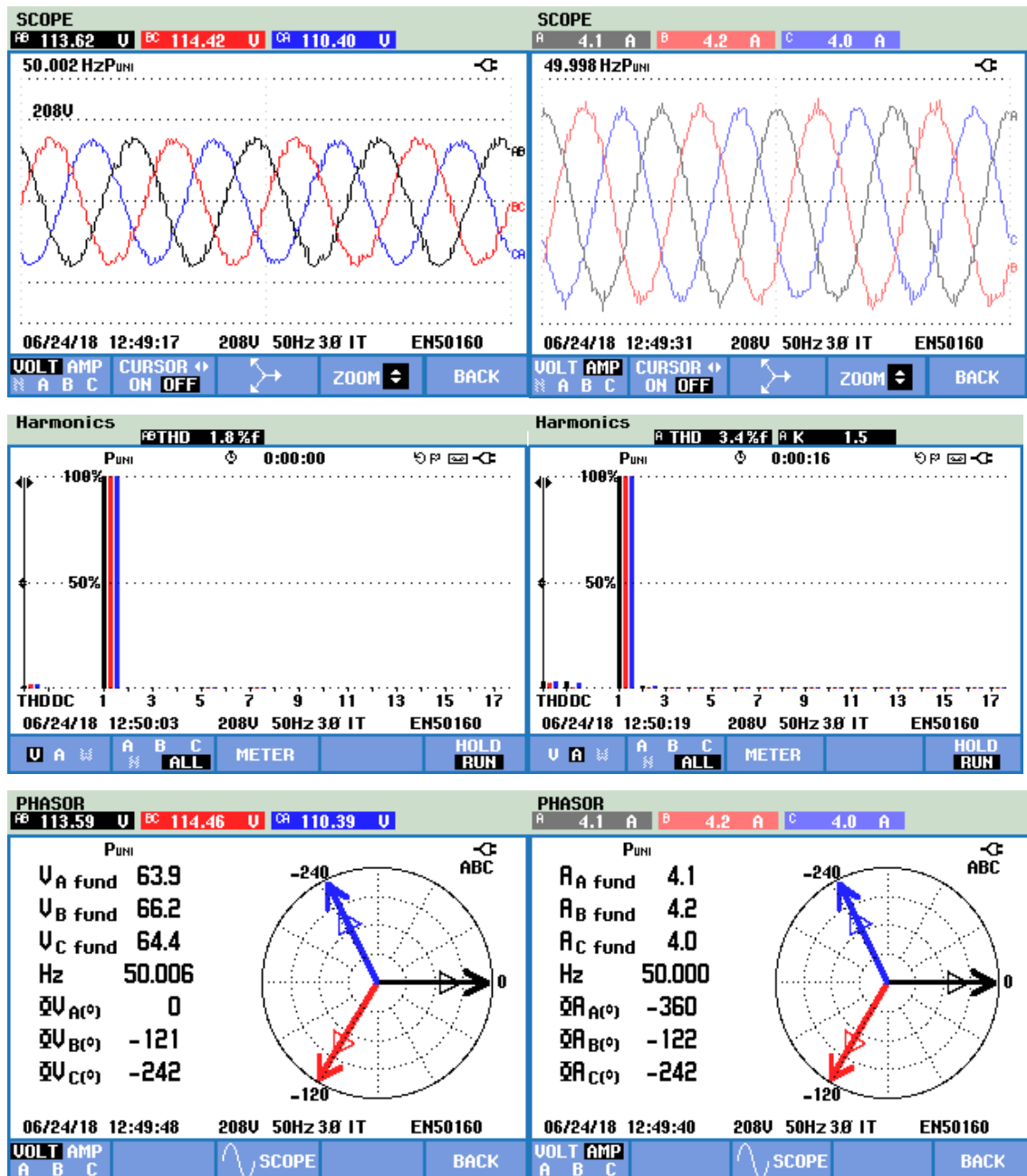


Figure 5-22. Compensated grid voltage and current in case of linear load with Indirect SRFT control



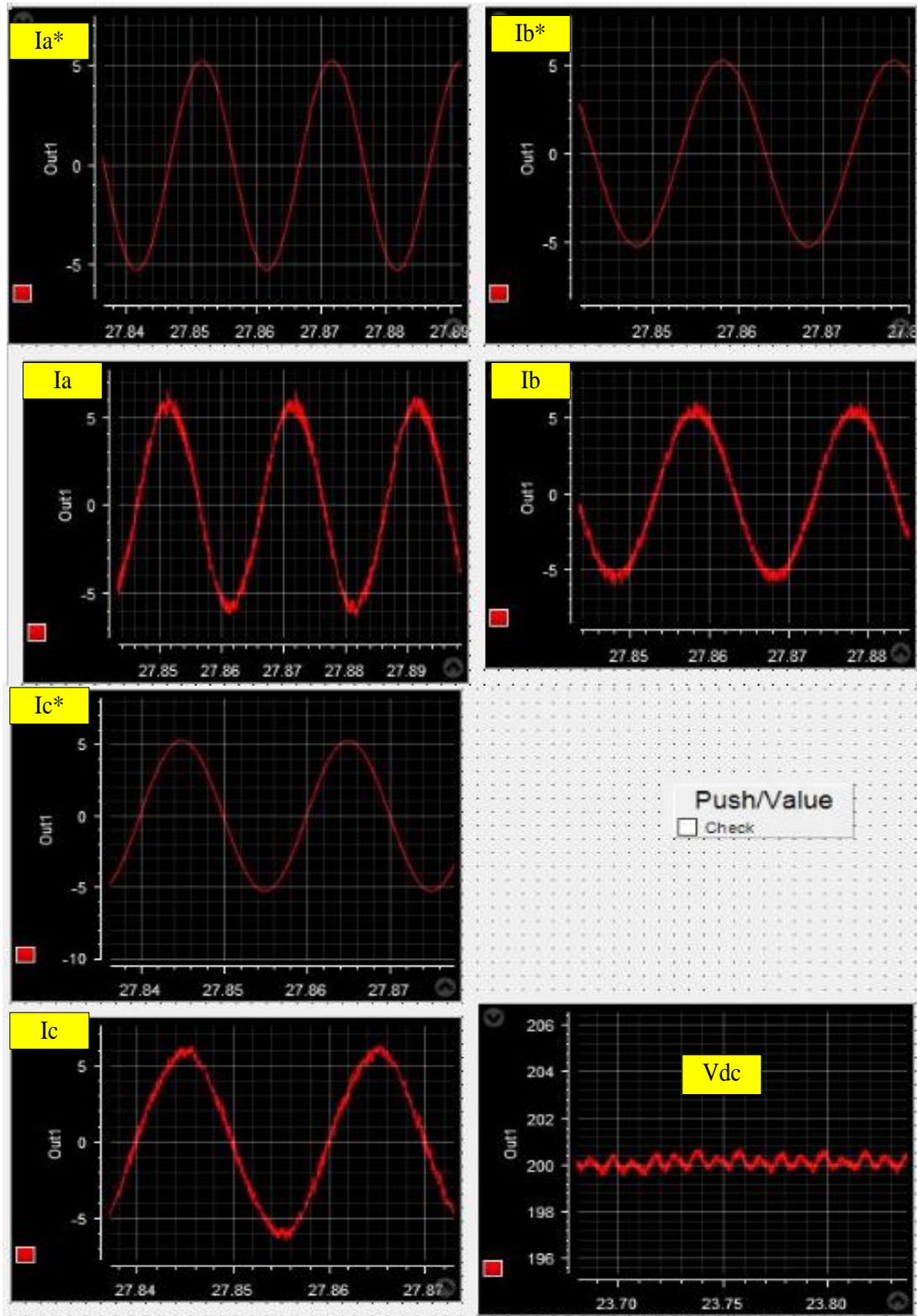


Figure 5-23. Reference grid currents, actual grid currents and dc-link voltage in case of linear load with Indirect SRFT control

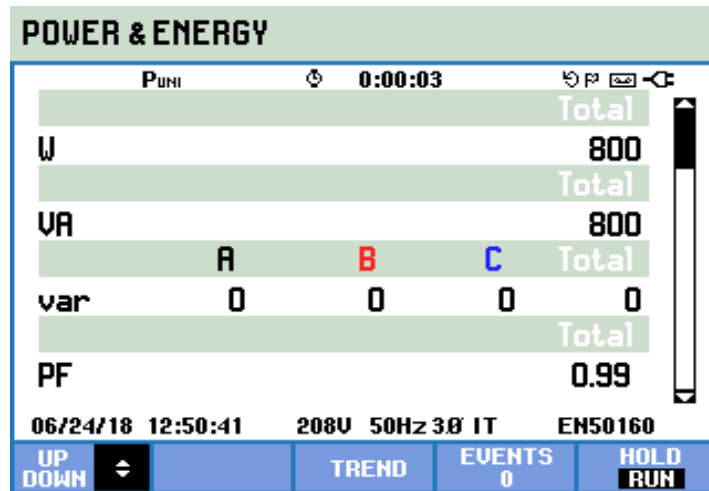


Figure 5-24. Grid power analysis in case of linear load with Indirect SRFT control

## 2) Non-Linear Load

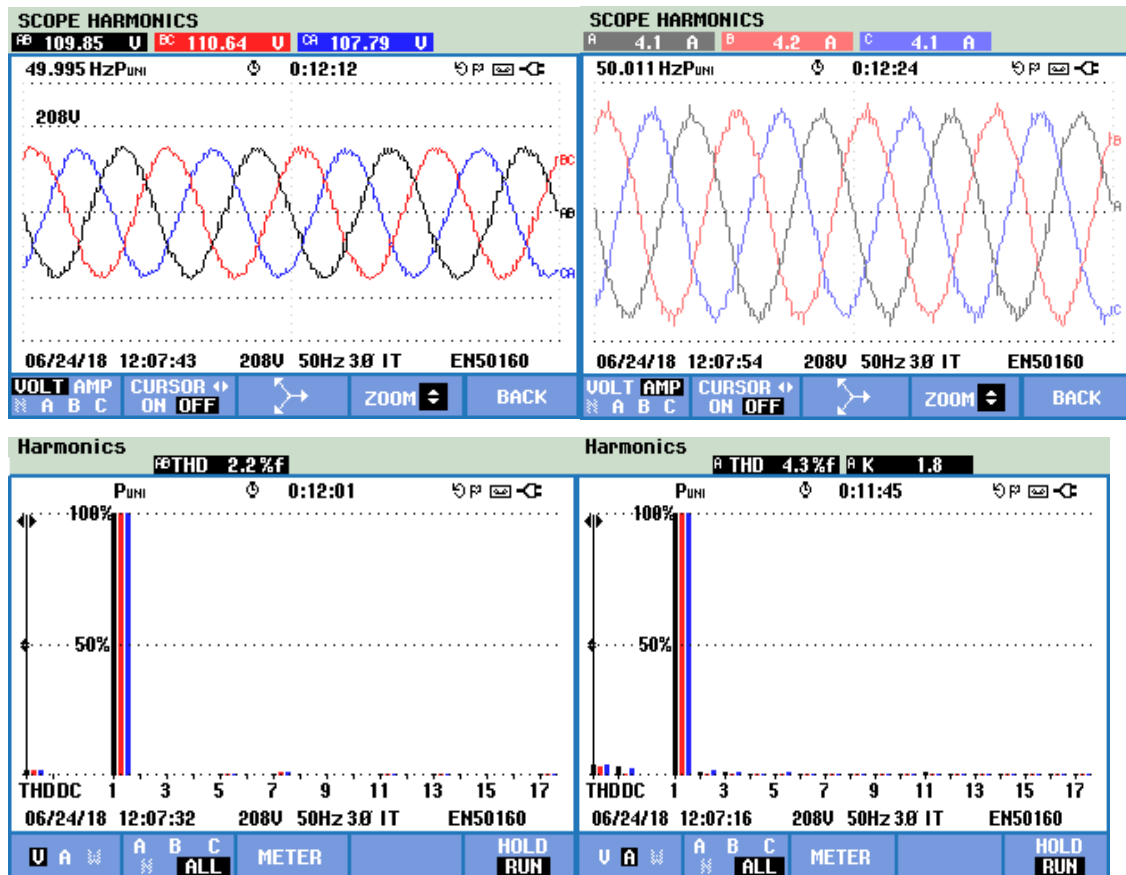
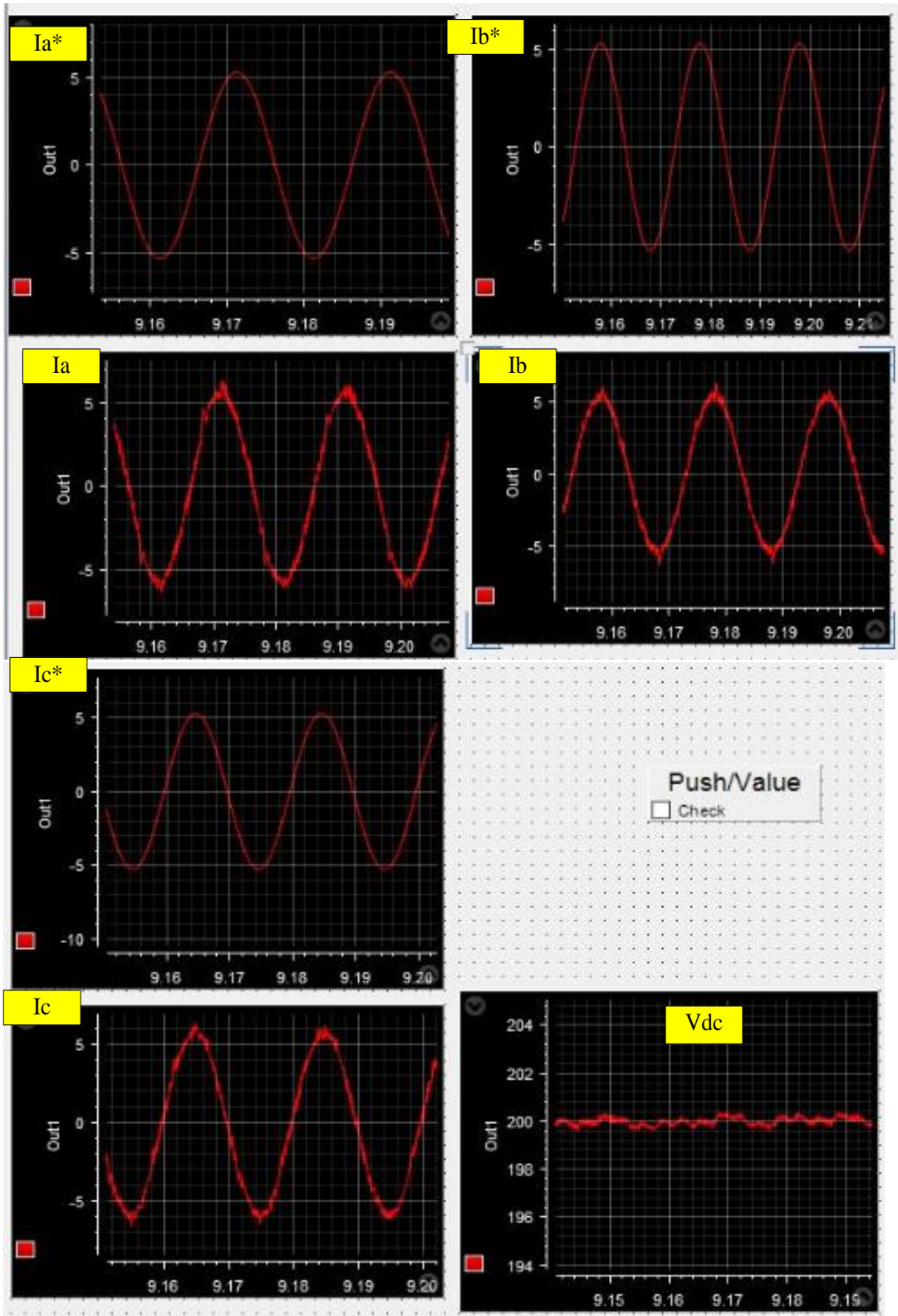


Figure 5-25. Compensated grid voltage and current in case of non-linear load with Indirect SRFT control



**Figure 5-26. Reference grid currents, actual grid currents and dc-link voltage in case of non-linear load with Indirect SRFT control**



### 5.6.6 Results for Compensation of Composite Load through SRFT Control:

This section compiles the waveforms, THD profiles, phasor analysis, power and energy details of grid currents and PCC voltages for composite load (a combination of reactive, non-linear and unbalance load) when DSTATCOM is connected and SRFT control algorithm is used.

#### 1) Without compensation

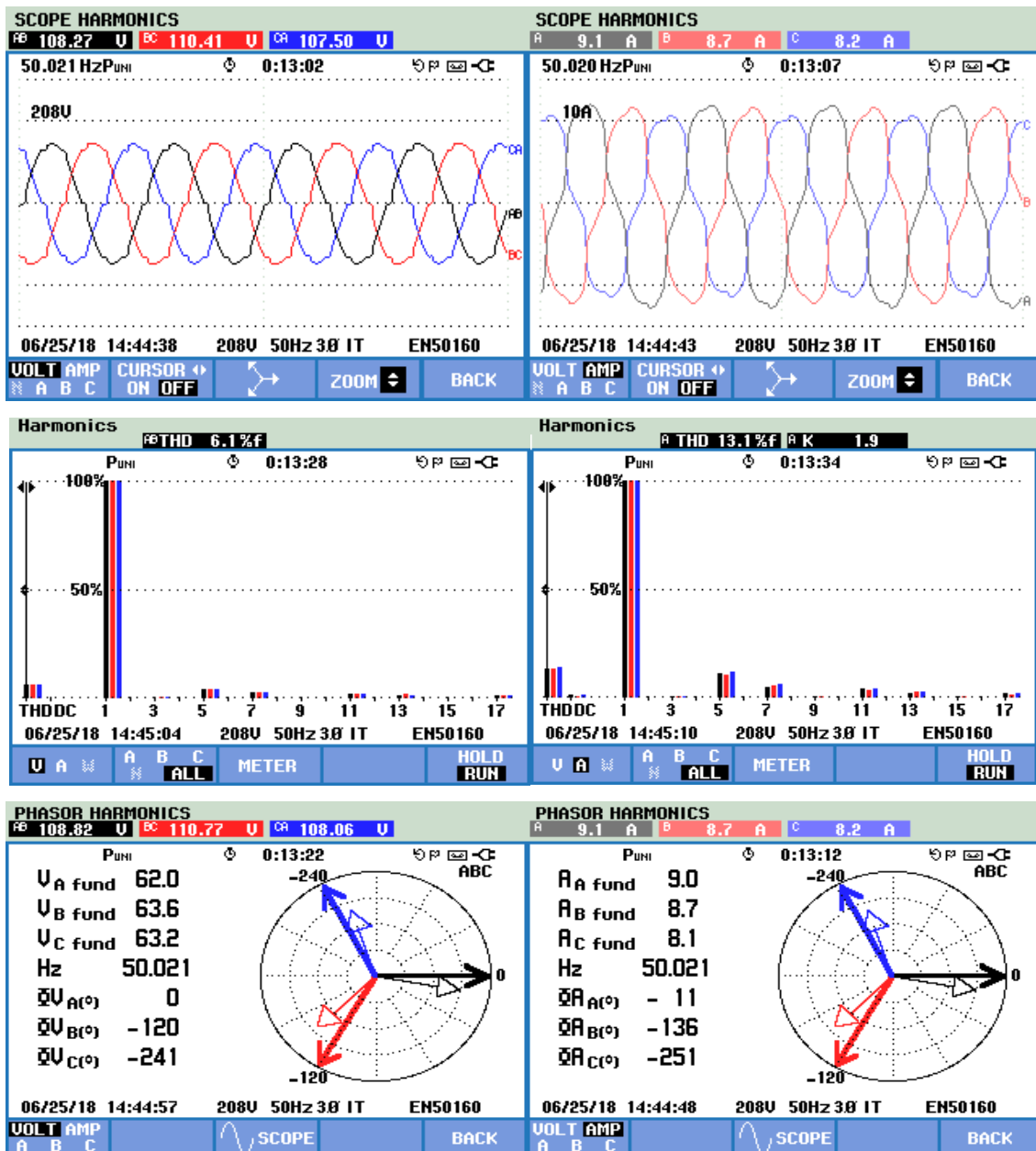


Figure 5-27. Grid voltage and current in case of composite load without compensation

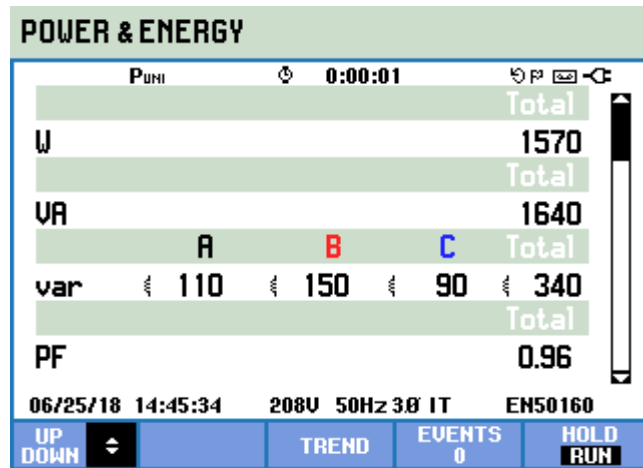


Figure 5-28. Phasors of grid voltage and current with power analysis in case of composite load

## 2) Compensation Applied

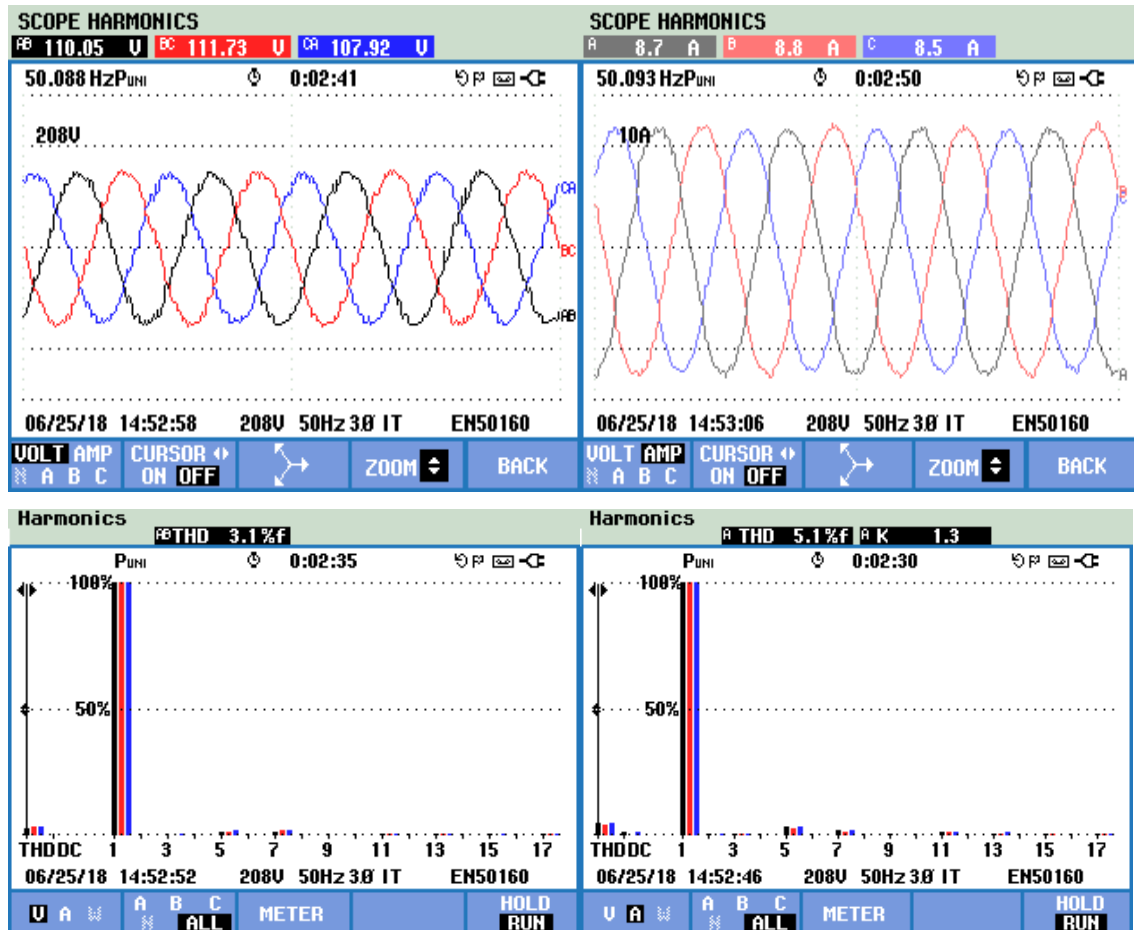


Figure 5-29. Compensated grid voltage and current waveforms and THD in case of composite load with SRFT control

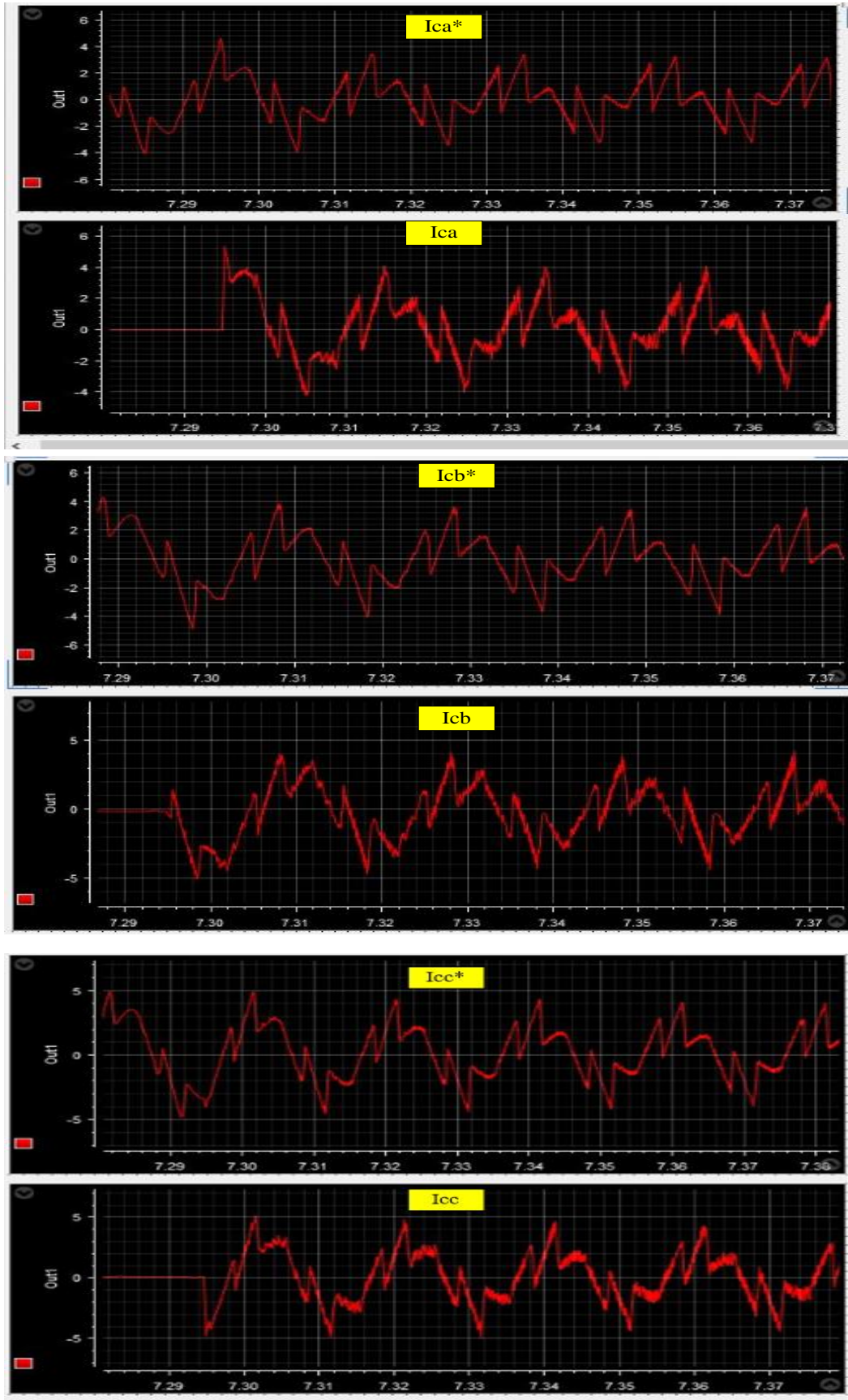


Figure 5-30. Reference VSI currents, actual VSI currents in case of composite load with SRFT control

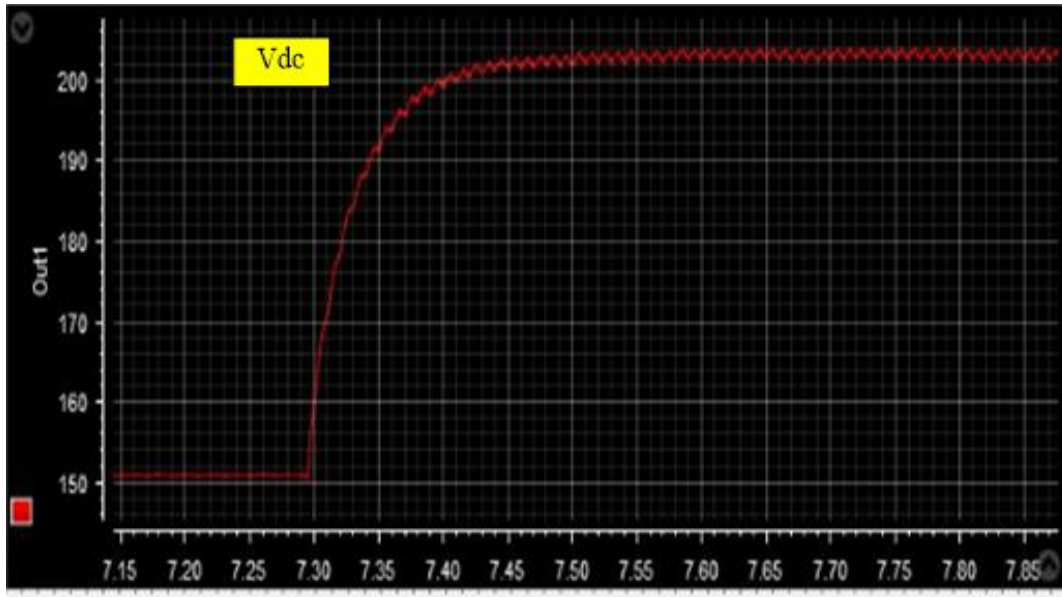


Figure 5-31. Actual DC-link voltage in case of composite load with SRFT control

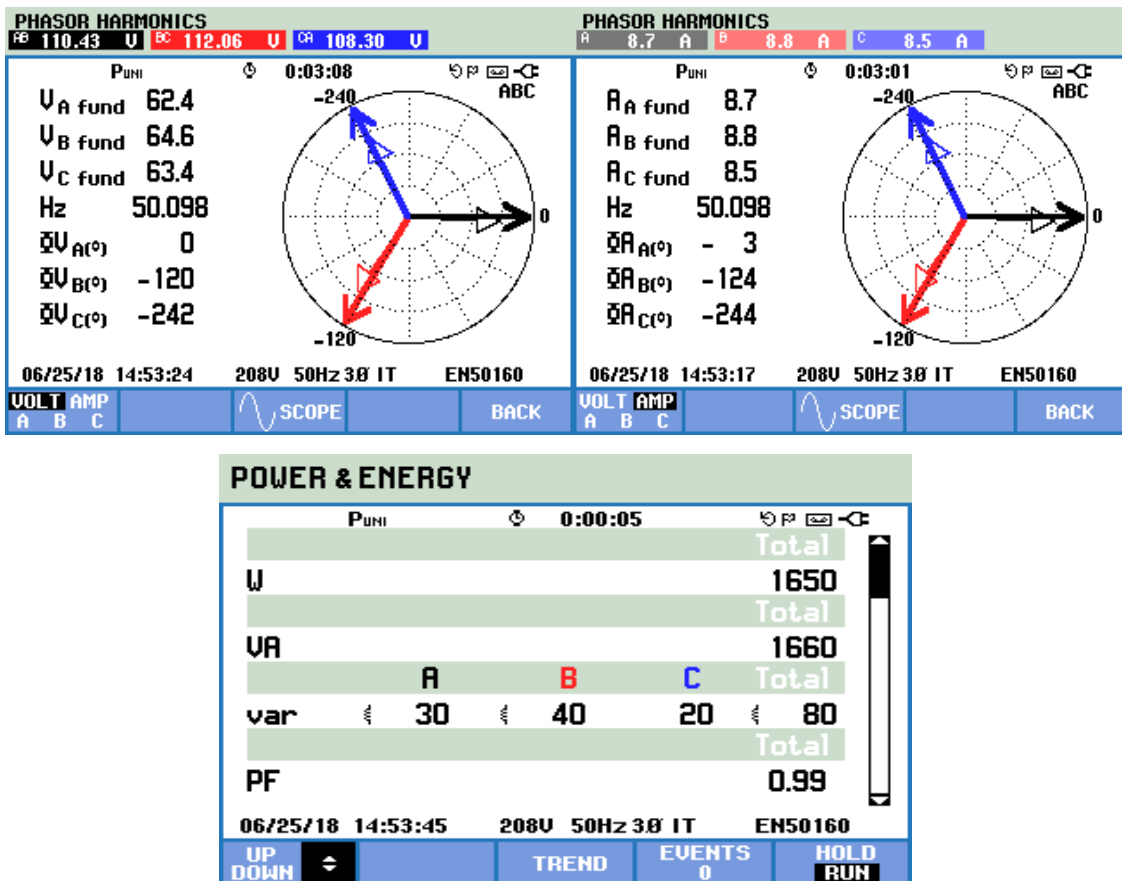


Figure 5-32. Phasors of grid voltage and current with power analysis in case of composite load with SRFT control

## 5.7 Observations

It is observed that the developed hardware is working fine for all the control algorithms used. The DSTATCOM model developed is able to compensate the load reactive power, load harmonics and unbalances and thus making the grid current sinusoidal, balanced and in phase with grid voltage.

Linear load: A linear load is connected to 3-phase, 110 volts ac source. The load draws a real power of 740 W and reactive power of 460 VAR having power factor of 0.85. DSTATCOM is used to compensate the load reactive power. It is seen that the DSTATCOM successfully compensates load reactive power and thus making grid to operate at unity power factor. Table 5.2 summarizes the results obtained for compensation of linear load for different control algorithms.

Non-linear load: A non-linear load is connected to 3-phase, 110 volts ac source. Due to non-linear load the voltage THD of PCC is 4.2 % and grid current THD is 19 %. DSTATCOM is used to compensate the load harmonics and thus reduce THD in PCC voltage and grid current. It is seen that the DSTATCOM successfully compensates load harmonics and thus reducing THD in PCC voltage and grid current. Table 5.3 summarizes the results obtained for compensation of non-linear load for different control algorithms.

Composite load: A composite load is connected to 3-phase, 110 volts ac source. The load is a combination of non-linear load and 3-phase unbalanced load drawing a real power of 1570 W at power factor of 0.96, voltage THD at PCC is 6.1 % and grid current THD is 13.1 %, the three phase load currents are unbalanced 9.1, 8.7 and 8.2 amperes respectively. DSTATCOM is used to compensate the load reactive power, unbalance and harmonics. It is seen that the DSTATCOM successfully compensates load reactive power and thus making grid to operate close to unity power factor, reduces the THD in PCC voltage and grid currents and also balance the 3-phase grid currents. Table 5.4 summarizes the results obtained for compensation of composite load for different control algorithms.

**Table 5.2. Hardware Results for compensation of linear load using DSTATCOM**

	Grid Voltage (V)			Grid Current (A)			Voltage THD (%)	Current THD (%)	Real Power (W)	Reactive Power (VAR)	Power factor
	Vab	Vbc	Vca	Ia	Ib	Ic					
<b>Without Compensation</b>	108.87	109.96	106.57	4.7	5	4.7	1.3	0.4	740	460	0.85
<b>Unit Template control</b>	112.70	112.47	108.71	4.1	4.3	4.1	2.4	6	790	0	0.99
<b>IRPT Control</b>	112.27	112.69	109.65	4.1	4.2	4.1	2.8	5.3	790	0	0.98
<b>SRF Control</b>	113.38	114.28	111.06	4.2	4.3	4.1	1.8	3.4	810	0	0.99
<b>Indirect SRFT Control</b>	113.62	114.42	110.40	4.1	4.2	4.0	1.8	3.4	800	0	0.99

**Table 5.3. Hardware Results for compensation of non-linear load using DSTATCOM**

	Grid Voltage (V)			Grid Current (A)			Voltage THD	Current THD
	Vab	Vbc	Vca	Ia	Ib	Ic		
<b>Without Compensation</b>	111.08	111.79	109.01	4.0	4.1	4.0	4.2	19
<b>Unit Template control</b>	113.47	114.47	110.65	4.1	4.2	4.0	3.7	8.7
<b>IRPT Control</b>	110.66	110.34	107.75	4.1	4.2	4.1	2.9	7.4
<b>SRF Control</b>	110.95	111.02	107.93	4.1	4.3	4.1	2.2	4.4
<b>Indirect SRFT Control</b>	109.85	110.64	107.79	4.1	4.2	4.1	2.2	4.3

**Table 5.4. Hardware Results for compensation of composite load using DSTATCOM**

	Grid Voltage (V)			Grid Current (A)			Voltage THD (%)	Current THD (%)	Real Power (W)	Reactive Power (VAR)	Power factor
	Vab	Vbc	Vca	Ia	Ib	Ic					
<b>Without Compensation</b>	108.27	110.41	107.50	9.1	8.7	8.2	6.1	13.1	1570	340	0.96
<b>SRFT Control</b>	110.05	111.73	107.92	8.7	8.8	8.5	3.1	5.1	1650	80	0.99



## **5.8 Conclusion**

In this chapter the design and hardware implementation of a DSTATCOM is presented. The design of all components in DSTATCOM is explained with all specifications. The control of DSTATCOM is explained with help of a block diagram. The hardware model is tested for four different control techniques under different load conditions and the results are presented. The results show that the system is able to compensate for load reactive power, unbalance load currents, and load harmonics satisfactorily with all control techniques used.

## CHAPTER 6 CONCLUSION AND FUTURE WORK

### 6.1 Main Conclusion

The main objective of this work is to understand working of a PV system, MPPT in PV system, integration of PV to grid and improve power quality in the grid. The electrical equivalent model of a photovoltaic is studied to understand output characteristics of photovoltaic. Designing of boost converter and its application for MPPT in PV system is studied. MATLAB-SIMULINK model is developed for MPPT in photovoltaic system using boost converter and obtained simulation results are presented. A hardware model for the designed MPPT system is also designed and developed.

The two-stage grid connection for integration of PV array to the grid and power quality enhancement is studied. The boost converter in the two-stage model is controlled using Incremental conductance algorithm for MPPT in PV array and the VSI is controlled using four different techniques:

- i) Unit template based current control algorithm
- ii) IRPT based current control algorithm
- iii) SRFT based current control algorithm
- iv) SRFT based indirect current control algorithm

MATLAB-SIMULINK models for all the four control techniques are developed and simulation results are presented. The models developed shows the capability of the grid connected two-stage PV system to successfully inject PV power into grid and simultaneously compensate load reactive power and harmonics. A hardware model of DSTATCOM is developed in laboratory and its performance with above mentioned control techniques to compensate reactive power, harmonics and load unbalance is recorded and compared.

### 6.2 Future Work

The future work is to study, understand and implement following:

- Different configurations of DSTATCOM and their application in 3-phase four/three wire systems.
- Study and apply other conventional and soft computing control techniques like fuzzy control, neural network, genetic algorithm etc. for MPPT and VSI control.
- Hardware implementation of grid connected two-stage PV system.
- Integrating battery storage in PV system.
- Study hybrid renewable energy systems.

## REFERENCES

1. S. K. Sahoo, "Renewable and sustainable energy reviews solar photovoltaic energy progress in India: A review," *Renewable and Sustainable Energy Reviews*, Volume 59, June 2016, Pages 927-939.
2. G. S. Sisodia, P. Singh, "The Status of Renewable Energy Research on India," *Energy Procedia*, Volume 95, September 2016, Pages 416-423.
3. K. Kapoor, K. K. Pandey, A. K. Jain, Ashish Nandan "Evolution of solar energy in India: A review," *Renewable and Sustainable Energy Reviews*, Volume 40, December 2014, Pages 475-487.
4. H. Bellia, R. Youcef and M. Fatima, "A detailed modeling of photovoltaic module using MATLAB," *NRIAG Journal of Astronomy and Geophysics*, Volume 3, Issue 1, June 2014, Pages 53-61.
5. A.V. Pavan Kumar, Alivelu M. Parimi and K. Uma Rao, "Performance Analysis of a Two-Diode model of PV cell for PV based generation in MATLAB," *2014 IEEE International Conference on Advanced Communications, Control and Computing Technologies*, May 2014, Pages 68-72.
6. L.UMANAND, "Design of Photovoltaic systems", [Video-lectures] NPTEL, Available: <https://nptel.ac.in/courses/117/108/117108141/#>.
7. R. Garg, A. Singh, S. Gupta, "PV Cell Models and Dynamic Simulation of MPPT Trackers in MATLAB," *2014 International Conference on Computing for Sustainable Global Development (INDIACom)*, March 2014, Pages 6-12.
8. N. Karami, N. Moubayed and R. Outbib, "General review and classification of different MPPT Techniques," *Renewable and Sustainable Energy Reviews*, Volume 68, Part 1, February 2017, Pages 1-18.
9. J. Prasanth Ram, T. Sudhakar Babu and N. Rajasekar, "A comprehensive review on solar PV maximum power point tracking techniques," *Renewable and Sustainable Energy Reviews*, Volume 67, January 2017, Pages 826-847.
10. P. Verma, P. Mahajan, and R. Garg, "Comparison of Intelligent and Conventional MPPT Algorithms for PhotoVoltaic system under Partially Shaded Conditions," *2017 Recent Developments in Control, Automation & Power Engineering (RDCAPE)*, October 2017, Pages 505-510.
11. N. Mohan, T. M. Undeland, W. P. Robbins, "Power Electronics: Converters, Applications, and Design," 3<sup>rd</sup> edition, WILEY, 2002.
12. D.P. Hohm and M.E. Ropp, "Comparative study of maximum power point tracking algorithm using an experimental, programmable, maximum power point tracking test bed," *Conference Record of the Twenty-Eighth IEEE Photovoltaic Specialists Conference - 2000 (Cat. No.00CH37036)*, September 2000, Pages 1699-1702.
13. S. Thakran, J. Singh, R. Garg and P. Mahajan, "Implementation of P&O Algorithm for MPPT in SPV System," *2018 International Conference on Power Energy, Environment and Intelligent Control (PEEIC)*, April 2018, Pages 242-245.
14. M. Farhat, O. Barambones, L. Sbita "A real-time implementation of MPPT-based on P&O method," *2016 5th International Conference on Electronic Devices, Systems and Applications (ICEDSA)*, December 2016, Pages 1-5.

15. S. S. Choi, J. D. Li, and D. M. Vilathgamuwa, "A generalized voltage compensation strategy for mitigating the impacts of voltage sags/swells," *IEEE Transactions on Power Delivery*, Volume 20, Issue 3, July 2005, Pages 2289–2297.
16. G.T. Heydt, "Electric Power Quality, Stars in a Circle Publication," 2<sup>nd</sup> edition, West Lafayette, Ind,1994.
17. O. Ozgonenel, T. Yalcin, I. Guney and U. Kurt, "A new classification for power quality events in distribution systems," *Electric Power Systems Research*, Volume 95, February 2013, Pages 192-199.
18. W.E. Reid, "Power quality issues-standards and guidelines," *IEEE Transactions on Industry Applications*, Volume 32, Issue 3, May/Jun 1996, Pages 625-632.
19. *IEEE Recommended Practice and Requirements for Harmonic Control in Electric Power Systems*, IEEE Std. 519, 1992.
20. *IEEE Recommended Practice for Monitoring Electric Power Quality*, IEEE Std. 1159,1995.
21. *IEEE Recommended Practice and Requirements for Harmonic Control in Electric Power Systems*, IEEE Std. 519, 1992.
22. *IEEE Standard Definitions for the Measurement of Electric Power Quantities Under Sinusoidal, Nonsinusoidal, Balanced or Unbalanced Conditions*, IEEE Std. 1459, 2010.
23. H. Akagi, "New trends in active filters for power conditioning," *IEEE Transactions on Industry Applications*, Volume 32, Issue 6, December 1996, Pages 1312-1322.
24. A. Sannino, J. Svensson and T. Larsson, "Power-electronic solutions to power quality problems," *Electric Power Systems Research*, Volume 66, Issue 1, July 2003, Pages 71-82.
25. B. Singh, A. Chandra, and K. Al-haddad, "Power Quality Problems and Mitigation Techniques" Wiley Online Library, February 2015.
26. B.N. Singh, B. Singh, A. Chandra and K. Al-Haddad, "Design and digital implementation of active filter with power balance theory," *IEE Proceedings - Electric Power Applications*, Volume 152, Issue 5, September 2005, Pages 1149-1160.
27. M. Singh, V. Khadkikar, A. Chandra and R.K. Varma, "Grid interconnection of renewable energy sources at the distribution level with power-quality improvement features," *IEEE Transactions on Power Delivery*, Volume 26, Issue 1, January 2011 Pages 307-315.
28. G. Tsengenes, G. Adamidis, "Investigation of the behavior of a three phase grid-connected photovoltaic system to control active and reactive power," *Electric Power Systems Research*, Volume 81, Issue 1, January 2011, Pages 177-184.
29. B. Singh, C. Jain and S. Goel, "ILST control algorithm of single-stage dual purpose grid connected solar PV system," *IEEE Transactions on Power Delivery*, Volume 29, Issue 10, October 2014, Pages 5347-5357.
30. C. Jain and B. Singh, "Luenberger observer based control algorithm for single-phase two-stage multifunctional grid connected solar energy conversion system," *2014 9th International Conference on Industrial and Information Systems (ICIIS)*, December 2014, Pages 1-6.

31. B. Singh, D.T Shahani and A. K. Verma, "Power balance theory based control of grid interfaced solar photovoltaic power generating system with improved power quality," *2012 IEEE International Conference on Power Electronics, Drives and Energy Systems (PEDES)*, December 2012, Pages 1-7.
32. B. Singh, D. T. Shahani, A. K. Verma, "IRPT based control of a 50 kW grid interfaced solar photovoltaic power generating system with power quality improvement," *2013 4th IEEE International Symposium on Power Electronics for Distributed Generation Systems (PEDG)*, July 2013, Pages 1-8.
33. A. K. Verma, B. Singh, and D. T. Shahani, "Grid interfaced solar photovoltaic power generating system with power quality improvement at AC mains," *2012 IEEE Third International Conference on Sustainable Energy Technologies (ICSET)*, September 2012, Pages 177-182.